AIR PLASMA SPRAYING OF SOFC COMPOSITE CATHODES

by

Bradley White

A THESIS SUBMITTED IN PARTIAL FULFILLMENT OF
THE REQUIREMENTS FOR THE DEGREE OF

MASTER OF APPLIED SCIENCE

In

The Faculty of Graduate Studies

(Mechanical Engineering)

UNIVERSITY OF BRITISH COLUMBIA

October 2006

Abstract

Air plasma spraying (APS) has been used to produce porous composite cathodes containing $(La_{0.8}Sr_{0.2})_{0.98}MnO_3$ (LSM) and yttria stabilized zirconia (YSZ) for use in solid oxide fuel cells (SOFCs). Preliminary investigations focused on determining the range of plasma conditions under which each of the individual materials could be successfully deposited. A range of conditions was thereby determined that were suitable for the deposition of a composite cathode from pre-mixed LSM and YSZ powders. A proof of concept SOFC containing a plasma sprayed composite cathode was then produced and tested to confirm the desired electrochemical properties of the coating had been obtained. Many composite cathodes were then produced using different combinations of parameter values within the identified range. Successful coatings were then characterized for composition and microstructure using EDX and SEM. As a result of these tests, combinations of input parameter values were identified that are best suited to the production of coatings with microstructures appropriate for use in SOFC composite cathodes. A selection of coatings representative of the types of observed microstructures were then subjected to electrochemical testing to evaluate the performance of these cathodes. From these tests it was confirmed that the coatings that appeared to have the most suitable microstructures showed the best performance. Finally, a procedure was developed to allow for the deposition of cathode symmetric cells entirely by APS using porous metal interconnect substrates. This will allow for the electrochemical evaluation of cells produced as part of future optimization studies using a production process similar to that expected to be used in the eventual commercial production of SOFCs by APS.

Keywords: Solid Oxide Fuel Cell, Air Plasma Spraying, Composite Cathode, LSM, YSZ

Table of Contents

Abstract ii

Table of Contents iii

List of Tables v

List of Figures vi

Acknowledgements ix

1.0 Literature Review 1

1.1 Introduction 1
1.2 The Plasma Spray Process 3
1.2.1 Overview 3
1.2.2 Coating Production 4
1.2.3 Plasma Spray Process Parameter Identification, Characterization and Stability 5
1.3 SOFC Cathodes 11
1.3.1 Cathode Function and Materials 11
1.3.2 Cathode Conductivity and the Oxygen Reduction Reaction 12
1.3.3 Cathode Composition and Structure Modification 14
1.3.4 Cathode Fabrication 18
1.3.5 Modeling and Reduced Temperature SOFCs 20
1.4 SOFC Fabrication by Plasma Spray 29
1.4.1 Plasma Spray Processing of SOFC Electrolytes 29
1.4.2 Plasma Spraying of SOFC Cathodes 31
1.4.3 Plasma Spraying of Interconnect Coatings 34
1.4.4 Integrated Fabrication of SOFCs by Plasma Spraying 36
1.5 Experimental Design and Coating Optimization 42
1.5.1 Parameter Development and Application of Factorial Experimental Design to Plasma Spray Coatings 43
1.5.2 Uniform Design Theory and Application to Plasma Spray Coating Optimization 50
1.6 Literature Review Summary 54

2.0 Air Plasma Spray System Description and Experimental Setup 56

3.0 Plasma Spray Feedstock Preparation 59

3.1 Introduction 59
3.2 Experimental Procedure 60
3.3 Results and Discussion 60

4.0 Single Material Coating Production and Parameter Range Screening 64

4.1 Introduction 64
4.2 Experimental Procedure 64
4.3 Results and Discussion 64

5.0 Initial Composite Coating Production and Proof of Concept Cathode Testing 68

5.1 Introduction 68
5.2 Experimental Procedure 68
5.3 Results and Discussion 69

6.0 Preliminary Coating Optimization Study 75

6.1 Introduction 75
6.2 Experimental 75
6.3 Results and Discussion 75

7.0 Cathode Electrochemical Evaluation 83

7.1 Introduction 83
7.2 Experimental Procedure 83
7.3 Results and Discussion 84

8.0 Symmetric Cell Production by APS 93

8.1 Introduction 93
8.2 Experimental Procedure 93
8.3 Results and Discussion 94

9.0 Conclusion 98

9.1 Summary 98
9.2 Recommendations for Future Work 100

References 102

List of Tables

Table 1: Air plasma spray input parameters..... **6**

Table 2: L9(34) Orthogonal Design [111]..... **50**

Table 3: U12(124) Uniform Design Table [111]..... **50**

Table 4: Maximum and minimum values for each input parameter that allows for the production of a viable LSM/YSZ composite coating..... **67**

Table 5: Relative deposition efficiency of LSM and 4.7 mol% YSZ over a range of plasma conditions (YSZ particle size -32+10μm). All ratios are on a mass basis..... **70**

Table 6: 9-4-40 Uniform Design Grid..... **76**

List of Figures

Figure 1: Axial injection air plasma spray torch schematic..... **4**

Figure 2: Cathode reaction paths (reproduced from information in [30])..... **13**

Figure 3: Powder feed hopper system..... **57**

Figure 4: APS system power and gas supplies..... **57**

Figure 5: Plasma torch and manipulator robot..... **57**

Figure 6: APS system control console..... **58**

Figure 7: Manipulator (right) and sample mounting system (left) control consoles..... **58**

Figure 8: Typical optical micrograph of plasma spray grade (La0.8Sr0.2)0.98 MnO3 (x40 magnification)..... **59**

Figure 9: Typical optical micrograph of plasma spray grade 4.7 mol% YSZ (x40 magnification)..... **60**

Figure 10: Particle size distribution of the as received LSM powder..... **61**

Figure 11: Particle size distribution of the a) -106+75μm, b) -75+45μm, c) -45+32μm, and d) -32μm sieved LSM powder..... **62**

Figure 12: Particle size distribution of -75+45μm unsintered LSM powder after feeding..... **63**

Figure 13: As received LSM powder after feeding (x40 magnification) showing clumping of broken agglomerates..... **63**

Figure 14: XRD patterns of, a) as received LSM feedstock and plasma sprayed LSM coatings produced with, b) 20% Ar, 80% N2; c) 55% Ar, 40 % N2, 5% H2; d) 0% Ar, 80% N2, 20% H2..... **65**

Figure 15: YSZ substrate holder and mask..... **68**

Figure 16: SEM image of LSM /YSZ composite coating #2 containing 23.9 wt% YSZ..... **70**

Figure 17: SEM cross section image of LSM /YSZ composite coating #2 deposited on a YSZ electrolyte substrate. Coating contains 31.9 wt% YSZ..... **70**

Figure 18: SEM image of LSM /YSZ composite coating # 4 containing 14.5 wt% YSZ..... **71**

Figure 19: Variation in YSZ relative deposition efficiency with total plasma enthalpy..... **72**

Figure 20: APS LSM/YSZ composite cathode on YSZ electrolyte..... **73**

Figure 21: I-V characteristics of an SOFC with a plasma sprayed LSM/YSZ cathode, YSZ electrolyte, and Pt anode tested in H2/Air at 1000°C..... **74**

Figure 22: Micrograph of surface of coating #16 from UD table, containing 33.8 wt% YSZ.... **78**

Figure 23: Micrograph of surface of coating #10 from UD table, containing 36.9 wt% YSZ.... **79**

Figure 24: Micrograph of surface of coating #8 from UD table, containing 31.7 wt% YSZ..... **79**

Figure 25: Micrograph of surface of coating #19 from UD table, containing 14.3 wt% YSZ.... **80**

Figure 26: Micrograph of surface of coating #1 from UD table, containing 29.4 wt% YSZ..... **80**

Figure 27: Micrograph of surface of coating #32 from UD table, containing 25.1 wt% YSZ.... **81**

Figure 28: Micrograph of surface of coating #25 from UD table, containing 26.1 wt% YSZ.... **81**

Figure 29: Micrograph of surface of coating #26 from UD table, containing 33.6 wt% YSZ.... **82**

Figure 30: Micrograph of surface of coating #35 from UD table, containing 30.1 wt% YSZ.... **82**

Figure 31: Top surface of LSM/YSZ coatings produced under identical conditions (30%N2, 100mm, 217A, 217slpm) on (bottom) zirconia and (top) stainless steel..... **84**

Figure 32: Cross section of coating produced on zirconia substrate at 30%N2, 100mm, 217A, 217slpm..... **85**

Figure 33: Top surface (top) and cross section (bottom) of a LSM/YSZ composite cathode deposited on a thick YSZ electrolyte (100mm, 220 slpm, 30%N2, 250A, -45+32μm LSM, -32+25μm YSZ)..... **87**

Figure 34: Top surface (top) and cross section (bottom) of a LSM/YSZ composite cathode deposited on a thick YSZ electrolyte (150mm, 200 slpm, 50%N2, 220A, -75+45μm LSM, -45+32μm YSZ)..... **88**

Figure 35: Top surface (top) and cross section (bottom) of a LSM/YSZ composite cathode deposited on a thick YSZ electrolyte (150mm, 220 slpm, 50%N2, 150A, -75+45μm LSM, -45+32μm YSZ)..... **89**

Figure 36: Top surface (top) and cross section (bottom) of a LSM/YSZ composite cathode deposited on a thick YSZ electrolyte (180mm, 180 slpm, 70%N2, 220A, -75+45μm LSM, -32+25μm YSZ)..... **90**

Figure 37: Electrochemical Impedance Spectra of LSM/YSZ cathode half cells tested at 950°C. 100mV AC amplitude, 1 MHz to 0.1 Hz frequency range..... **91**

Figure 38: Electrochemical Impedance Spectra of LSM/YSZ cathode half cells tested at 860°C. 100mV AC amplitude, 1 MHz to 0.1 Hz frequency range..... **91**

Figure 39: Electrochemical Impedance Spectra of LSM/YSZ cathode half cells tested at 780°C. 100mV AC amplitude, 1 MHz to 0.05 Hz frequency range..... **91**

Figure 40: Electrochemical Impedance Spectra of LSM/YSZ cathode half cells tested at 715°C. 100mV AC amplitude, 1 MHz to 0.01 Hz frequency range..... **92**

Figure 41: Arrhenius plot showing ASR vs. 1/T for both cells tested..... **92**

Figure 42: Cross section of plasma sprayed electrolyte (80% N2, 220 slpm, 250 A, 150mm). **95**

Figure 43: Surface view micrographs of cathodes deposited on substrate (top) and on plasma sprayed electrolyte (bottom). Coating compositions 31-35wt% YSZ and porosities 16-19%. Both cathodes deposited using -75+45μm LSM, -45+32μm YSZ, 183 slpm, 77% N2, and 217A at 100mm..... **97**

Acknowledgements

I owe a debt of gratitude to all of the people and organizations that have contributed to this project.

I would like to thank the NRC Institute for Fuel Cell Innovation for both the assistance of many of their staff members and the use of their fine facilities. I would also like to thank Northwest Mettech Corp. for their financial, technical, and in-kind support of this project.

This work would also not have been possible without the assistance and insight provided by the entire UBC SOFC research group, in particular Nir Ben-Oved and Dave Waldbillig. Their generous sharing of time, experience, and considerable expertise has greatly improved the quality of this work. They have also helped me solve many of the (numerous) problems encountered and no doubt helped me avoid many others.

Most of all, I would like to thank my supervisor, Dr. Olivera Kesler, from whom I've learned much over the last two years. Without her guidance, insight, and unwavering support, none of this work would have been possible.

I would also like to thank my friends for providing encouragement and, from time to time, much needed distractions. Last, but certainly not least, I would like to thank my parents, whose backing, both moral and financial, I've always been able to count on.

1.0 Literature Review

1.1 Introduction

Solid oxide fuel cells (SOFCs) are electrochemical energy conversion devices that could potentially provide a low pollution, high efficiency alternative to heat engines for many power generation applications. SOFCs have the ability to use a wide variety of fuels including hydrocarbons, alcohols, hydrogen and carbon monoxide. The high operating temperature of SOFCs (~800°C) yields high quality waste heat that is suitable for use in co-generation and combined heat and power systems, further improving overall system efficiency. SOFCs are well suited for applications that require moderate to large amounts of power including stationary electricity production for both centralized and distributed power generation as well as auxiliary power generation for mobile applications [1]. The ability to utilize hydrocarbon fuels allows SOFCs to make use of the existing fuel delivery infrastructure with little or no modification required. Furthermore, the fuel flexibility of SOFCs makes them a suitable technology for a transition from our current fossil fuel economy to one based on hydrogen, biofuels, and other renewable energy sources.

The physical structure of an SOFC consists of a fully dense ceramic electrolyte between porous ceramic electrodes. Multiple cells are connected together in series or parallel in a stack to achieve high voltages or currents. Ceramic or coated metallic interconnects provide an electrical connection between cells and also supply reactants to the electrodes. The use of solid components eliminates the risk of leak posed by hazardous materials such as acids and alkaline solutions found in many other types of fuel cells. SOFCs have been produced with various geometries, the most common being tubular and planar (or flat plate) configurations. Other geometries include segmented-cell-in-series, single phase, single chamber, and monolithic designs. Of these, tubular designs were the earliest and consequently are presently the most well developed. Large tubular SOFCs are currently in operation as power plants in several locations worldwide. Japan in particular has an extensive SOFC test program with many prototypes in place at various locations throughout the country [2]. While to date, most of the prototypes in place are of the tubular configuration, Japan is increasingly looking to planar SOFCs due to their higher power density. Planar SOFCs, while at a comparatively early stage of development, have achieved higher power densities and reduced ohmic losses compared to the tubular configurations. One study has attempted to combine the desirable characteristics of the tubular and flat plate designs [3]. While better performance was obtained from this configuration the resulting structure is considerably more complex than the standard flat plate design. The

development of this new cell geometry is still very much in its infancy, although it could eventually compete successfully against the more established SOFC geometries.

Compared to other fuel cell types, SOFCs are a relatively new technology and are further from commercialization. The principal limiting factors to widespread implementation of the technology are high material and manufacturing costs, time consuming fabrication processes, and insufficient reliability and durability. The introduction of improved manufacturing techniques could potentially remedy many of these deficiencies. The traditional fabrication of an SOFC involves the deposition of a single cell component followed by a high temperature sintering step. This process is repeated until the entire cell has been assembled. The use of multiple sintering steps is necessitated by the nature of the materials being used. For instance, temperatures required to achieve gas tightness in the electrolyte can result in over sintering or decomposition of cathode materials if all of the layers were to be sintered simultaneously. Thus, more complex sintering steps involving multiple temperatures are required to avoid material degradation during fabrication. In the case of planar cells the supporting electrode is tape cast. Following pre-sintering, the electrolyte is deposited by any number of processes e.g. screen printing, electrochemical vapour deposition, etc. The two layers are then co-sintered. Finally, the other electrode is deposited and the entire cell is again co-sintered. Tubular cell fabrication is carried out in a similar manner, but with extrusion replacing the tape casting step. This manufacturing process introduces a number of undesirable effects. Each sintering step takes a number of hours and can introduce high stresses upon cooling if there is a mismatch of thermal expansion coefficients (TECs) between layers. This process also allows for only minimal control of spatial variations in the resulting microstructure of the cells. Finally, these fabrication techniques are not ideally suited for mass production due to the length and complexity of the multiple steps involved.

There is also much interest in lowering the material costs of SOFCs by lowering their operating temperature. This would allow for the use of cheaper metallic materials for the cell interconnects. In order to achieve lower temperature operation it is necessary to improve the performance (i.e. conductivity and reaction kinetics) of the ceramic electrolyte and electrodes. Improved reaction kinetics, and to some extent improved conductivity, can potentially be accomplished by exercising greater control over the microstructure and properties of the ceramic layers. This level of control is hard to achieve with traditional processing techniques and represents another barrier to commercialization. For example, grading the composition and microstructure of cell layers is one potential strategy that has been shown to improve cell performance and reliability. Unfortunately, current manufacturing steps are unable to produce layers with a graded composition without significant increases in processing time and complexity.

Plasma spraying has recently emerged as a manufacturing process with the potential to overcome many of the limitations of traditional processing routes. Plasma spray technology has been used for some time to deposit interconnect layers in tubular SOFCs. The process has also been applied to deposit the electrodes and electrolytes of tubular cells with varying degrees of success. Because of the potential advantages in performance of planar SOFCS, the remainder of this literature review will focus on research investigations related to this cell geometry.

1.2 The Plasma Spray Process

1.2.1 Overview

Plasma spray technology is a subset of thermal spraying. In addition to plasma, other thermal spray technologies include combustion and electric/wire-arc. The operating principle of all thermal spray techniques is the same: to heat and accelerate molten particles and deposit them on a surface. These technologies differ in the way this heating is accomplished. Thermal spraying is a well established technology and the process is well understood. Plasma spraying is generally the preferred technology for depositing ceramics due to the extremely high temperatures generated; values greater than 10,000 K are not uncommon. Plasma spraying can be used to spray virtually any ceramic with a stable liquid phase.

Plasma spraying uses an electric arc to heat and ionize gases, typically argon, helium, hydrogen and nitrogen, to produce an energetic plasma. The gasses are fed into the torch in varying amounts depending on the desired properties of the plasma. Particles of the material to be sprayed are fed into the hot plasma; they absorb heat and are accelerated towards the substrate at speeds of around 500 m/s. The two principal variations of plasma spraying are air plasma spraying and vacuum plasma spraying, where air and vacuum refer to the conditions under which the process is carried out. Air plasma spraying (APS) involves spraying in normal air at atmospheric pressure and vacuum plasma spraying (VPS) is carried out in an evacuated chamber (~0.1 atm). Vacuum spraying has been extensively used for producing experimental SOFCs. Ceramics have been sprayed for a variety of applications, typically protective coatings for thermal, corrosion and wear resistance. Ceramic coatings are usually sprayed from powder feedstocks which have been processed to control the agglomerate size of the powder. In conventional DC plasma spray torches the powder is injected radially into the hot gas zone [4]. Recently, an axial injection DC torch has been developed, which can be seen schematically in Figure 1 [5]. Axially injected powders tend to have more uniform thermal histories, which results in more uniform coatings and higher deposition efficiencies.

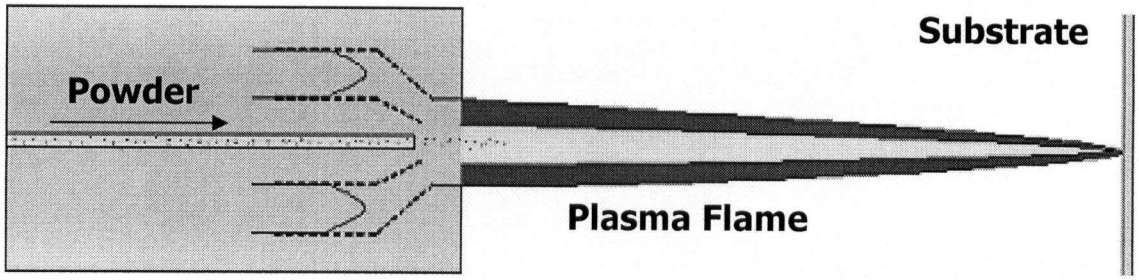

Figure 1: Axial injection air plasma spray torch schematic

Ceramics have also been successfully sprayed by feeding a sintered rod into the torch. This technique is more complex and is much more limited in the number of materials that can be used. Plasma spraying has also been carried out by spraying liquid feedstocks of ceramic precursor materials. These precursor materials react in flight to form the desired material, which is then collected or deposited directly onto a substrate. This technique has been used successfully to synthesize alumina, zirconia and yttria stabilized zirconia (YSZ) [6]. The coating deposition mechanisms for solution precursor plasma spraying have been found to be substantially different from traditional plasma spraying of ceramic powders [7]. Often, the coating material will be in a vapour state following synthesis. The coating will then be produced by the condensation of this vapour on a substrate in a vapour deposition process as opposed to liquid droplet deposition that occurs when depositing powders directly.

In this work we intend to take advantage of the relative simplicity and low cost of APS and the advantages of the axial injection torch design in the production of SOFC composite cathodes from powder feedstock.

1.2.2 Coating Production

Plasma sprayed coatings are produced through the build-up of individual molten particle impacts on the substrate. In flight, the molten particles for the most part retain the spherical shape of the powder fed into the torch, although some deformation does occur due to the aerodynamic forces encountered in flight. Upon impact, the tremendous kinetic energy of the particles causes them to deform into pancake shaped "splats". Depending on the initial particle size, velocity, viscosity, and wettability of the ceramic material, the individual splats can have thicknesses ranging from about 1 – 20 μm [8, 9]. These splats rapidly solidify; typical cooling rates are in excess of 10^6 K/s. The coating builds up as molten particles impact initially on the substrate and then on previously impacted and cooled splats. This process continues until the desired coating thickness has been achieved. For most thermal spray applications the desired coating thickness usually ranges from 20 μm up to about 1 mm. As a result of the high cooling rates, the deposited materials usually have a fine grained nano-crystalline or amorphous structure.

Since incoming particles generally impact on previously solidified particles, distinct boundaries usually remain between the splats. Other typical features of the resultant coating are porosity, both open and closed, micro cracks which form due to high thermal stresses during solidification, and the incorporation of unmelted particles which become trapped in the coating [9, 10]. These features all have an impact on the coating characteristics, and performance and can be either desirable or undesirable, depending on the intended application.

The nature of substrate used can have a significant effect on coating quality. The vast majority of ceramic coatings are used to enhance the performance (wear, thermal, chemical, etc.) of a metal surface. In some instances plasma spraying has been used to produce free-standing ceramic components; though careful control of the process parameters and the mould design are needed to achieve acceptable quality [11]. The substrate can affect coating parameters such as the structure of the initial splats, coating adhesion and lifetime. The adhesion between the coating and the substrate is a mechanical bond between the splats and the substrate surface. The rougher the substrate surface the better the adhesion of the coating generally is. Substrates are usually roughened by sand blasting or chemical etching prior to deposition of the coating. The roughness of the substrate can also affect the structure of the splats on the surface. A rougher substrate surface has been found both theoretically and experimentally to lead to thicker splats of smaller diameter and contribute to splashing of molten particles upon impact [8].

The quality of the adhesion can also be affected by the formation of oxides on the metal surface. This can particularly be a problem in high temperature environments where hot gases reach the substrate surface through porosity and micro cracks in the coating surface and oxidize the metal. These oxides not only weaken the underlying metal, but can weaken the mechanical bond between coating and substrate leading to coating spallation. This problem can be avoided through the deposition of a bond coat on the substrate surface prior to the deposition of the ceramic [12]. The bond coat will protect the underlying substrate, but thermally grown oxides generated by oxidation of the bond coat will also eventually lead to coating spallation. This scenario is most often encountered when dealing with plasma sprayed thermal barrier coatings (TBCs). The excessive oxidation of metal substrates (cell interconnects) in SOFC systems would lead to a degradation of the cell's electrical performance; operating conditions would therefore be selected to avoid this occurrence.

1.2.3 Plasma Spray Process Parameter Identification, Characterization and Stability

There are a number of plasma spray input parameters that are generally acknowledged to have a significant effect on the quality of coatings produced. A list of these parameters can be

seen in Table 1. These input parameters will have a direct influence on resulting process parameters that can be measured. These process parameters include torch voltage, plasma enthalpy, particle velocity, deposition efficiency, and coating quality (as defined by the coating parameters relevant to the particular application) [13-21]. The input parameters related to the torch can be set through the torch operation interface. Substrate temperature can be harder to control, as it is dependent on other input parameters such as current, plasma composition, standoff distance, and torch velocity. Control of substrate temperature can be exercised by using real-time monitoring of the temperature to provide feedback to control an active substrate cooling system. The effect of variations of the input process parameters has been extensively investigated both theoretically and experimentally in a number of studies. For many of the parameters, some effects of these variations are intuitive. For instance, the torch velocity will clearly impact the per pass thickness of the deposited coating; a faster moving torch will deposit less material and result in a thinner coating for a given number of passes. In general though, it can often be very difficult to quantitatively identify the consequences of changing just one of these parameters, as effects can be coupled to more than one parameter. Many studies have, however, attempted to analyze the effects of individually varying the input parameters described above.

Feedstock Parameters	Torch Operation Parameters	Torch Movement Parameters
• Particle Size	• Plasma Gas Flow Rate	• Torch Traverse Speed
• Carrier Gas Flow Rate	• Plasma Gas Composition	• Spray Angle
• Powder Mass Flow Rate	• Arc Current	• Standoff Distance
	• Substrate Temperature	

Table 1: Air plasma spray input parameters

In radial injection torches, the powder carrier gas (usually Argon) flow rate as well as the position of the injector will have a direct impact on particle velocity and trajectory, which will in turn affect the thermal conditions the particles encounter. The effect of varying these particle injection parameters has been investigated both theoretically [13] and experimentally [14,15,16]. The results of these investigations all show that for a particular set of plasma conditions, particle size, and powder composition, there is a carrier gas flow rate and injection location that yields the optimum particle trajectory, usually defined as maximum dwell time in the centre of the plasma jet. These studies all demonstrate that the principal effect of varying the carrier flow rate is the depth of injection of the powder into the plasma jet. One study has explored the impact of the carrier gas flow rate on plasma temperature for a new axial injection, plasma electrode type plasma spray gun [17]. It was found that increasing carrier gas flow rate had a cooling effect on the plasma jet. This plasma gun design is relatively unique, and this effect does not seem to be

significant in torches of other designs. Axial particle velocity is almost entirely dependent on momentum transfer from the plasma gas to the particles. The effect of powder particle size was also theoretically explored for radial injection geometry [13]. The results were what would intuitively be expected: larger particles tended to penetrate deeper into the plasma jet, accelerated more slowly, and maintained their velocity longer than did the smaller, lighter particles. This effect also leads to the in-situ particle size distribution differing significantly from that of the feedstock. Larger particles tend to be found in the area of the plasma jet furthest from the injection site while smaller particles are more common closer to the powder feed site [25]. Two studies have also explored the consequence of increasing powder feed rate [18,19]. Both found that increasing powder mass flow rates decreased particle temperature and velocity. These effects were caused by having the overall plasma energy, which remained unchanged, absorbed by more particles. Increasing powder feed rate also increases deposition rate, although the relationship may not be linear due to changes in deposition efficiency caused by the lower energy of individual particles.

The torch operation input parameters (torch current, plasma gas composition and flow rate) determine the plasma conditions. Electrode voltage and torch power are determined by the electrode current setting and the plasma gas composition. The energy content of the resulting plasma is directly related to the electrical energy consumed by the. Higher plasma energies generally translate into higher plasma temperatures and higher plasma jet velocities due to greater expansion of the gasses at higher temperatures. The highest temperatures and jet velocities are consistently predicted and observed to occur in the centre of the plasma jet [13, 14]. Plasmas for spraying are generally classified either as nitrogen based or argon based, depending on which gas makes up the majority of the plasma composition. Either hydrogen or helium is typically also present as a secondary plasma gas, usually accounting for no more than 20% by volume of the composition. Nitrogen based plasmas generally exhibit higher voltages and therefore higher plasma energy content than argon based ones. Increasing the proportion of either hydrogen or helium will also increase the voltage and plasma energy. The temperature of the plasma jet will determine the temperatures experienced by the powder particles [14, 15, 20]. Temperatures that are too high will vaporize the powder particles and prevent deposition; low temperatures could result in particles remaining unmelted and not adhering to the substrate upon impact. The degree of powder melting and/or decomposition is also related to particle size; particles that are too small for a given plasma are more likely to be vaporized, while particles that are too large will be more likely to remain solid or partially solid. The desired plasma temperature will of course depend on the material being sprayed as well as the desired application.

It has been consistently found that the highest deposition efficiencies occur when most of the particles are fully molten upon impacting the substrate [15, 20]. Molten particles will deform on impact, resulting in the splats that are the basis of sprayed coating microstructures. Unmelted particles can become entrapped in the coating by molten particles, which results in increased coating porosity. Particle velocity has also been found to have a significant effect on splat formation and coating quality [14, 15, 21]. As would be expected, higher particle velocities result in flatter splats. Higher velocities also tend to result in better coating adhesion and lower porosity due to greater compaction. These relationships have been verified both by theoretical models [8, 14, 15] and through characterization of deposited coatings [15, 18]. Control over jet and particle velocity can also be exercised by changing the torch nozzle size. Narrower nozzles constrict the gas flow and produce a faster moving plasma jet, which results in faster moving particles [15]. Supersonic nozzles have also been used for thermal spraying, but are typically found in high velocity combustion spraying and are rarely used for plasma based spraying [12].

The physical positioning and movement of the torch relative to the substrate during spraying also influence the final coating characteristics. As mentioned above, the torch velocity affects the per pass thickness of the deposited coating. The torch velocity also influences the local substrate temperature. A slow moving torch will linger over a region of the substrate longer and cause greater heating of the substrate in that location. As well, the torch standoff distance, the axial distance between the torch and substrate, will affect the substrate temperature. The substrate temperature is another important factor for splat formation, coating adhesion and residual thermal stresses. Spraying on cold substrates usually results in less symmetrical splat shapes due to splashing and lower deposition efficiency due to poorer splat adhesion [8, 15, 16]. This effect has been both observed and predicted. It has been found that there is a substrate transition temperature, below which splashing can be expected to occur for a particular combination of substrate and spray material [8]. For this reason the substrate is usually preheated to a few hundred degrees prior to deposition by passing the torch over its surface. Excessive substrate heating has the drawback of causing the formation of an oxide layer on the substrate surface which can degrade coating adhesion and must therefore be avoided [16]. Substrate temperature can be monitored and controlled during the plasma spray process through active cooling, typically with cool air jets aimed at the substrate. Torch standoff distance will have a more direct impact on the coating porosity and deposition efficiency through its effect on the thermal history of sprayed particles. Greater standoff distances have been found to lead to lower deposition efficiencies and higher coating porosities [13, 15, 18]. This trend is caused by an increasing number of cold, solid particles being present the further the torch is moved away from the substrate. These solid particles tend to either not adhere to the substrate or are entrapped and cause porosity. It has been shown that a compromise distance must be found that balances particle cooling and

substrate overheating effects [13, 18]. The angle of the torch with respect to the substrate will also influence the coating properties. Spraying at off normal angles has been found both experimentally and theoretically to decrease the thickness of individual splats and the resulting coating, decrease splat adhesion, and increase porosity. It has been recommended that 45° is the minimum spray angle that can be used to produce quality coatings [14].

Clearly, it is important to be able to monitor the process parameters resulting from controllable process variable settings. In particular, in-situ monitoring of particle temperature, velocity and size distribution as well as monitoring of the plasma conditions can provide real time information for diagnostic and control purposes. These measurements can be correlated with coating quality indicators such as porosity and deposition efficiency, which can only be evaluated after spraying. Thus, it becomes possible to monitor the quality of a coating during deposition and make adjustments to the process input parameters as needed. In-situ measurement also allows for monitoring of the plasma spray equipment's long term stability with regards to mechanical degradation. The measurement techniques described in the following paragraph have been used extensively for real time monitoring.

In-flight particle analysis must be done through remote optical sensing techniques because of the extremely high temperatures in the plasma jet. Two separate experimental setups have been utilized to perform these measurements. The first uses Laser Doppler Velocimetry, based on the Doppler shift of reflected light from a moving particle, to determine in-flight particle velocity [22]. A method known as phase Doppler anemometry has been used to evaluate the size of in-flight particles based on the characteristics of scattered laser light. Particle size and velocity measurements can be carried out with one piece of equipment call a phase Doppler particle anemometer. Particle temperature measurements are made by radiation emission thermometry using a two colour pyrometer. Two colour pyrometers can also be used to determine the temperature of the surface of a coating during deposition. Two colour pyrometers are used because they rely on the ratio between a long and short wavelength intensity, which remains unchanged in the presence of dust or anything else obscuring the image. Single wavelength pyrometers would measure any drop in intensity due to opaqueness as a drop in temperature. Thus, in an environment, such as a plasma spray booth, where the presence of powder is expected, the data from a two colour pyrometer will likely be more reliable. Two colour pyrometers also do not normally require knowledge of the emissivity of the body being imaged and are less sensitive to any changes in emissivity that may occur over the course of an experiment. One such instrument was developed to measure the temperature in real time of the surface of a steel billet sprayed onto a ceramic substrate [23]. The instrument used was based on a high resolution (32,000 pixels) charge coupling device camera and was sensitive enough to

detect temperatures as low as 200°C. For this particular camera material (InGaAs) the long and short wavelengths were positioned at the long wavelength end of the camera's response range (0.9 to 1.7μm). This provided for maximum sensitivity at low temperatures near 200°C. This camera has now been successfully integrated into a manufacturing process under development for the fabrication of tools for the automotive industry.

Another experimental setup alternatively used an optical sensor head to image in-flight particles as they pass the sensor's field of view [24, 25]. By analyzing flight time and radiation intensity, both relative and absolute, it is possible to obtain estimates of particle velocity, temperature and size. Both setups seem to yield reliable results; however, no study has been found that compares the accuracy and precision of the two methods. Using these measurement techniques it has been possible to obtain a full set of experimental data for particle velocity, size and temperature within the plasma jet. This detailed information can be used for: adjusting plasma spray settings to produce optimized coatings, comparison to theoretical models of particles in plasma jets, and for providing input data for coating production models.

Over time, the extremely high voltages and currents involved in the generation of the plasma jet results in the gradual erosion of the electrode material. This erosion causes changes in the torch power over time, even if all spray input parameters remain constant. A change in torch power will influence the velocity and temperature of the in-flight particles and will have an impact on the coating quality. Without good data on the degradation rate and amount it would be very hard to produce coatings with reproducible characteristics. Through the use of the in-flight particle measurements for size, temperature and velocity previously described, as well as data obtained from the torch control system on electrode voltage, power, and plasma enthalpy, it is possible to monitor electrode degradation and to compensate to ensure consistent coating quality. Data from a study of the long term stability of a plasma torch indicates that, over time, the plasma torch loses power [24, 25]. This drop in torch power corresponds to a decline in the value of electrode voltage, plasma jet enthalpy, particle temperature and velocity. A relationship was also discovered between the change of particle temperature and the final porosity of the coating [24]. Changes were also found to occur in the cross sectional distribution of in-flight particle temperature, velocity and size distributions [25]. From these investigations it is clear that the degradation rate of the torch does not occur at a constant rate. However, it was determined that, for the torch examined, the monitored torch parameters remained nearly stable for over the first 12 hours of operation [24]. Thus, by replacing the electrodes regularly, it should be possible to avoid most of the unpredictable effects of torch degradation on coating quality. The above trends have been observed for a radial injection torch. It has been predicted by a manufacturer that the

trend for axial injection torches will be the opposite: a gradual increase in torch power over time [26]. No long term studies have, however, been found that investigate this effect.

All of the studies examined dealt exclusively with the effects of the various system parameters in radial injection torches. Nevertheless, there is sufficient similarity between radial and axial systems to conclude that the same parameters should be considered in this work. The parameters chosen to be examined for their effects on coating quality were: powder feedstock size, powder feed rate, carrier gas flow rate, plasma gas flow rate, plasma gas composition, arc current, nozzle diameter, and standoff distance. As monitoring of in-flight particle characteristics (e.g. temperature, velocity, diameter) requires specialized equipment not presently available for use in this project, these will not be monitored.

1.3 SOFC Cathodes

1.3.1 Cathode Function and Materials

The cathode (also referred to as the air electrode) is one of three electrochemically active layers in a SOFC; the other two being the anode and the electrolyte. The primary function of the cathode is to reduce oxygen according to the following reaction:

$$\frac{1}{2} O_2 \text{ (gas)} + 2e^- \rightarrow O^{2-} \text{ (electrolyte)}$$

The oxygen reduction reaction will normally occur at so called triple phase boundaries (TPBs) where ionically conducting, electronically conducting, and gas phases all come into contact with one another. If mixed electronic and ionic conducting (MIEC) materials are used, then reactions will take place wherever the MIEC material contacts the gas phase. The effective performance of this function introduces a number of necessary material requirements [27, 28]. First, the cathode material must be electronically and, preferably, ionically conductive. This allows electrons and ions to reach the triple phase boundaries and provides conduction paths to complete the cell circuit. The cathode must also be permeable in order to allow the oxidant to reach the ionically and electronically conducting phase boundaries. The cathode must be sufficiently catalytic to limit the activation polarization of the reduction reaction. The cathode material must also be stable in high temperature, oxidizing environments to prevent corrosion of the cathode layer during operation. As well, the material should not undergo any phase changes within the operating temperature range, from room temperature up to about 1000°C. Finally, the cathode material must be compatible both chemically and mechanically with the other cell layers which it contacts, the electrolyte and interconnect. Having chemical compatibility prevents the reaction of cell components to create undesired phases which may degrade cell performance. Mechanical compatibility is primarily achieved by ensuring that adjacent layers have similar TECs to prevent

high differential thermal expansions from occurring during fabrication and operation, leading to thermal stresses that could cause mechanical failure of the cell through cracking or de-lamination of the cell layers.

Due to the high operating temperatures involved, most metals are not suitable for use in the cathode because of the excessive oxidation that would occur. Those that would be suitable, noble metals such as platinum and palladium, are much too expensive. Accordingly, all SOFCs use mixed or electronically conducting ceramic oxides in the cathode [27, 28]. Rare-earth perovskite-type oxides in particular exhibit the electrical properties desired for use in cathodes. Materials such as lanthanum cobaltite and indium oxide have both been used for cathodes in the past but have been phased out in favour of lower cost materials. By far the most common cathode material presently used with YSZ electrolytes, and hence the focus of this project, is strontium doped lanthanum manganite ($La_{1-x}Sr_xMnO_3$ or LSM). Lanthanum manganite is a p-type perovskite and its electronic conductivity can therefore be increased through substitution of a lower valence ion onto either A or B sites. Strontium doping increases the Mn^{4+} content of the $LaMnO_3$ through substitution of La^{3+} by Sr^{2+} and is preferred to other dopants (e.g. calcium) because it possesses superior electrical conductivity in oxidizing environments [27, 28].

In addition to being electronically conductive, LSM also exhibits limited oxygen ion conductivity. LSM has a relatively high TEC of around $12x10^{-6}$ K^{-1} and does not form any reactive phases with YSZ at temperatures below 1250°C [27, 28]. The performance of the cathode, and consequently the entire cell, is very much dependent on the inherent material properties as well as the fabrication and assembly techniques applied in the manufacture of the cell. The relationship between cathode polarization losses and physical characteristics has been extensively explored and modeled, although there is rarely agreement in the literature. The extent of the disagreement led one investigator to remark: "the most important 'parameter' in determining the reaction rate (the area specific resistance) as well as the kinetic details is the name of the laboratory, which made the LSM cathode" [29]. It has been suggested that much of the irreproducibility arises from the incorporation of foreign impurities, notably silica phases which form at the cathode/electrolyte interface, during fabrication and testing of the cells.

1.3.2 Cathode Conductivity and the Oxygen Reduction Reaction

The identification and explanation of the various polarization mechanisms that lead to a lowering of cathode performance has been the focus of many studies. There are three polarization mechanisms which have been found to occur in SOFC cathodes: activation polarization, ohmic polarization, and mass transport polarization. Activation polarization is related to the amount of activation energy required to allow the oxygen reduction reaction (ORR) to

occur. The higher the cathode activity is, the faster the ORR will proceed and the higher the overall cell performance will be. Much effort has been expended in better understanding this mechanism, as the ORR has been identified as the rate limiting step in SOFCs [27,30]. Ohmic polarization is determined mostly by the resistance of the electrolyte, but also by the conductivity of the cathode, both electronic and ionic, and it affects the speed of charge transfer both in the cathode bulk and between the cathode and neighbouring cell components. Improving the conductivity of the cathode will lead to slightly lower ohmic polarization and an improvement in cell performance. The third cathode polarization mechanism is concentration polarization, which occurs due to mass transport limitations. At very high current densities a concentration gradient will develop near the electrode surface as, the reactants are consumed faster than they can diffuse to the reaction sites. This lower oxidant concentration near the reaction sites will cause a drop in cell voltage and a corresponding decline in cell performance. Concentration polarization is primarily a function of reactant pressure and cell geometry [31].

Activation and ohmic polarizations are directly related to electrochemical processes in the cell. The ORR can be broken down into a number of steps: adsorption, dissociation, diffusion and charge transfer [32]. Three different reaction paths have been identified for the ORR: the electrode surface path, the bulk path, and the electrolyte surface path. These three reaction paths are diagrammed in Figure 2. All of these reaction mechanisms have been found to occur simultaneously. The speed with which each of the mechanisms proceeds in LSM cathodes depends on external parameters such as temperature and O_2 partial pressure, material properties such as dopant level, microstructural properties such as porosity, and geometric properties such as cathode layer thickness. It has been indicated that, in general, surface processes dominate O_2 reduction [33], although this conclusion has been challenged [34]. Differing values of the above parameters will determine which of the reaction paths dominates [30]. A systematic study has been carried out using secondary-ion mass spectrometry to identify the reaction paths at various cathodic polarization overpotentials [35]. It was discovered that the reaction paths vary with changing overpotential. This knowledge can be used to design optimized cathode/electrolyte interfaces. Identification of the reaction polarization mechanisms is mainly done through AC electrochemical impedance spectroscopy (EIS) and conductivity measurements [27 -36].

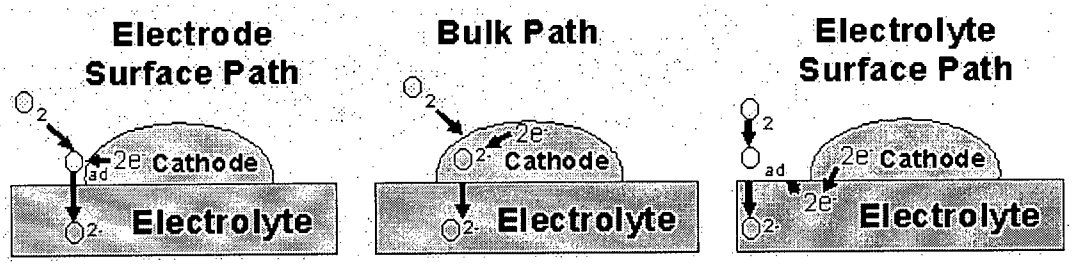

Figure 2: Cathode reaction paths (reproduced from information in [30])

The dependence of LSM cathode performance on the surrounding temperature and oxygen partial pressure (PO_2) has been extensively studied. Through conductivity and EIS measurements over a variety of temperature and PO_2 conditions, it has been shown that cathode conductivity is higher at higher temperatures and PO_2's [32, 37]. It is also possible to use EIS to examine the rate limiting steps of the ORR under changing operating conditions. As expected, oxygen diffusion became a rate limiting step at very low PO_2's; this corresponds to the concentration polarization discussed above. At higher PO_2's the rate limiting steps were found to be oxygen disassociation and adsorption [32]. It has been reported, however, that it can be very difficult to definitively identify particular reaction mechanisms from EIS measurements. It has also been shown that IS measurements can be extremely sensitive to slight variations in cell composition and construction, making it very difficult to obtain reproducible results [38].

Varying the amount of Sr dopant in LSM has been found to affect the properties of the cathode. As mentioned above, adding Sr significantly enhances the conductivity of $LaMnO_3$ through substitution of La^{+3} cations by Sr^{+2} cations. The higher the level of doping, the higher the conductivity and the lower the activation energy required up to a maximum. The fraction (x) of Sr which yields maximum conductivity is not, however, clearly established. It is most commonly reported to occur around x = 0.5, but values as low as x = 0.15 have been reported [27, 28]. However, increasing the dopant amount increases the TEC of LSM and has been found to decrease the stability of $LaMnO_3$ by raising the PO_2 at which disassociation occurs. Increasing the amount of Sr dopant will also raise the sintering temperature of the LSM [27]. Thus, it is necessary to pick a dopant level which strikes the best balance between maximizing the electrical performance of LSM while still providing good stability and thermal compatibility with neighbouring cell components. One study used EIS to study the effect of varying Sr content in LSM-YSZ composite cathodes on a YSZ electrolyte [39]. It was found that while cathode material properties and geometry had a strong influence, no clear relationship could initially be established between Sr content and impedance. The same measurements were performed again after a current had been passed through the cathode. From these measurements it was determined that the electrode with a LSM composition of $La_{0.85}Sr_{0.15}MnO_3$ had the lowest electrode resistance. However, the LSM composition most frequently used, and the composition used throughout this project, is $La_{0.8}Sr_{0.2}MnO_3$, suggesting that this composition provides an acceptable compromise between electrical properties and thermal compatibility.

1.3.3 Cathode Composition and Structure Modification

While LSM is technically a mixed conductor, its oxygen ion conductivity is not sufficient for good performance. To remedy this deficiency, SOFCs typically use a composite cathode with

LSM providing electronic conduction and YSZ providing oxygen ion conduction. The use of composite cathodes extends the TPBs from the cathode/electrolyte interface into the cathode bulk, greatly increasing the number of available reaction sites and lowering the polarization resistance of the cathode. LSM/YSZ composite cathodes have been compared to pure LSM cathodes using EIS [32]. It was found that composite cathodes had an additional impedance arc associated with the presence of LSM/YSZ phase boundaries. The other impedance arcs were found to occur at similar frequencies for both pure and composite cathodes, but with the composite cathodes having lower impedance. This indicates that the same rate-limiting reaction mechanism is present, but the composite cathodes have increased TPB length, which improves performance [32]. This study only examined a 50/50 vol. % mixture of LSM/YSZ and does not provide any information on the optimum cathode composition.

Another study also found a clear relationship between polarization resistance and TPB length [40]. This study similarly observed that TPB length was greatly increased in LSM/YSZ composite cathodes. EIS was also used in an experiment examining the effect of varying the volume fraction of YSZ in a composite cathode [37]. It was found that there is an optimum LSM volume fraction for which cathode polarization resistance is minimized. This minimum was detected at 42.5% LSM. It was suggested that at this volume fraction, the connectivity of both the electronic and ionic conducting phases is maximized, and that significant variation from this value results in decreasing connectivity for one or the other of the phases. It was also found that varying the composition from 30% to 100% LSM did not change the activation energy, indicating that the rate limiting mechanism was the same in all cases studied [37]. Other studies have, however, indicated that the use of composite cathodes does lower the activation polarization of the cathode [31, 32]. A separate experiment achieved similar results to those in [31, 32] when the LSM volume fraction was varied from 40% to 100% [41]. The only additional result obtained was a measurement of cathode-electrolyte interface resistance; this was found to be lowest at 40% LSM and increased with an increasing amount of LSM.

In addition to considering cathode composition, cathode microstructure has also been found to play an important role in determining cathode performance. Another strategy to increase the length of TPBs has been to increase the active electrochemical area at the interface between LSM and YSZ phases through modification of the electrolyte surface. Structured YSZ electrolytes were created by placing a layer of coarse YSZ particles on the electrolyte surface prior to the deposition of the LSM layer [42]. It was found that as the effective surface area of the interface was increased, polarization resistance dropped. With a 60% increase in effective surface area, a three-fold drop in polarization resistance was observed when operating at 950°C. SOFCs with structured interfaces were also found to show better performance in terms of voltage output and

power density compared to those with standard interfaces at all current densities above 0.2 A/cm^2. A separate study examined similar structures in a composite cathode resulting from the introduction of a coarse layer of YSZ particles at the cathode-electrolyte interface [36]. The addition of a layer of coarse YSZ was found to substantially reduce polarization resistance when the cell was operated at 750°C and 850°C; but little improvement was noted at 1000°C. The proposed explanation for this was a broadening of the electrochemically active zone of the cathode at higher temperatures which would greatly increase the TPB length and reduce the relative effect from the structured interface.

The effect of initial particle size of the LSM phase on cathode performance has been studied as well. The charge transfer resistance of three LSM cathodes prepared from powders with mean particle sizes of 1.54μm, 5.98μm and 11.31μm was evaluated over 100 hours of operation [43].The cathode with the largest starting particle size, 11.31μm, had significantly higher initial resistance, but this resistance remained relatively stable over the 100 hours of the test. It was found that the cathode with the smallest starting powder size, 1.54μm, gave the lowest initial charge transfer resistance. This was found to be due to the presence of larger numbers of active sites for oxygen reduction being present with the smaller particles. However, the performance of this cathode rapidly decayed and by 100 hours had a charge transfer resistance significantly higher than that of the other two cathodes. This degradation was caused by grain growth and sintering at the high operating temperatures, which was experienced to the greatest extent with the smallest particles. The cathode with the intermediate starting particle size had an initial resistance between that of the other two cathodes that remained relatively stable. Over the 100 hours of the test, the cathode with the intermediate starting particle size had the lowest overall charge transfer resistance.

The size of LSM grains in the cathode layer has also been found to affect cell performance by comparing coarse, fine, and mixed coarse/fine grained LSM in LSM/YSZ composite cathodes [44]. No information was provided concerning the preparation of LSM with differing grain sizes or the sizes of the grains investigated. It was found that the mixed grained cathode exhibited lower polarization resistance than both the coarse and fine grained cathodes. The fine grained LSM cathode was again found to be the worst performing. As was the case in the papers reviewed above, the composite LSM/YSZ cathodes were found to outperform pure LSM cathodes. The mixed grained cathodes were found to have much better adhesion to the electrolyte substrate and a greater number of cathode/electrolyte contact points. This improved interfacial contact led to an increase in the length of TPBs and a corresponding drop in polarization resistance. It was also reported that the active area of the cathode could be maximized through the use of a 1:1 YSZ/LSM volume ratio for cathode preparation. It was found that if levels of YSZ were too high

there would be an increased chance that zirconate (predominantly $La_2Zr_2O_7$) phases would form at the YSZ/LSM interfaces during sintering of the cell. A low level of strontium dopant in LSM also increases the likelihood that these reactive phases will form. $La_2Zr_2O_7$ is undesirable as it is highly non-conductive with a resistivity about 2.5 times higher that that of the surrounding YSZ phase [28]. Zirconates arise where Mn diffuses from the LSM into solid solution in the YSZ, leaving behind a chemically active La_2O_3 phase. The substitution of non-stoichiometric LSM ($(La_{0.8}Sr_{0.2})_{0.95}MnO_3$) has also been shown to prevent zirconate formation [33].

The thickness of the cathode layer has also been shown to affect cathode performance. The performance of composite cathodes of varying thickness at a number of different temperatures has been examined [36]. It was found that polarization resistance declined with increasing cathode thickness up to a thickness of 11μm, the largest value measured. The sensitivity of polarization resistance to changes in thickness was found to be much higher at the lower temperatures. The reasons for the decrease in resistance with increasing thickness were not stated explicitly, but it is likely to be related to an increase in the TPB length. The ideal thickness for the cathode layer was not explored, but it was indicated that a minimum in polarization resistance had been observed in other studies to occur at 25μm. It would be expected that cathode performance would be maximized when the thickness of the cathode is close to that of the electrochemically active region. Another study did not, however, find a correlation between cell thickness and cell overpotential [40]. It is possible that the inconsistency in the published results on this issue is due to the effect of other factors, such as porosity or material composition, overwhelming the effects of changing thickness.

The studies that have just been discussed all examined composite cathodes that possessed a uniform mixture of LSM/YSZ across the electrode thickness. Work has also been done that examines the potential benefits of grading the cathode composition. Graded cathodes will typically vary from pure YSZ near the electrolyte to pure LSM near the interconnect. One study examined the performance of graded cathodes and found a five fold reduction of polarization resistance in the graded cathode compared to constant composition LSM/YSZ cathodes [45]. The use of graded cathodes is thought to also improve the mechanical stability of the cell by reducing the thermal stresses arising from TEC mismatch of the pure materials used in the cathode. In graded cathodes the TEC mismatch between layers is very small and the thermal stresses are distributed throughout the cathode volume and therefore less intense. In conventional cathodes these stresses are concentrated at the interfaces between the cell layers. Graded cathodes also eliminate the distinct interfaces that give rise to interfacial electronic and ionic resistance. It was observed that the electrical conductivity of the cathode could be further

increased by introducing a graded layer comprised of LSM and interconnect material, $La_{0.84}Sr_{0.16}CoO_3$ (LSCo or LSC) next to the interconnect.

Most studies to date on graded cathodes have focused only on varying composition across the electrode layer. It is expected, however, that significant additional performance increases can be realized by also grading the grain size and porosity in the cathode; these effects were examined by one research group [46]. The desired structure would have a fine microstructure consisting of nano-scaled grains and pores near the electrolyte/cathode interface. The desired electrode composition and structure was achieved through the use of a combustion chemical vapour deposition process. The result is a very large surface area available for oxygen adsorption which enhances electrode activity. Away from the electrolyte, the microstructure is coarser, with larger grains and pores. This allows unhindered transport of oxygen through the cathode layer to the reaction sites. A cathode fabricated with a graded composition and microstructure was found to have a four fold reduction in interfacial resistance between the cathode and electrolyte layers compared to that of cathodes fabricated with only compositional grading.

Due to the significant advantages in performance, this project will focus on the fabrication of LSM/YSZ composite cathodes. Due to the fabrication technique being used however, there will be a limited ability to control some aspects of cathode composition and microstructure. Plasma spraying from powder feedstock generally requires special powder preparation (e.g. spray drying) which results in fairly broad particle size distributions (~1-100μm). Practical methods of separating the powders sizes, such as sieving, still result in fairly broad distributions and are of no use for particles less than ~25μm. While cathode composition can be controlled to some extent by adjusting the amount of each material in the initial feedstock, differences in the relative deposition efficiency of each material will make it difficult to achieve the exact desired compositions. Finally, grain size in the coating will for the most part be extremely fine due to the very rapid cooling experienced by the molten drops upon impact on the substrate; any grain structure introduced in the feedstock will only be preserved in partially molten particles that happen to be present in the coating. While plasma spraying is quite compatible with producing graded coatings, there are many additional complexities in the fabrication process as a result. So while graded cathode layers will be part of a future continuation of this work, they will not be part of the initial stages of this project which are presented here.

1.3.4 Cathode Fabrication

The performance of SOFC cathodes has been clearly shown to be sensitive to the composition and morphology of the starting materials used for fabrication and on operating conditions. An additional set of factors affecting cell performance arise from the cell fabrication

techniques employed. Traditionally, planar SOFCs are fabricated first by deposition of the ceramic materials followed by sintering of individual layers and co-sintering of multiple layers. The deposition method used has been found to influence the cathode quality [47]. The simplest method is wet powder spraying, in which cathode material powder is dispersed in a solvent and then sprayed on top of the electrolyte. The main problems with this technique are material loss due to over spray and the sensitivity of the final coating quality on drying conditions. Screen printing is currently the most widely used method for depositing cathode materials, as it eliminates the shortcomings of wet powder spraying. However, screen printing is a more complex route requiring specialized equipment and multiple processing steps.

After the cathode layer has been deposited, it is then usually co-sintered with the previously deposited anode and electrolyte layers. One of the principal problems arising during co-sintering is the development of bending stresses in the cell due to differential shrinkage rates of the various cell layers [47]. These stresses can lead to warping of the cell and cracking or delamination of the cell layers. In order to find the optimal conditions to co-fire a three layer cell (anode/electrolyte/cathode), the parameters in the sintering process have been systematically explored [48]. Shrinkage of the various layers during sintering was minimized to acceptable levels by reducing the amount of binder used in the powder slurries. Sintering temperature for co-firing was determined by the temperature required to produce a fully dense electrolyte layer. Unfortunately, it was found that this temperature lead to the porosity level in the cathode being too low. This problem was remedied by introducing carbon powder into the LSM slurry, which when burnt off, left behind a sufficiently porous cathode layer. Despite having sufficient porosity, the cathode microstructure was not optimized; this led to significant losses occurring in the cathode layer during cell operation. While a working cell was produced, this study clearly shows that considerable compromises need to be made when using the co-firing procedure. The conditions necessary to produce one cell layer with suitable properties may be far from optimal for the manufacture of the other cell layers. This provides some of the motivation to develop new manufacturing techniques not subject to this limitation.

The effect of the co-firing temperature on the interfacial resistance between an LSM cathode and YSZ electrolyte has also been examined [49]. It was found that interfacial resistance increased with an increase in co-firing temperature from 1350 to 1500°C. There was found to be a decrease in the TPB length which is believed to have occurred due to a modification of the surface composition of the electrode during firing. However, the decrease in TPB length was not sufficient to explain the increase in interfacial resistance. The additional increase was discovered to be caused by the formation of $La_2Zr_2O_7$ at the interface which inhibited the diffusion of adsorbed oxygen atoms. $La_2Zr_2O_7$ was found to occur in cells co-fired over the entire temperature

range examined, with the amount increasing with the co-firing temperature. From this result it is clear that co-firing should be conducted at the lowest temperature which still results in a sufficiently dense electrolyte layer. Excessively high co-firing temperatures are detrimental to both the mechanical stability and the electrical performance of the cell and must be avoided.

From these studies it can be seen that there is a large potential advantage to utilizing thermal spray or other deposition techniques that can eliminate the need for co-firing of the cell layers. One technique currently under development for cathode fabrication is flame assist vapour deposition, a variation of chemical vapour deposition also known by the term combustion chemical vapour deposition [50]. In this deposition technique the LSM is synthesized in-flight from a solution of precursor chemicals. The deposition temperature (substrate temperature) was found to be influenced both by the ethanol/water ratio in the solution and by the flow rate of the atomizing air. It was noticed that a fairly high deposition temperature (~700°C) was necessary to produce LSM in a crystalline phase. A high precursor solution flow rate was found to leave some of the precursors unreacted in the flame zone. The precursors did continue to react at the substrate, but the resulting coating had an unacceptably high density. The concentration of the precursor solution was found to influence the particle size in the produced coating. Standoff distances that were too low were found to result in a dense coating damaged by thermal shock effects, while very large standoff distances resulted in a coating with poor adhesion to the substrate. In this study all of the parameters were considered individually. It is possible that a superior coating could be produced through application of a factorial design technique to simultaneously optimize all parameters. Some of the results of this experiment could potentially be applied to other thermal deposition techniques (e.g. plasma spray) in which the coating material can be synthesized in-situ from precursor chemicals.

Plasma spray is another deposition technique under examination for depositing SOFC layers as it too would eliminate many of the problems associated with the traditional wet powder/sintering route. The application of PS to SOFC fabrication is discussed at length in Section 1.4.

1.3.5 Modeling and Reduced Temperature SOFCs

An area of particular interest in SOFC research is the development of reduced temperature SOFCs that would operate at temperatures below 800°C, rather than above 1000°C as is the case now for most tubular and many planar SOFCs. Lower temperature operation would allow for the use of cheaper, metallic interconnects between cells, in place of the expensive perovskite ceramics currently used. Operating at lower temperatures would also reduce the degradation arising from thermal stresses, sintering in operation and the formation of non-conductive phases.

Standard planar SOFCs are not suitable for operation at these lower temperatures because cell performance would be unacceptably poor. There are two primary routes to the development of reduced temperature SOFCs: the optimizing of the geometry and microstructure of cells in order to reduce losses, and the development of new materials which exhibit higher conductivity and catalytic activity at lower temperatures than traditional materials.

Theoretical calculations are frequently used to determine the maximum possible performance that can be obtained from a particular electrode material or set of operating conditions. Theoretical models are also developed to examine the effects of various parameters on cathode performance; the data can then be used to optimize those parameters. In general, there are so many factors affecting cell performance that modeling is often the only way to gain insight into the effects of individual parameters. One article examined the development of cell performance models with varying levels of complexity [30]. At the most simplistic level, cathode performance is a function of cathode layer thickness, cathode reaction rate and ionic conductivity. Models with increasing complexity bring in considerations such as the electrode particles and inhomogeneities in local current distributions. It was found that in order to achieve a fast bulk path it is important to enhance oxygen surface exchange. It was also shown that in order to achieve low polarization resistance it is necessary to either have a porous, electronically conductive, single phase cathode with high surface area or a composite cathode layer.

Models are often developed to examine a specific aspect of cell performance. For example, a model was developed to examine the relationship between TPB length and overpotential in a pure LSM electrode [40]. The data obtained from this model correspond well to experimental data and show several interesting features. First, there is a threshold value for the TPB length, below which the overpotential increases dramatically. It was also found that the surface oxide ion concentration decreases with a decreasing length of the TPBs. Correspondingly, the limiting current was found to increase with increasing TPB length. In addition, it can be seen that the decrease in overpotential rapidly levels off as the TPB length increases. Thus, the excessive lengthening of the TPBs is not a viable strategy to reduce electrode overpotential beyond a certain level. Equations have also been developed to model the dependence of activation polarization on multiple parameters relating to the electrode structure [31]. Activation polarization is found to be dependent on parameters such as electrode thickness, grain size, porosity and ionic conductivity. It was shown that for a porous LSM/YSZ cathode with a YSZ grain size of 5μm, electrode activity will increase significantly with increasing thickness up to around 100μm, after which the effects of increasing thickness become negligible. The results of the developed model corresponded very well with values obtained from experiments. It was expected that overall cell performance would also peak with a composite cathode thickness near 100μm. The experiments

performed found this not to be the case, as the investigators were unable to produce a cathode of this thickness that was free of cracks and with sufficient porosity. A similar conclusion on the effect of cathode thickness was reached based on the model developed in [30]. It was found that for a very porous, mixed conducting cathode there was a thickness beyond which no reductions in polarization would be observed; although a typical value for the maximum thickness was not presented. This thickness was found to be a function of the ionic conductivity of the cathode and the ease with which the ORR proceeds at the cathode. It was also shown that the use of composite electrodes, rather than pure LSM ones, can easily lead to an order of magnitude increase in the rate of charge transfer and hence activity of the air electrode [31].

Another study looked specifically at developing equations to determine the DC polarization behaviour of a cell from EIS measurements [51]. EIS measurements are more reproducible than straightforward polarization measurements and it is thought that use of this technique would yield more reliable and reproducible polarization data. The study was successful in accurately determining both the exchange current density as well as the cathodic limiting current density from EIS measurements. The investigators then went on to establish the PO_2 and temperature dependence of these values, again using only EIS measurements. It was also determined that the limiting process in the cathode was the diffusion of adsorbed oxygen on the electrode surface.

The above models were all constructed using analytical relationships. More complex models have, however, taken advantage of numerical techniques to model the complex phenomena within electrode layers. One such study used finite element methods (FEM) to model the polarization resistance arising in a three dimensional interface between the electrode and electrolyte during operation at 850°C [42]. The values for electronic and ionic conductivity used in the model were determined from experimental measurements. The structure of the model was based on SEM micrographs of the cathode/electrolyte interface of a prepared cell. The number of the YSZ particles at the interface was gradually increased to enlarge the surface area of the interface by up to 50% compared to an interface with no YSZ particles. The calculated polarization resistance values arising from the FEM model corresponded very closely to those observed in experiments performed on the prepared cells. It is therefore possible to build "virtual" cells to evaluate new cell structures. The principal advantage to these computational models is the ability to conduct many experiments very rapidly and without complex fuel cell test stands on carefully controlled structures within an SOFC.

Many models have been constructed to explicitly examine and optimize parameters related to reduced temperature operation. One such study used calculations to evaluate the ohmic drop, overpotential and current density in a thin, mixed conducting cathode layer at a reduced operating

temperature (700°C) [52]. It was determined that low ohmic losses, small overpotentials and very high current densities are achievable with existing mixed conducting electrode materials. Calculations, however, only included "typical" values for the various material properties used and reference was not made to particular MIEC materials. This study particularly focuses on true mixed conducting materials in which the limiting reaction mechanism is diffusion of oxide ions through the electrode materials.

Another model was developed to examine the polarization resistance at various temperatures and the potential for improving the electrode structure [36]. It was noted that the observed polarization resistances during operation at 850°C and 700°C did not correspond to the values predicted by the model. Based on this finding, it was concluded that the limiting factor contributing to electrode polarization resistance was something other than ionic conductivity, possibly a lack of electron or gas percolation throughout the entire structure. A calculation was also performed to determine the polarization resistance of an ideal LSM/YSZ composite cathode layer. The value obtained was an order of magnitude lower than that of the best existing composite cathodes. This result suggests that significant performance improvements might be obtainable from currently used materials which could potentially allow for lower operating temperatures.

Electrode models are frequently based on the assumption that TPB interface charge transfer processes are the dominate contribution to area specific resistance (ASR). There are some studies that suggest that the polarization losses in mixed conducting electrodes arise instead from generation and transport of oxide ions within the porous cathode structure [53]. By comparing values obtained from a model based on oxide ion generation and transport to experimental data, it was discovered that the oxygen surface exchange coefficient of the YSZ was much too low for the area specific resistance values that were observed. It was suggested that there were other processes which increase the transfer of oxide ions into ionically conducting phases. The increase was theorized to be predominately due to a contribution from the electronically conducting phase (LSM), the mechanism of which was not identified. The presence of redox cations such as Tb^{4+}/Tb^{3+} in the surface region of the cathode was also found to enhance oxide ion transfer by increasing the rate of oxygen surface exchange. However, to enhance this rate notably, 10-30 mol% of these cations must be added; this significantly lowers the oxygen ion conductivity in the ionically conductive phase and is therefore not a viable option for improving performance. Oxide ion transfer was also thought to be enhanced through the addition of a noble metal catalyst as they promote the dissociation of oxygen into charged species; no evidence of this effect was, however, observed in this experiment.

Some groups have taken the pursuit of optimized cathodes beyond the modeling stage and have attempted to prepare optimized cathode layers using conventional materials. One study examined the performance of a cathode with a double layer structure at reduced temperatures [54]. A thin LSM/YSZ composite layer was introduced between a 45μm YSZ electrolyte and a pure LSM cathode in an anode supported cell. Maximum power densities of 0.90, 0.52, 0.26, and 0.14 W/cm^2 were obtained at 800, 750, 700, and 650°C respectively. As the operating temperature was decreased the current density at which the peak power occurred also decreased, the value being about 2.75 A/cm^2 at 800°C and approximately 0.25 A/cm^2 at 650°C. The H_2 fuel flow rate was held constant in all trials at 250 ml/min, which translates into a fuel utilization of approximately 16% at 2.75 A/cm^2 and 1.5% at 0.25 A/cm^2. A high air flow rate of 500 ml/min was also provided to the cell. It was also discovered that the rate of air flow significantly affected the peak power density of the cell; higher airflows greatly improved performance at large current densities. This investigation was also able to relate the polarization characteristics of the cell to the results of impedance testing. It is suggested, much as in [50], that impedance testing could be used to provide much of the information that is usually obtained from direct polarization measurements.

Another group fabricated an optimized cathode using a wet spray technique to deposit a 20μm thick YSZ electrolyte and a 5μm LSM cathode on a conventional NiO/YSZ anode [55]. Cell testing was performed at 850°C using both pure H_2 and CH_4 as fuel. The H_2 fed cell achieved a peak power density of 0.12 W/cm^2 and an open circuit voltage of 0.9 V, results which were deemed promising. The methane fed cell performed much more poorly due to the slow kinetics of methane oxidation. Suggestions for further improvement included optimization of the anode and improvement of the cathode/electrolyte interface in order to slow degradation. Another group pursued a similar strategy, fabricating an anode supported cell with a 4-10μm YSZ electrolyte layer and a LSM cathode whose thickness was not reported [56]. This study succeeded in obtaining an extremely high power density (1.934 W/cm^2), current density (nearly 6 A/cm^2) and open circuit voltage (1.1V) at an operating temperature of 800°C. Air supplied to the cell during this test was provided by ambient airflow. Unfortunately, no information on fuel flow or utilization rates was provided. However, it seems likely that fuel utilization rate is relatively low as no significant mass transport effects were observed during the test. Nevertheless the results of this study show that the thickness of the electrolyte is of critical importance when operating at reduced temperatures with conventional materials. Compared to the results presented here from [54], the cell in [56] has significantly better performance. The main difference between these cells appears to be the thicknesses of the electrolytes, as fabrication techniques, composition and the structure of other components as well as test conditions are similar. These results also help to confirm what was suggested by theoretical models, namely that conventional SOFC materials

can provide excellent performance at reduced temperatures if cell layers are adequately optimized. It would be expected that even better performance could be obtained through the use of optimized cathode and anode layers in conjunction with a very thin electrolyte.

The other main route to achieving reduced temperature operation is through the use of new materials which exhibit better ionic and electronic conductivity at lower temperatures. One new ceramic material with high electrical conductivity and close thermal matching to YSZ that has been explored for use in SOFC cathodes is $LaNi_{0.6}Fe_{0.4}O_3$ [57]. It was discovered, however, that when co-fired with a YSZ electrolyte at temperatures above 1300°C, a dense, insulating layer of $La_2Zr_2O_7$ was formed between the cathode and the electrolyte that prevented operation. This demonstrates the importance of evaluating the chemical compatibility of materials with promising electrochemical properties. Another such project examined the performance of a composite graded cathode using GDC rather than YSZ as an ionic conductor [58]. The performance of both half cells and full cells was compared to conventional cells fabricated with LSM/YSZ graded composite cathodes. EIS testing of the half cells showed that the LSM/GDC cathode had significantly lower polarization resistance than the conventional cathode at 700°C. While little difference in performance of the complete cells was noted at operating temperatures above 950°C, the cathode fabricated with GDC showed notably higher performance when operated at 750°C. The improvement was found to occur primarily in the activation region of the cell polarization curve.

GDC has also been identified as a suitable ionic conductor for use at temperatures as low as 500°C, although no suitable electronic conductor has as of yet been identified for use at this temperature [53]. As previously mentioned, GDC has also been incorporated into cathodes which have been graded for composition and microstructure [46]. The following power densities were recorded for this cell: 0.551 W/cm^2 at 850°C, 0.481 W/cm^2 at 800°C, 0.319 W/cm^2 at 700°C, and 0.138 W/cm^2 at 600°C. The test was conducted with ambient air as an oxidant. Again, no information on fuel utilization was reported, but from the polarization curve it is apparent that fuel utilization was low as no significant mass transport effects were observed over the range of current densities examined. These power densities were achieved despite the presence of a relatively thick YSZ electrolyte (240μm). If one were to replace this electrolyte with a thin layered one, such as fabricated in [56], it would be expected that the reduced temperature performance of the cell could be further improved.

Lanthanum strontium cobalt iron oxide (LSCF) is a candidate material for replacing LSM in cathodes for reduced temperature operation. Unlike LSM, LSCF is a true mixed ionic electronic conductor. As such, it would be expected to exhibit increased electrochemical activity as the

TPBs would be effectively extended throughout all surfaces with open porosity within the bulk of the electrode, rather than being limited to physical interfaces between ionically and electronically conducting phases. LSCF is not suitable for use with YSZ electrolytes due to the formation of non-conducting phases. One study looked at both electrolyte supported and anode supported cells which used LSCF/SDC (samaria doped ceria) composite cathodes [59]. The electrolyte supported cell used lanthanum strontium gallium manganite (LSGM) as the electrolyte and included SDC interlayers between the electrodes and the electrolyte in order to prevent interdiffusion between these layers. This cell structure was found to be very stable over 1000 hours of operation. In particular, the bi-layered electrode structures were found to be resistant to chromium contamination (the mechanisms of which are discussed below). The cells were tested at temperatures ranging from 650 to 800°C. Peak power densities were reported to range from 0.29W/cm^2 at 650°C to 0.67 W/cm^2 at 800°C. The anode supported cells in this study used a thin YSZ electrolyte and a LSCF/SDC composite cathode with a SDC interlayer. Similar performance to the electrolyte supported cell was obtained with a peak power density of 0.648 W/cm^2 at 800°C. No fuel utilization information was provided for tests of either of these cells; it again appears to be significantly low so as not to limit the performance of the cell. When current density was held constant and fuel flow reduced, the anode supported cell did show excessive concentration polarization at high fuel utilization levels, (>80%) due to slow diffusion of reactants and products through the thick anode layer.

Another study examined the performance of a cell with a Ni/GDC cermet anode, 100μm GDC electrolyte and a LSCF/GDC composite cathode at temperatures between 500 and 700°C [60]. Silver particles were distributed on the cathode surface and were thought to improve the rate of oxygen adsorption. While the anode was found to have adequate performance at 500°C, it was found that refinement of the cathode structure is necessary before operating temperatures this low can be realized. Use of a functionally graded cathode structure would be one possibility for achieving this. The entire cell did however show good performance at 700°C, yielding a peak power density of 0.67 W/cm^2. As measurements of performance were calculated from EIS measurements performed at open circuit conditions, the effects of fuel utilization were not considered. The improvement over the 0.46 W/cm^2 reported in [59] at 700°C is most likely due to the use of GDC rather than YSZ as the electrolyte material. Note that this improvement was achieved in spite of the fact that the GDC electrolyte was more than three times thicker than the YSZ electrolyte in the previous study. The effect of adding GDC to the MIEC LSCF has been examined in greater detail [61]. EIS testing between 550°C and 700°C indicated that 50 wt% GDC was the optimal fraction to combine with LSCF in the cathode over this temperature range. This combination produced an order of magnitude reduction in interfacial polarization resistance between the electrolyte and cathode layers compared to a pure LSCF cathode. The explanation

for this performance improvement was that the addition of a highly ionically conducting material (i.e. GDC) expanded the electrochemically active area of the cathode further from the electrolyte interface. It was suggested that this cell would be able to perform effectively down to temperatures of 600°C. It should be noted that one drawback to the use of these materials was noted. It was discovered that these cathode materials require relatively low temperature sintering (~900°C) and the cell must therefore be processed in such a way that no high temperature sintering steps follow the cathode sintering step. This requirement, however, was not reported to have caused any difficulty in this or any of the other studies examined that made use of these cathode materials.

One of the foremost motivations for reducing the operating temperature of SOFCs is to allow the use of oxidation resistant metallic materials, rather than expensive ceramics, to provide an electrical connection between cells in a stack. The primary requirements of the interconnect are as follows: it must be dense and impermeable to any reactant gasses, it must be chemically and thermally compatible with both anode and cathode materials, it must be stable in both oxidizing and reducing environments and it must be have adequate electrical conductivity without ionic conductivity [27, 28]. In high temperature SOFCs, rapid oxidation would quickly degrade metallic materials used in the cell. The only materials suitable for use as interconnects in this harsh environment are electrically conducting perovskite ceramics, such as lanthanum chromate, which are typically very expensive and difficult to manufacture. By reducing operating temperatures, the rates of oxidation can be reduced sufficiently to allow cheaper, easy to form metallic materials to remain stable in the operating environment. The metals usually considered for use are chromium containing alloys which preferentially form protective chromium oxide layers. The growth rate and electrical properties of this chromium oxide layer have been examined both in unmodified and mixed conducting ceramic coated alloys [62]. As would be expected, it was found that mixed conducting ceramics did not inhibit growth of an oxide layer, and in the case of the LSCo coated interconnect the growth rate of the oxide layer was four times faster than on the uncoated interconnect. The conclusion was that pure electronic conducting ceramics must be used to coat metallic interconnects. Pre-oxidation of the interconnect alloys was also found to be an effective means for limiting the growth of an oxide layer during operation.

Chromium contamination of the cathode is another major issue arising from the use of metallic interconnects. During operation at elevated temperatures the Cr species will evaporate from the alloy and migrate into the cathode, where it deposits at the cathode/electrolyte interface and interferes with the oxygen reduction reaction. One study endeavoured to quantify the degradation due to this process in a LSM cathode over a period of extended operation [63]. It was found that Cr contamination caused a large, rapid increase in cell overpotential after just a few

hours of operation. Using EIS measurements, an initial decrease followed by an increase was observed in the cell polarization resistance. The increase in overpotential was found to be caused by an increase in charge transfer and diffusion resistance as ohmic resistance remained relatively stable. It was again suggested that protective ceramic coatings on alloy interconnects would be useful for preventing Cr evaporation and the subsequent contamination of the cathode, in addition to protecting the alloy from excessive oxidation. A similar study was performed examining the extent of Cr degradation in LSM and LSCF cathodes at 900°C [64]. As expected, it was found that the presence of a Cr alloy interconnect caused a rapid degradation in cell performance, measured as a decrease in electrode potential. However, the decrease in potential was much larger in the LSM cathode than in the LSCF cathode. The degradation was attributed to Cr deposition at the electrolyte/cathode interface which obstructed adsorption and diffusion processes on the electrode surface. In the LSM electrode it was found that the evaporated Cr was combining with Mn from the cathode and forming a spinel phase on the surface of the YSZ electrolyte at the LSM/YSZ interface. Cr_2O_3 phases were also detected on the electrode surface. In the LSCF only a small amount of Cr containing crystalline phase, randomly distributed, was noted on the electrode and SDC electrolyte surface. It was concluded that Mn is an effective nucleation agent for the deposition of Cr. The LSM electrode was found in general to be less tolerant to surface contamination due to the dominance of surface processes. The results of this study indicate that LSCF cathodes in reduced temperature SOFCs could allow for the use of uncoated metallic interconnects, achieving one of the primary goals of temperature reduction.

Theoretical modelling of cathodes confirms what has been observed experimentally, namely that substantial performance improvements can be realized through the use of a composite structure. From an inspection of the results of various efforts to achieve reduced temperature operation it appears that the thickness of the electrolyte, and to a lesser extent that of the cathode, are the most important factors to control. Cells with highly optimized structures using conventional materials (LSM and YSZ) in the electrolyte and cathode were able to achieve performance equal to or greater (as in [56]) than that obtained from cells utilizing new materials with higher conductivity, providing ample justification for their continued study. It would be expected that an optimized cell structure using these new materials would outperform those from the studies reported on in this review. It seems likely that use of the materials and cell structures described here will allow for the effective operation of SOFCs at temperatures below 700°C and a realization of the benefits of reduced temperature operation.

1.4 SOFC Fabrication by Plasma Spray

1.4.1 Plasma Spray Processing of SOFC Electrolytes

Studies carried out to examine the fabrication of SOFC electrolytes by plasma spraying have focussed on YSZ for high temperature SOFCs and LSGM for reduced temperature use. The primary difficulty in fabricating a good electrolyte by plasma spraying is that plasma sprayed ceramic coatings typically contain too much porosity and have extensive microcracking, which conflicts with the gas tightness requirement to prevent fuel crossover in the electrolyte layer. While this problem can and has been solved by producing a very thick electrolyte layer, this is generally undesirable as it greatly increases ohmic polarization in the cell. Thus, the primary focus of these studies is producing a dense, thin electrolyte by plasma spraying.

One study specifically examined the effect of powder preparation techniques on the properties of a VPS YSZ electrolyte [65]. Two YSZ powder morphologies were examined: agglomerated/sintered and fused/crushed. No information was provided on the exact preparation methods used for creating the two powders. While no particle size is given for either powder, from the micrographs of the powders it appears that both have an average particle size of approximately 30 μm. The agglomerated powder appears to have a morphology that is roughly spherical while the crushed powder appears to mostly consist of jagged particles. For the one set of plasma conditions examined in the study, it appeared from micrographs that the agglomerated and sintered powder produced a denser, more homogenous layer, although no porosity measurements were conducted.

The most common approach to producing a gas tight YSZ electrolyte involves the application of a post spray treatment to densify the plasma sprayed layer. A pair of studies examined the densification of YSZ electrolytes produced by APS for tubular SOFCs, which have electrolyte requirements similar to those of planar cells [66, 67]. In these studies, porous APS YSZ electrolyte layers were impregnated with solutions of yttria and zirconia nitrate and then subjected to elevated temperatures. This process was successful in achieving both reduced porosity and increased ionic conductivity. 150 μm thick YSZ layers were dipped in the nitrate solutions and then subjected to 500°C for 30 minutes. This process was repeated to gradually increase the density of the electrolyte. It was found that after 10 repetitions of impregnation with the nitrate solution and heating, the gas permeability for air had decreased from $2.9 \times 10^{-6} cm^4/gs$ in the as sprayed layer to $2.5 \times 10^{-7} cm^4/gs$, a level deemed acceptable for use in an operating SOFC and comparable to that typically found in VPS YSZ layers. It was also found that this post spray treatment increased the ionic conductivity by 30% over the as sprayed layer when measured

between 600 to 900°C. By increasing the number of treatments the performance can be further improved, but the effectiveness of these treatments decreases as the number of cycles is increased. In general it is desired to keep the number of cycles as low as possible as they add significantly to the processing time.

Another study looked at the effects of post spray heat treatment, electrolyte thickness and the addition of manganese oxide (MnO_2) on the gas permeability, microstructure and composition of an APS YSZ electrolyte deposited on a porous LSM cathode layer [68]. It was found that there was a sudden decrease in gas permeability of 60 μm layers as the sintering temperature was increased (sintering time was held constant at 3 hrs). This decrease occurred at ~1550°C in pure YSZ electrolytes and ~1400°C in electrolytes with a MnO_2 layer at the cathode/electrolyte interface. Furthermore, the presence of MnO_2 suppressed the formation of lanthanum zirconate, an undesirable reactive phase that forms due to diffusion of Mn from the LSM into the YSZ in solid solution. When 5 wt% MnO_2 was mixed with the YSZ powder it was again found that the formation of lanthanum zirconate was suppressed with the added benefit that no MnO_2 is observed after sintering, as was the case when MnO_2 is instead deposited in a layer at the interface. The dramatic decrease in permeability observed was attributed to the transformation of the open porosity and micro-cracks in the as-sprayed layer to spherical, closed porosity. It was also found that gas permeability decreased with increasing electrolyte thickness, as would be expected. Finally, it was also observed when the electrolyte thickness drops below 50 μm the permeability increases dramatically, most likely due to incomplete overlapping of the splats.

The use of spark plasma sintering (SPS) as a post spray heat treatment to rapidly densify YSZ has also been explored [69]. This study explored both sintering temperature (1200-1500°C) and the number of sintering cycles. Soak times in this study were 3 minutes, compared to 3 hours in the previous study using traditional furnace sintering methods. The density of the plasma sprayed samples was significantly increased with the heat treatment from 5.24 g/cm^3 in the as sprayed sample to 5.53, 5.71 and 5.89 g/cm^3 at 1200, 1400 and 1500°C respectively for 3 SPS cycles. By comparison, the theoretical maximum density of YSZ is 5.90 g/cm^3. Increasing the number of cycles was also found to increase the density; however the effect was less noticeable at higher temperatures. The resistivity of the YSZ was also decreased with increasing sintering temperature. It was found that after the SPS treatment the splat structure of the coating had been completely transformed to a granular structure as the result of active atomic diffusion between the YSZ grains. Multiple SPS cycles were better than a single extended cycle for improving the strength, hardness and thermal conductivity of the coating. As the study was carried out using freestanding discs of YSZ, no information is available on the formation of reactive phases, such as lanthanum zirconate, during the SPS procedure.

Plasma spraying has also been investigated for depositing electrolyte materials for reduced temperature operation, specifically LSGM [70, 71]. LSGM has important advantages over YSZ which make it better suited to processing by plasma spray techniques. First, LSGM has a much lower melting temperature (~1500°C) than YSZ (~2400°C), which allows for the deposition of higher density films containing fewer unmelted or partially melted particles at lower plasma energies. LSGM also has higher ionic conductivity which enables somewhat thicker deposits to be used without having as great an effect on the cell performance. It was found that as sprayed LSGM coatings exhibited an amorphous structure due to the high cooling rates involved during deposition. Post spray heat treatment was successful in restoring the crystal structure to that of the feedstock material. Crystallinity began to reappear after heat treatment at 500°C, with full crystallinity being restored after treatment at 700°C. However, the ionic conductivity was still much lower than a LSGM specimen prepared by sintering methods when measured at temperatures below 800°C. Results from this study seem to suggest that under some circumstances post spray heat treatment will be required for LSGM electrolyte layers and that it may be difficult to achieve good performance at reduced temperatures, below 800°C.

1.4.2 Plasma Spraying of SOFC Cathodes

The deposition of LSM for SOFC cathodes by plasma spraying has been extensively studied. One of the principal challenges in depositing LSM by PS is producing a coating with sufficient porosity and gas permeability. For good operation, more porosity is needed than is usually produced during plasma spraying, and, unlike the fuel electrode, one cannot rely on reduction to achieve the necessary level of porosity. An added challenge when fabricating composite cathodes is the desire to simultaneously deposit both YSZ and LSM.

One study examined the characteristics of an APS LSM layer after heat treatment [72]. One set of plasma torch parameters was used to deposit cathode layers from LSM powder with a particle size of about 100 μm onto YSZ substrates. Some of the layers were then subjected to post spray heat treatments at temperatures between 800 and 1000°C for 1 hour. The heat treatments were at low enough temperatures and duration to avoid the formation of undesired reactive phases. While both treated and untreated LSM were crystalline, the grain size in the treated specimen was larger, close to that of the raw powder. The electrical conductivity of the treated sample was found to be three orders of magnitude higher than that of the as sprayed LSM and was nearly identical to that of sintered and screen printed specimens. Increasing the heat treatment temperature reduced the cathodic overpotential. This was thought to be due to the slight reduction of the LSM during spraying which was re-oxidized during the heat treatment,

though there was no evidence of this degradation in the XRD analysis. It was also found that the LSM layer had porosity of about 35%, which is sufficient for good gas transport in the cathode.

Other research has been carried out examining the fabrication of LSM/YSZ composite cathodes using VPS techniques. One such study compared composite cathodes with different compositions and thicknesses to single phase LSM cathodes also prepared by VPS [73]. When the LSM and YSZ powders were fed separately the result was a layered structure. A more homogenous structure was achieved when the powders were premixed by dry tumbling. The powders were also mixed by fine wet grinding of sub-micron LSM and YSZ particles followed by slurry-drying using an atomisation process. In both cases the mixed powders were fed from a single hopper. EIS testing of the cathodes showed that separate feeding of the powders in a roughly 50/50 vol. % mixture resulted in the cathode with the lowest polarization resistance. This was attributed to an increase in electrode activity resulting from the large unsintered agglomerates and porosity present in the YSZ feed powder. It was expected that for similar levels of porosity, the cathode sprayed from premixed powders should out perform the cathode sprayed from separate hoppers due to the improved connectivity. This, however, does not yet appear to have been confirmed through testing. Mixtures with a higher LSM content, 70 vol. %, had a polarization resistance similar to that of a single phase cathode due to the lack of percolation of the YSZ phase.

A separate study by the same researchers examined the fabrication of functionally graded composite cathodes by VPS and flame spraying (FS) [74, 75]. In this study the performances of graded cathodes were compared to constant composition and two-layer composite cathodes also fabricated by VPS and FS. With EIS testing it was found that the two-layer and graded cathodes had significantly lower polarization resistance than those with a constant composition, with the two-layer cathode performing the best. It was concluded that more work needs to be done to optimize the composition of the graded cathode layer to fully realize the benefits of this structure. Interestingly, it was found that flame spraying can achieve a performance level comparable to that of vacuum plasma spraying at significantly lower cost.

Work has also been done which examines the use of pore forming material for increasing the porosity of APS planar cathodes [76]. Two separate pore forming techniques were explored; mixing carbon with LSM powder prior to spraying to act as a pore former, and the spraying of LSM ceramic precursors containing residual organic material followed by annealing. Three types of carbon were examined as pore formers; extremely fine carbon black powder, and hollow and solid carbospheres. In each case these techniques were applied to single phase LSM cathodes. All of the as-sprayed LSM coatings were heat treated at 1000°C to burn off residual carbon and

to achieve the perovskite crystal structure in the LSM necessary for electrical conduction. It was found during spraying that in order to ensure good feeding of the powders a fairly narrow particle size distribution was required. It was also observed that particles less than about 50μm in diameter produced coatings which were too dense, while particles larger than about 180μm produced coatings with poor adhesion as a result of incomplete melting. The optimum LSM particle size range for giving a porous, well adhered coating was between 90 and 180μm. The carbon black powder could not be mixed evenly with the LSM due to the large differences in particle size and, when sprayed, a layer of carbon on the coating surface resulted. Both types of carbospheres could be mixed well with the LSM. The solid carbospheres were found to give substantially higher porosity than the hollow ones. This was thought to occur because the solid carbon particles would persist longer, more effectively preventing a dense coating from forming before being burned away. With both types of carbospheres, it was found that no more than 20 wt% could be added to the LSM before the coatings would have a layer of carbon on the coating surface and a much higher density. The latter effect was attributed in part to the heat of combustion of the carbon. In all cases amorphous LSM resulted, requiring heat treatment to restore the perovskite structure. The highest porosity obtained was 40%, achieved with 15 wt% of solid carbospheres. The resulting pores in this coating had diameters mostly ranging between 60 and 140μm. Spraying of LSM precursors followed by annealing did not result in a coating with much porosity. It was suggested, however, that by combining the resin and carbosphere techniques, even higher porosity could be achieved. Finally, in these tests only one set of spray parameters was used, and by optimizing the torch parameters the authors believe that still higher porosity could be obtained.

Spray techniques, both spray pyrolysis by flame spraying and plasma spray synthesis, have also been used to synthesize cathode powder feedstocks and coatings from precursor compounds in order to reduce material costs. Spray pyrolysis by flame spraying tends to yield powdery, poorly adhered coatings. One study used this technique to fabricate nano-composite LSM/YSZ particles from La, Sr, and Mn nitrate precursors and YSZ sol [77]. Fine particles (~1μm) containing well dispersed YSZ and LSM phases were successfully created. Subsequent heat treatment of these particles increased the crystallinity, though the observed structural changes seemed to be dependent on the heating rate. It was concluded that more study was needed to fully understand the crystallization mechanisms in these particles. Other studies have instead focussed on developing coatings directly from precursors using plasma torches, yielding solid coatings in one step, but with much finer microstructural details than when spraying from coarse powder feedstocks. One project used a non-sintered, spray dried powder feedstock of precursors to fabricate spinel coatings [78]. Unsurprisingly, it was found that the plasma conditions and powder injection parameters heavily influenced the coating composition and structure. The

coatings consist of many thin layers created by agglomerate splats; unlike traditional feedstock materials however, the individual splats possessed a composite structure. The outer parts of the powder agglomerates were found to always melt and stick together, forming a cohesive coating. However, within the agglomerates, some of the precursors could remain un-reacted under some plasma conditions. These results would seem to suggest that small agglomerates and long residence times would be desirable for achieving good coatings with this technique. It is also unknown whether other types of ceramic coatings could be successfully created using this technique, particularly LSM and other perovskites that are highly susceptible to decomposition.

While LSM cathodes have been fabricated by APS, to date only single phase cathodes have been examined. However, previous composite LSM/YSZ cathodes work, particularly that using VPS, will provide some useful insights into how to achieve similar success by applying APS.

1.4.3 Plasma Spraying of Interconnect Coatings

As mentioned previously, the transport of chromium from chromia containing metallic or ceramic interconnects to the cathode/electrolyte interface can degrade cell performance over time. One strategy to counteract this is to use coatings on the interconnect materials to block the transport of chromium, either as a vapour or by solid state diffusion, to this interface. The materials for these coatings must have several characteristics: effective seal for chromium containing vapours, thermal and chemical compatibility with adjacent components (interconnect and electrodes), mechanical stability over time under SOFC operating conditions, resistance to solid state diffusion of chromium and high electrical conductivity to minimize ohmic losses [79]. Perovskite materials have been considered for use in this role. Recently several groups have begun to examine thermal spraying for the deposition of these protective layers.

One study evaluated different thermal spray methods (HVOF, VPS and APS), substrate chemistries (Cr-5Fe-1Y_2O_3, Ni-40Cr and Ni-20Cr), and coating compositions (LSM, LSC and $La_{0.7}Ca_{0.3}CrO_3$ (LCC)) for the deposition of protective interconnect layers [79]. The thermal spray process was optimized using fractional factorial design (see section 5) for the following spray parameters which were believed to influence the chemistry of the coatings: the amount of oxygen in the carrier gas (for HVOF), enthalpy, powder feed rate, spray distance, and sample preheat temperature. The coated interconnects were evaluated for chemical compatibility and conductivity. With each thermal spray method, decomposition of the perovskites was noted when deposition was done at high enthalpy. It was suspected that under high enthalpy conditions, the molten droplets developed a La_2O_3 skin. Over an extended period of time (many months), the La_2O_3 absorbed water from the air, resulting in the presence of significant quantities of $La(OH)_3$. The end result is that coatings that were initially dense and well adhered gradually turned into fine

powder which could be easily removed. It was found that decomposition of the perovskites could be avoided by reducing the enthalpy and powder dwell time and by using powders with larger particle sizes. In each case, the coating of the metallic substrates increased the oxidation rate. The LSC was found to be an inappropriate material as it allowed rapid diffusion of Cr through the protective layer and resulted in thick oxide scales that contributed to a high contact resistance. In general, the best combination of coating/substrate in terms of oxide growth rate and Cr diffusion was reported to be LSM/Cr-5Fe-1Y_2O_3. LSM was also found to give the lowest contact resistance of the three coating materials examined.

Other studies have also examined the deposition of LSC, LCC, and LSM protective coatings onto a structured Cr-5Fe-1Y_2O_3 interconnect by VPS [80, 81]. Torch power, powder injection angle, plasma gas flow rate, chamber pressure, powder feed rate, and spray distance were optimized for each material to achieve a dense protective layer. The decomposition of the powders could be limited by decreasing the torch power and increasing the jet velocity. However, too low torch power resulted in a coating that was not sufficiently dense and poorly adhered. Because of the presence of the gas channels and the need for surface roughness below 5μm, chemical etching was found to the best method for surface conditioning of the substrate (interconnect) prior to deposition of the coating. All of the coating materials were found to be successful in preventing the formation of reactive chromium containing phases in the cathode. It was discovered that interconnects having gas channels with vertical sides could not be uniformly coated with a dense coating using VPS. This problem was remedied by redesigning the gas channels with a semi-circular cross section and varying the torch angle during deposition. It was also found that coating full sized (260mm x 260mm and 360mm x 360mm) interconnect plates at ambient temperature resulted in the formation of large cracks and bulges in the coating which eventually damaged the underlying interconnect. These cracks were the result of the presence of large thermal gradients in the plates during deposition which induced large thermal stresses. This problem was overcome by heating the interconnects to between 400 and 500°C during deposition. This greatly reduced the magnitude of the thermal gradients and prevented cracks from forming. It was found that the coated interconnects had much lower contact resistance than the uncoated plates and the resistance did not increase with time or during thermal cycling. The coated interconnects were also tested in a working fuel cell. Both the cell voltage and current remained very stable over the duration of the tests (about 2500 hours), with a degradation rate of less than 1% per 1000 hrs if equipment failures are neglected. No distinction was made between the performances of the various protective coating materials.

1.4.4 Integrated Fabrication of SOFCs by Plasma Spraying

While extensive effort has been put into developing a plasma spray process for individual cell layers, the ultimate goal is to fabricate multiple cell layers and/or an entire cell through continuous deposition. The target of integrated spray fabrication processes is to entirely eliminate the time consuming sintering steps now used and the resulting thermal stresses, and to take advantage of the flexibility of the thermal spray process to improve and optimize the microstructure of each cell component.

The most advanced integrated fabrication processes developed to date involve deposition by vacuum plasma spray of an SOFC consisting of fuel and air electrodes and an electrolyte. The preliminary stages of this development involved first developing a procedure for successfully fabricating each layer individually [82]. A dense, 30μm YSZ electrolyte was achieved through the use of a special Laval type supersonic nozzle to deposit the powder at velocities between mach 2 and 5. This nozzle also produces a larger high temperature core in the plasma jet which allows for a larger fraction of the injected powder to be melted. It was also found that fine grained powders with a size of -22μm+10μm produced the densest electrolytes. Graded composite anodes were deposited by injecting NiO and YSZ powders separately, using the location of the injection sites to control the thermal environment encountered by each powder. The use of a nozzle with a wider opening and thus slower plasma jet velocities allowed sufficient porosity to be introduced into the layer. Single phase LSM cathodes were produced similarly, using a nozzle specifically designed to yield a broad, low intensity temperature profile in the jet, thereby avoiding decomposition of the LSM. It was found that by introducing oxygen into the LSM carrier gas, reduction of the powder could be prevented. Tests were also performed to compare the performance of a single cell with a plasma sprayed anode to one with a screen printed anode; both cells had a sintered YSZ electrolyte and LSM cathode. It was indicated that the plasma sprayed anode performed about the same as the screen printed one; however, no specific performance information was presented. Finally, anode/electrolyte half cells and full three layer cells were fabricated by plasma spraying, but having individual layer thicknesses greater than those for the individually fabricated layers.

The substrate and mechanical support for this cell was provided by a porous, metallic felt or mesh that allows for the uniform passage of oxidant and fuel gasses, thus eliminating the need for having a thick cell layer to provide mechanical support [1, 83 - 85]. During deposition, the substrate is resistively heated to reduce thermal gradients and stresses. Both nickel and ferritic steel have been used as supports. The nickel is more corrosion resistant and has higher

conductivity, while the ferritic steel provides a better match in terms of thermal expansion with the other cell components. From electrochemical testing it was found that despite having a lower open circuit voltage, the nickel supported cell performed much better, achieving a power density of 400 mW/cm^2 compared to only 200 mW/cm^2 for the ferritic steel one, measured at a cell voltage of 0.7 V. New materials which are both thermally compatible and corrosion resistant are reported to be under development. Most of the focus is on improving ferritic alloys for use as substrates. These alloys require an alumina content of between 4-6% to form a thin, dense, protective alumina scale that will remain stable over long operating periods. As alumina is a poor electronic conductor, a secondary material is introduced into the substrate, typically nickel, which is also resistant to corrosion and provides good electronic conductivity. Development of this material is still ongoing and no performance data were presented.

The next stage in the fabrication of entire cells by VPS involved refining the procedure described above to produce cell layers of the desired structure, composition, and thickness in a continuous deposition process to produce a cell suitable for operation at 800°C [86 - 89]. Dense YSZ and scandia stabilized zirconia (ScSZ) electrolytes were produced, again using a high velocity nozzle which provided for particle velocities of about 650 m/s. The resultant 30-40μm electrolyte layer was found to have 1.5-2.5% closed porosity. For fabricating the anode layer, the NiO and YSZ (or ScSZ) were injected separately at an increased standoff distance of 240mm.The particles also achieved a much lower velocity (~250 m/s), resulting in an anode layer porosity of 21vol. % after reduction. Composite LSM cathodes were produced in a similar manner, but the cathode was found to have lower porosity, 10-15%, due to the lack of a pore forming process. Both electrodes had a constant composition across their thickness (30-50μm). The above described conditions were applied in a continuous manner to produce a three layer cell. Electrochemical testing of both the YSZ and ScSZ based cells was performed. At 900°C and 0.7 V the YSZ cell had a power density of 0.580 W/cm^2, while the ScSZ cell had a power density of 0.770 W/cm^2; the performance difference was attributed entirely to the increased ionic conductivity of the ScSZ. The YSZ cell achieved power densities of 0.430 W/cm^2, 0.280 W/cm^2, and 0.190 W/cm^2 while the ScSZ cell had performance of 0.590 W/cm^2, 0.430 W/cm^2, and 0.300 W/cm^2, at 850, 800, and 750°C respectively and 0.7 V. EIS testing revealed that the cathode contribution to the cell polarization resistance was by far the most significant component, contributing about 65% of the total. Long term measurement of these cells showed a degradation rate of approximately 1%/1000 hrs, though testing had only been conducted for 2500 hrs at the time of publication.

An alternative process has been developed using a triple torch plasma reactor system in conjunction with a controlled atmosphere deposition chamber [89 - 91]. Graded anode and

electrolyte layers were deposited in a similar manner as described above by adjusting the process parameters and deposition atmosphere. The geometry of this particular torch is very similar to an axial injection torch; the main difference being the converging electrodes in this design. It is observed that the powder particles are all melted upon impact and remain molten for some time after, allowing, in the case of the electrolyte, for a very dense coating with chemical bonding between splats and no lamellar structure. The resulting electrolyte layer is 40 to 70μm in thickness. The deposition of a single phase LSM cathode was, however, carried out instead by injection of aqueous precursor solutions in a process known as thermal plasma chemical vapour deposition (TPCVD). After injection, the precursors are vaporized and transported towards a cooled substrate, where they react and condense on the previously deposited YSZ electrolyte. Nucleation of particulates can occur prior to deposition if the boundary layer in front of the substrate is not very thin; this leads to higher porosity in the coating. The boundary layer thickness can be controlled by the torch power, plasma jet velocity, and standoff distance. It takes somewhat longer to build up a coating with TPCVD, about 30 min for a 200μm thick layer (compared to 2 min for a 300μm anode layer deposited by VPS). The resulting cathode structure was found to be sufficiently porous but has not been optimized. Electrochemical testing yielded a peak power of 0.325 W/cm^2 with a current density of about 0.65 A/cm^2 (cell voltage ~0.5V) and 900°C.

To improve the porosity of the sprayed cathode layer and reduce material costs, the use of radio-frequency plasma spray technology has been explored for the deposition of perovskites using in-situ synthesis from precursor solutions in a TPCVD process [83, 84]. Aqueous nitrates of the desired elements are fed and atomised into the RF plasma torch. RF plasma technology generates plasma by passing a high frequency (500 kHz) current through an induction coil, the energy of which is coupled to the gas volume. The powder or aqueous feedstocks are generally injected axially. RF plasma torches produce a much larger volume of slower moving plasma than traditional DC plasma torches while jet core temperatures are similar. RF plasma torches offer the possibility of much longer residence times for the feedstock; sufficient to allow reaction of precursors and formation of a coating. The coatings are formed through condensation of the vapour phase of the perovskite material, leading to coating build up through the growth of columnar crystals, as in other PVD processes. The resulting coating has been found to have an open porosity exceeding 20 vol%. The pores formed by this process also offer relatively straight migration paths which should allow for efficient transport of gasses in the cathode layer. Fabricating perovskites using this process with a single pure phase has proven difficult, requiring very careful control. To date, only a strontium doped praseodymium cobaltite ferrite ($Pr_{0.58}Sr_{0.4}Co_{0.2}Fe_{0.8}O_3$) coating has been successfully deposited. While improved performance of TPCVD over DC-VPS cathodes is expected, electrochemical testing has not yet been carried out.

A similar method has, however, been used to deposit LSM coatings from aqueous nitrate precursor solutions using a cold temperature vacuum plasma RF reactor [92]. The resulting LSM coatings had high porosity (no exact figure was given) but were amorphous. Annealing for 1 hour at 750°C was required to achieve crystallization of the layer. The electrical properties of the cathode layer, most notably the conductivity, were highly dependent on the plasma conditions. It was found that coatings processed with higher oxygen content in the plasma exhibited much better conductivity, as the precursor nitrates were more fully oxidized. Much more work remains to be done to develop anode and electrolyte deposition processes with this technique in order to achieve integrated fabrication of a complete cell, though the technique appears to hold promise.

Numerous other variations of thermal spray technology have been explored in order to achieve better properties in the cell layers [91]. DC/RF hybrid plasma spraying was successfully used to fabricate both electrodes and electrolytes. It was found that this method produced an anode containing Ni particles with a high specific surface area. This allowed the Ni content and consequently the TEC of the anode layer to be reduced, providing a better match with the electrolyte. Testing of a cell prepared using this hybrid system revealed an OCV of 1.01V with a 40μm thick electrolyte. It was noted that while there was significant porosity in the electrolyte, it was mostly closed and the gas permeability was very low. A peak power of 0.731 W/cm^2 was achieved with this cell. It was felt that further improvements could be made, particularly in the cathode layer, to enhance the length of TPBs. Induction plasma spraying has been successfully used to create freestanding interconnect plates. Dense YSZ electrolytes have also been successfully deposited through the use of induction plasma spraying with the addition of a supersonic nozzle. Ni/YSZ cermets for the anode layer were also sprayed with this technology, but with limited success. It was found that the coating quality was very sensitive to the torch standoff distance due to the different cooling rates of the Ni and YSZ particles. Experiments involving the deposition of LSM from aqueous precursors using the induction torch were not successful as it was found that the torch power was not sufficient to completely react the La, Sr, and Mn.

While vacuum plasma spraying has been the focus of the most developmental effort, atmospheric plasma spraying has also been under investigation for integrated fabrication of SOFCs. The earliest work looked at applying APS to the fabrication of tubular SOFCs. One study compared the performance of a tubular cell using both APS and VPS (an extruded calcia stabilized zirconia tube was used as a support and VPS and APS were used to fabricate the electrolyte) [93]. The electrolyte density was found to be significantly higher when using VPS, with gas permeability through the electrolyte an order of a magnitude lower than when APS was used.

One other point of interest in this study was the use of nickel alloy/Al_2O_3 cermet as the interconnect material. No reason is given for the use of this material rather than a perovskite ceramic, as is usually the case in this type of cell. Performance testing of this cell indicated that it was possible to achieve a fuel utilization of 87.1% and an overall cell efficiency of 38% at 0.7 V. 1 and 10 kW stacks have been assembled using this fabrication technique; they have been operated for over 3000 hours with only slight degradation. Another study looked at the application of APS to a tubular cell in which an extruded LSM cathode acted as the cell support, and the electrolyte and anode were applied by VPS and APS respectively [94]. APS was found to be particularly useful in this case, as a functionally graded anode layer was required in order to reduce the thermal stresses encountered when operating at high temperatures (~1000°C). This cell achieved a maximum power density of 0.31 W/cm^2 at ~0.6 A/cm^2 and 0.5 V and had an OCV of 0.95 V. Performance was found to be much improved over a cell that was entirely fabricated by plasma spraying due mainly to improvements in the structure of the cathode layer which reduced the cathodic activation and diffusion overpotential substantially.

APS has also been used with some success in a few attempts at integrated fabrication of planar cells. One study examined a cell with a Ni/YSZ anode, LSGM electrolyte and LSM cathode fabricated using APS and intended for use at intermediate temperatures [95, 96]. The as-sprayed LSM was also found to retain the crystal structure of the feedstock powder, but with a slightly finer grain structure caused by rapid cooling during deposition. The LSGM electrolyte was deposited onto the cathode layer and formed a dense layer of about 50μm in thickness. It was found that the as sprayed LSGM was amorphous and required heat treatment above 700°C for an undisclosed period of time to recrystallize. A porous Ni/YSZ anode was finally deposited onto the electrolyte to complete the cell. EIS testing of the LSGM electrolyte found that, after exposure to temperatures above 750°C for recrystallization, the sprayed LSGM layer had ionic conductivity nearly as high as a pellet prepared by sintering. Testing of a single cell at 600 and 700°C revealed an OCV of 0.95V and 1.045V respectively, indicating that the electrolyte was reasonably gas tight. Peak power densities of 0.08 and 0.15 W/cm^2 were obtained at the respective temperatures; there was no indication of the voltage/current conditions at these points.

Another study fabricated an optimized cell structure for intermediate temperature operation having a Ni/YSZ anode, YSZ electrolyte and a LSC cathode by APS [97]. The cell layers were consecutively deposited onto a porous Ni-plate substrate that was roughened by grit blasting prior to deposition of the anode layer. The electrolyte was optimized for porosity using a nine trial, three level orthogonal experimental design using four spray parameters: torch current, argon flow rate (primary plasma gas), hydrogen flow rate (secondary plasma gas) and powder feed rate. No information was provided on the experimental design method or target responses used to

optimize the electrode layers. In addition to the four parameters mentioned in conjunction with the electrolyte optimization, the electrode optimization also considered standoff distance. By decreasing the torch current and relative hydrogen content and increasing the powder feed rate and standoff distance, the particle temperature and velocity were decreased sufficiently to create the required porous structure for the electrodes. As is often the case with perovskites, it was found that the LSC tended to decompose during spraying. To avoid this, the powder feed rate was increased and the hydrogen content of the plasma decreased. The deposited LSC layer was also found to have an amorphous structure; heat treatment at 800°C for 2 hrs was applied following spraying in order to restore crystallinity. The OCV of the cell was found to be about 0.95V, indicating that there was a small amount of gas leakage through the 80μm electrolyte. Electrochemical testing of the cell was carried out in a humidified H_2/O_2 environment. At 700, 750, and 850°C the peak power of the cell was measured as 0.1 W/cm^2 (@ 0.4V, 0.2 A/cm^2), 0.15 W/cm^2 (@ 0.45V, 0.35 A/cm^2), and 0.41 W/cm^2 (@ 0.45V, 0.9 A/cm^2) respectively. The resistance of the electrolyte was found to be the largest contributor to cell losses, accounting for 78% of the voltage loss at 700°C and 56% at 850°C. Cathode activation losses were the next largest contributor, accounting for 17% of the losses at 700°C and 31% at 850°C. Anode losses and losses due to interfacial effects were found to be very small at all temperatures tested. Monitoring over 20 hrs of testing at a steady current density of 0.5 A/cm^2 and various temperatures revealed some degradation of the cell and a corresponding rise in overpotential. The degradation was found to be primarily the result of Ni sintering in the anode and YSZ/LSC reaction at the electrolyte/cathode interface, resulting in the formation of a non-conductive phase. This interfacial reaction was found to be most noticeable at 850°C, while the effect was much less noticeable at 800°C. This indicated that this particular combination of materials is only suitable for use at reduced temperatures, preferably below 800°C. It is suggested that further work remains to be done to reduce the thickness of the electrolyte that can be achieved with APS and improving the microstructure of the LSC/YSZ interface.

APS has also been explored for use in fabricating SOFCs based on proton conducting electrolytes and electrodes [98]. A proton conducting SOFC was deposited with a barium calcium niobate (BCN) electrolyte, Ni/BCN anode, and a LSM cathode. The cathode layer was first fabricated by uniaxial pressing of pellets followed by sintering. The electrolyte and anode layers were then deposited onto the cathode using APS and flame spraying, respectively. The primary focus of this study was on the physical and mechanical properties of the cell materials rather than on electrochemical performance. The strength of the plasma sprayed BCN was found to be about half of that of the bulk material, while the anode layer was weaker yet, due mainly to its higher porosity. In all tests of the mechanical strength of complete cells, failure was always observed to initiate in the cathode layer. Mechanical failure of cells occurred when a bending stress of

approximately 35 MPa was applied; which is between the strength of the LSM (~25MPa) and of the BCN (~50 MPa). The three layers were found to be thermally compatible, each having a TEC of between 11 and 12.6 ppm/K. The adhesive strength of the cells was measured to be 0.24 MPa and failure again always initiated in the cathode layer. Interestingly, the adhesive strength of a stack with the same materials was found to be substantially higher, 0.42 MPa; no explanation is provided for the discrepancy. While mechanically it appears that a cell fabricated from these components is feasible, much work remains to evaluate the electrochemical performance of such a device.

Cathodes produced as part of these integrated fabrication processes have again either been single phase cathodes (either LSM or LSC) produced by APS or LSM/YSZ composite cathodes produced by VPS. In the future, it is hoped that the composite cathodes produced in this project will be combined with other cell layers being presently developed by colleagues to allow for integrated production of an SOFC by APS.

1.5 Experimental Design and Coating Optimization

Experimental design involves a detailed laying out of an experimental plan in advance in such a way that the collected data can be analyzed, and useful information extracted [99]. The first step in any experimental design process is the identification of process inputs (controlled factors) and the desired outputs (responses). A model, e.g. linear or quadratic, can then be fitted to the data by performing a regression analysis to yield information about the entire experimental space. The more experimental data one has, the more accurate the model will be. For example, a linear model for an experiment with two controlled inputs, X_1 and X_2, where Y is the response, could look something like:

$$Y = \beta_0 + \beta_1 X_1 + \beta_2 X_2 + \beta_{12} X_1 X_2$$

In this model, β_0 would be the response when X_1 and X_2 are both 0. $\beta_1 X_1$ and $\beta_2 X_2$ terms would be the main effects of the process inputs, and the $\beta_{12} X_1 X_2$ term would account for interaction between the two inputs, which may or may not be important in a given experiment. With sufficient experimental data, in this case 4 experimental points, the unknown β values can be determined. In practice, once the number of important input factors becomes larger than about 2, it becomes very time consuming and expensive to explore all possible combinations of factors. For example, to explore 3 levels of 4 factors would require 3^4 or 81 runs. Many experiments require many more factors to be considered. Thus, many statistical methods have been developed to dramatically reduce the number of experiments necessary to evaluate a large experimental space. The most common are known as fractional factorial designs, as a specific fraction (e.g. ½, ¼, etc.) of combinations of input values required to perform a full factorial analysis are chosen.

The following section will examine some examples of the application of fractional factorial experimental design and derivative techniques, specifically Taguchi and Response Surface methods, to the optimization of the properties of plasma sprayed coatings. Following that will be a more thorough examination of the uniform design approach, the method selected for use in this project, to experimental design and examples of its application to thermal spray experiments.

1.5.1 Parameter Development and Application of Factorial Experimental Design to Plasma Spray Coatings

For experiments requiring few experimental runs, a relatively simple and straightforward fractional factorial design approach can be used. This approach was used in one study examining the sensitivity of Cu-Ni-In and Inconel 718 coatings to variations in plasma spray process parameters [100]. In this experiment 2 levels of 8 input parameters were examined using 16 experimental runs. In each run only one parameter was varied at a time; this enabled the examination of the effects of each individual parameter on the coating quality directly. Higher order interactions (those between 2, 3 or more factors) tend to become less and less important; for the purpose of this study any interactions higher than second order were neglected. The inputs considered for the purposes of this study were: standoff distance, primary plasma gas flow rate, secondary plasma gas flow rate, carrier gas flow rate, torch current, powder feed rate, gun traverse speed, and whether or not cooling air jets were used. The coatings were characterized for 6 properties: hardness, deposition efficiency, adhesive strength, lap shear, the percentage of oxides present, porosity, and the percentage of unmelted particles. The Inconel 718 coating was found to be most significantly influenced by the primary plasma gas flow rate. It was found that increasing this flow rate tended to increase the porosity of the coating as a result of reduced residence time and less complete melting of the powder. Short residence times also resulted in a smaller percentage of oxides being present in the final coating. The carrier gas flow rate and torch traverse rate were not found to significantly affect the properties of the Inconel 718 coating. There were also differences observed in the relative importance of some parameters between the two different types of equipment used in this experiment, though these differences were not explored in any great detail.

The Cu-Ni-In coating was found to be very sensitive to most of the parameters. Interestingly, the deposition efficiency was found to respond either positively or negatively to an increase in primary or secondary plasma gas flow rate, depending on the type of gas used. Increasing the primary gas flow of nitrogen increased the deposition efficiency (DE), while the opposite trend was found when the flow rate of argon as the primary plasma gas was increased. When hydrogen was introduced as a secondary plasma gas, the DE of the nitrogen based plasma decreased,

while for the argon based plasma, it increased. A similar effect was noted when the torch current was increased. This resulted in an increase in the DE in an argon based plasma and a decreased DE in a nitrogen plasma. The presence of air jets was also found to significantly affect the properties of the coating sprayed in nitrogen, but little effect was noted in the argon plasma. No attempt was made to provide an explanation for these results. It was also stressed that the testing procedures used to characterize the coating properties must be sufficiently precise so that any statistical noise generated from these be small enough so as to not overwhelm the effects of input parameter variation.

A widely used subset of fractional factorial designs are known as Taguchi designs, though much of Taguchi's work relies on commonly used statistical tools. The Taguchi method is capable of handling large studies requiring consideration of many parameters with relatively few trials. Taguchi makes widespread use of fractional factorial and orthogonal experimental arrays. The approach is most commonly used in industrial engineering and product development studies. It is geared primarily towards improving quality control and making processes more robust so that the quality of resulting products are less sensitive to process variations [99]. In particular, Taguchi analyses often make use of an inner and outer array experimental design to separate design parameters (inner array) from environmental variables (outer array). Impacts on product quality resulting from deliberately controlled process parameters are taken as a signal while the influence of environmental variability is considered noise. The results are then analyzed using a logarithmic signal to noise ratio, with a high value of this indicator being desired. The goal of these experiments is often to minimize the susceptibility of the product quality to variability in environmental parameters (e.g. ambient temperature).

Taguchi methods have been used in many instances for the development of plasma sprayed coatings. One study sought to analyze the influence of the plasma spray process parameters on the quality of a variety of wear resistant coatings [101]. The process parameters were developed for the following coating systems: tungsten carbide/cobalt, chrome carbide/nickel chromium and alumina/titania. In each system the goal was to optimize the coating microstructure, hardness and adhesion. For this study 2 levels of 7 parameters were examined in 8 trials. The process parameters studied here were: the primary and secondary plasma gas flow rates, nozzle size, powder feed rate, torch traverse speed, torch current, and standoff distance. For the tungsten carbide coating system it was found that one of the tests performed, Rockwell 15N hardness testing, was not precise enough to provide useful data. The variation in the results between two tests with the same parameter values was as large as the variation between runs with different parameter values. For the tungsten carbide coating, the primary plasma gas flow rate was found to be the most significant parameter contributing to the coating microhardness with higher flow

rates giving better hardness. For the chrome carbide coating high primary gas flow rates, small standoff distance, and low powder feed rates all contributed to the coating having the best hardness. The adhesion of both the tungsten carbide and chrome carbide coating systems were found to be most dependent on the torch traverse rate, with high traverse rates giving the lowest per pass thickness and the best coating adhesion. The alumina/titania coatings sprayed all had excellent properties and the parameter variations in the range explored in this study did not seem to significantly affect the coating quality.

A subsequent study focussed more specifically on the optimization of alumina/titania plasma sprayed coatings for use as an electrical insulator for simulated nuclear fuel tubes [102]. Deposition was carried out using a radial injection DC plasma torch at atmospheric pressure. The parameters under consideration in this study were the torch current, primary plasma gas flow rate, powder feed rate, and standoff distance. The resulting coatings were characterized for hardness (both macrohardness and microhardness), thickness, porosity, dielectric strength, roughness, electrical resistance, and deposition efficiency. The experimental design used nine runs and explored three levels for each parameter. Macrohardness (Rockwell 15t) was primarily effected by the powder feed rate, with a higher feed rate giving the hardest coatings, and to a lesser extent by the standoff distance and torch current. Microhardness (Vickers) was similarly dependent on the powder feed rate and varied to a lesser extent with standoff distance and primary gas flow rate. Coating thickness was almost entirely dependent on powder feed rate, with the other parameters having a very minor effect. The porosity was primarily influenced by the torch current and standoff distance, with high current and intermediate distances giving the lowest porosity. The dielectric strength was primarily a factor of the powder feed rate; low feed rates resulted in the highest dielectric strength. The other three factors contributed moderately and equally to the dielectric strength of the coating. Surface finish (roughness) was found to be principally influenced by the standoff distance, primary gas flow rate, and torch current, with large distances, higher flow rates and low currents giving the smoothest finishes. Electrical resistance in the coatings was mostly affected by the standoff distance; large distances gave the highest resistance. A low primary gas flow rate and intermediate powder feed rate also tended to produce a coating with high resistance. Finally, deposition efficiency was affected by both the primary gas flow rate and the powder feed rate, with high feed rates and intermediate gas flow rates giving the best deposition efficiency. Based on these experimental results an optimum set of conditions for depositing the alumina/titania coatings was determined.

Taguchi methods were also used to determine the effect of oxy-fuel spray process parameters on the properties of NiCrAl/Bentonite abradable coating for use in a gas turbine [103]. The goal of the project was to evaluate the effect of the process parameters, determine the

parameters which contribute most significantly to coating quality, and to better control these parameters to allow coatings to be produced to more exacting specifications with greater reliability. A 15 factor (12 independent parameters plus 3 interactions), 2 level, 16 run experimental grid was used. Independent parameters considered were: substrate preheat temperature, coating thickness, powder hardness, total gas flow rate, internal cooling air pressure, carrier gas flow rate, system type (manual pressure/flow control or mass flow, closed loop), standoff distance, external cooling air pressure, oxygen/acetylene flow ratio, powder feed rate, and substrate rotational speed. Interactions between the internal cooling air and total gas flow, total gas flow and system type, and oxygen acetylene ratio and total gas flow were also considered. Coatings were evaluated for erosion resistance, tensile strength, and macrohardness. Erosion resistance and tensile strength were found to be controlled by system type and the powder feed rate, with automatic control and low feed rates being preferred. The total gas flow rate, internal cooling air/total gas flow interaction, and total gas flow/system type interaction were also found to contribute to these properties; high total gas flow rate and internal cooling air pressures were found to be preferred. The tensile strength of the coatings was also found to be sensitive to the oxygen/acetylene ratio. The hardness of the coating was sensitive to some of the same factors as the other properties, namely powder feed rate, total gas flow rate, and system type, with all of the same preferences as previously mentioned. The hardness was also found to be related to the coating thickness and carrier gas flow, with thicker coatings and lower carrier gas flow giving better hardness. The next steps in the development of this coating system will involve finding the overall optimum set of spray parameters considering all properties, exploring different feedstocks produced using different production methods, and with a wider range of characteristics.

Another study used Taguchi methods to explore how the process parameters affect the properties of plasma sprayed zirconia and zirconia/MCrAlY TBC systems [104]. The goal of this study was to minimize the variability in the coating properties by determining the sensitivity of those properties to process parameters and noise factors (variability between different facilities). The coating quality was determined using a four point bend strength test; coatings performing the best in this test were considered to be of the best quality overall. Unlike the previous studies that have been reviewed, this study did not look at parameters relating to the torch (current, plasma gas flow, etc.) but rather at parameters related to the preparation and mounting of the substrate. Two levels of 7 factors (plus one interaction) were considered in a 8 run experimental grid: substrate panel orientation (axial or circumferential), specimen location (edge or centre), the interaction between orientation and location, substrate removal technique (milling or cutting), pre-test treatment (none or heat treatment), test temperature (room or elevated) and pre-stress condition (controlled or variable). Pre-stressing was performed either by controlled heating of the

substrate (accomplished by heating with external gas torches monitored and controlled by thermocouples mounted on the panel) or by passing the plasma torch over the panel several times prior to starting the powder feed (which provides variable heating as the torch passes over different areas of the panel). This pre-stress condition was found to be the dominant factor contributing to the performance of both the ceramic and ceramic/metallic coating systems, with the controlled approach being preferred. Heat treatment of the zirconia coating was also found to lower the measured strength of the coating by 7%; no details of the heat treatment used were provided. For the zirconia/MCrAlY system, performing the bend test at elevated temperature was found to lower the coating strength by 7%. This coating was also affected by an interaction between the panel orientation and specimen location. All other factors were considered to have a small contribution (<6%).

A second, 8 factor, 2 level linear array was used to evaluate the effect of noise originating from the use of different spray facilities. In this part of the experiment the pre-stress level was controlled for all samples and its place in the array taken by a new parameter, panel size (4"x2" or 2"x2"). The previous orientation/location interaction term was replaced by a panel size/specimen location interaction term. Most of the parameters considered in this test were found to have a nearly negligible impact on coating strength (≤2%). The only factor to contribute notably was a still small (5%) variability resulting from the use of heat treatment prior to testing of the zirconia/MCrAlY coating. The signal to noise ratio was found to be both very low and relatively insensitive to the facility used.

While Taguchi analysis is still widely used for product development, many researchers have sought to develop new fractional factorial experimental design procedures that overcome the shortfalls of Taguchi analyses. For instance, when dealing with problems requiring a large number of factors to be considered, the use of inner and outer arrays to deal with controlled and noise parameters separately can become very tedious [105]. Statisticians have also discovered numerous instances where specific assumptions used in a Taguchi analysis would lead one to a less than optimal solution. The use of signal to noise ratios in Taguchi analyses has also been called into question. Some experiments have shown that their use requires the performing of calculations that are more complicated than is necessary and, in some cases, can result in the loss of significant information. Signal to noise ratios can also result in non-significant factors appearing to have a larger influence than they actually do. It has been suggested that the use of means and standard deviations is a more effective approach. Problems have also been found with Taguchi's interpretation of life testing data, which requires that the collected data be statistically independent, which it is not. Taguchi experiments also usually involve carrying out one large, comprehensive experiment, where the relative importance of each factor may not be

known. It has been suggested that a more effective approach would be to initially conduct a series of smaller screening experiments followed by more detailed exploration of areas of apparent interest. This approach would be well suited to experiments where there is uncertainty as to which parameters are most important. The Taguchi approach has also been considered by some to be "too simplistic and not very realistic for most practical problems" [106]. Taguchi designs also tend to place less emphasis on the effects of interaction between multiple parameters, which can be significant in some situations.

Some studies, taking some of these critiques into consideration, have proceeded to use orthogonal experimental arrays similar to Taguchi's, but have also taken advantage of screening tests and more straightforward statistical tools. One study utilized this approach to optimize chrome carbide/nickel chromium coatings [107]. These coatings have been shown to be extremely sensitive to process parameter variation. Initial screening tests indicated that five factors were of significant importance: torch current, primary gas flow rate, standoff distance, target rotational speed and powder feed rate. Two levels of each parameter were examined. Separate sets of experiments were performed for coarse and fine powder lots, as these were found to respond differently to parametric variation. The coatings were characterized primarily for macrohardness and tensile strength. A half fraction, 16 run factorial matrix was used that allowed for all main and two-factor interaction effects to be determined. For both powder lots it was found that the hardness was significantly dependent on one main factor, rotational speed (lower speeds giving better hardness), and on three two-factor interactions: distance and powder feed rate, distance and rotational speed, and current and feed rate, with high powder feed rates and large standoff distances giving the hardest coatings. The coarse powder tended to yield higher and less variable hardness across the entire range of parameters. A confirmation run was performed to test the optimum set of parameters that had been determined. The resulting coating had a hardness significantly higher than any produced from the experimental grid.

A later study used an identical experimental approach to study the parametric sensitivity of alumina and chromium carbide/nickel chromium coatings produced by plasma spray [108]. Screening studies indicated that the alumina coatings were sensitive to variations in the secondary plasma gas flow rate, torch current, and standoff distance. The alumina coatings were characterized for macrohardness and porosity. An 8 run full factorial experimental grid was used to study 2 levels for each parameter. Torch current most significantly influenced the porosity of the coatings, with a high current, small standoff distance, and high secondary gas flow rate giving the lowest porosity. This would be expected, as these conditions would yield a very hot plasma in which most of the ceramic particles have been completely melted, and the low standoff distance would tend to prevent the particles from cooling and solidifying before impact. The hardness of

the alumina coatings appeared to be influenced primarily by an interaction between the 3 parameters. The chromium carbide/nickel chromium coatings were similarly studied using 3 parameters: primary gas flow rate, standoff distance, and torch traverse speed. No one factor or interaction appeared to dominate the macrohardness of these coatings, but the highest value was achieved with a combination of high flow, low traverse speeds, and large standoff distances. Confirmation runs again showed that the experimentally determined optimum values yielded superior coating attributes for both the alumina and chromium carbide/nickel chromium coatings.

Response surface methodology (RSM), which also stems from fractional factorial design, has been suggested as an alternative to Taguchi methods that is both more sophisticated and easier to use [106, 109]. This technique involves sequential experimentation moving initially from being relatively ignorant of parameter effects to complete understanding of the system. The experimental steps in RSM are fairly straightforward. First, initial screening tests are performed to determine which parameters are relevant. Then a 2 level factorial experiment is conducted with the relevant parameters to achieve a local linear approximation of the response function (the value of the characteristics that are being optimized for), which should indicate the direction of the optimum set of parameter values. Then, a series of single run experiments are performed by adjusting the parameter values sequentially in the direction of the optimum as indicated by the linear approximation. Eventually, a point of diminishing return for the value of the response function will be reached, indicating that the maximum is likely near. A second factorial design can then be conducted to determine the shape of the response surface in this area and determine the direction of further increase. If the response surface does not appear to increase or decrease significantly in any direction, then the maximum has likely been reached. An augmented factorial design known as a central composite design can then be performed to obtain a two dimensional representation of the surface in this area and to determine the exact nature of the area in and around the maximum. Even non-linear systems can be initially explored through the use of two level experiments, with higher order experiments being conducted only in the later stages.

This approach is significantly less complicated than the Taguchi approach, which would require the use of a higher order experiment for the entire system right from the start. RSM also does not require knowledge of the appropriate spacing of the parameter values, as this is revealed through the course of the initial screening tests. Thus, the power of RSM lies in its flexibility and requires little prior knowledge of the system being studied. The most obvious limitation to RSM would be in distinguishing local maxima from the global maximum in complicated response functions if these occurred in separate areas of the experimental space. To ensure that one has really found the absolute maximum it may be necessary to "ascend" the response function starting from widely separated areas of the experimental space and ensuring

that a large portion of the experimental space has been mapped, so that it can be stated with some confidence that the best combination of parameters really has been found. This could add significantly to the time and number of experiments required. On the other hand, if one has reason to suspect that the response function will be relatively straightforward, such that one obvious maximum is expected, then RSM would be an efficient way to proceed.

1.5.2 Uniform Design Theory and Application to Plasma Spray Coating Optimization

Both Taguchi and Response Surface methods rely on orthogonal designs. To be orthogonal the experimental matrix must meet certain conditions. For example, consider Table 2, an n x s experimental design where n denotes the number of experiments (9) and s the number of factors (4). In this example, q, the number of levels of each factor is 3. The notation $L_n(q^s)$ is normally used to identify an orthogonal array. To be an orthogonal design, each entry must occur in each column the same number of times and, in any two columns, each pair of entries must occur the same number of times [110]. Experiments using Taguchi or Response Surface methods generally rely on orthogonal designs for their experimental grids.

	Column			
Row	**1**	**2**	**3**	**4**
1	1	1	1	1
2	1	2	2	2
3	1	3	3	3
4	2	1	2	3
5	2	2	3	1
6	2	3	1	2
7	3	1	3	2
8	3	2	1	3
9	3	3	2	1

Table 2: $L_9(3^4)$ Orthogonal Design [111]

More recently a new method for generating experimental grids has been developed based on number theory, Uniform Design (UD). The principal goal of these designs is to develop grids which provide for a more uniform distribution of experimental points within the experimental space [110, 111]. Put another way, UD seeks to minimize the value of various measures of non-uniformity (discrepancies). UD has been proven to be capable of substantially reducing the number of experiments required compared to fractional factorial methods when a large number of factors with many levels are involved. UD tables have the notation $U_n(q^s)$, where n is the number of experiments, q is the number of levels, and s the number of factors under consideration. For example, Table 3 shows a $U_{12}(12^4)$ Uniform Design table for an experiment with 12 levels of 4 factors with 12 experimental trials. Each column

No.	**1**	**2**	**3**	**4**
1	1	10	4	7
2	2	5	11	3
3	3	1	7	9
4	4	6	1	5
5	5	11	10	11
6	6	9	8	1
7	7	4	5	12
8	8	2	3	2
9	9	7	12	8
10	10	12	6	4
11	11	8	2	10
12	12	3	9	6

Table 3: $U_{12}(12^4)$ Uniform Design Table [111].

contains elements 1 - q and they appear equally often, thus $q \leq n$ and q is a divisor of n.

Procedures such as the Forward Procedure and the Threshold-Accepting heuristic have been developed to generate UD tables for specific combinations of n, q and s. These tables are freely available and do not have to be manually produced. An experiment applying UD methods would follow these steps:

- Choosing factors (controlled parameters), their range of values, and the number of levels
- Choosing the appropriate UD table based on the number of factors, levels, and the number of experiments one wants to perform
- Perform the experiments according to the table and record the responses
- Use regression analysis to establish a suitable model that provides a good fit to the data
- Find the value of the factors that gives the optimal response (maximum or minimum) and perform validation experiments

UD is also more robust than other experimental design methods in that it is not particularly sensitive to the type of model used for analysis and can give good results with little or no knowledge of the model governing the system prior to it being studied. The simplest, and most common, model that is applied to UD results is a linear regression model where the response is expressed in terms of input variables and some unknown regression coefficients [112]. These inputs will usually consist of linear input variables corresponding to experimental factors, higher order terms, and interaction terms. Usually, the number of coefficients exceeds the number of experimental points, requiring a method such as step-wise regression or a Bayesian based penalized least squares method to be applied to systematically eliminate insignificant terms from the model. Stepwise regression is the most widely used variable selection technique in uniform design experiments. The significance of each variable is evaluated either using an F-test (based on the Fisher variance ratio distribution) or t-test (based on the t distribution). For each variable an F value (or t value) is calculated and compared to a critical value from the distribution for the number of degrees of freedom involved and the desired significance (i.e. confidence) level (0.05, 5% is typically used). If the calculated F-value exceeded the critical value from the distribution, the variable would be deemed significant and added to the model. The remaining variables are then evaluated in turn for their significance in the presence of previously added variables. It is also important to re-evaluate the significance of previously added variables as new ones are included to ensure that all are still found to be significant [113].

Drawbacks to the use of stepwise regression for variable elimination in uniform design have, however been identified [112]. In some situations the procedure has proven to lack stability and it ignores the stochastic errors that are inevitably present in the variable selection process. A penalized likelihood (penalized least squares) approach has been proposed which is an estimation rather than regression procedure. The penalized likelihood approach greatly reduces the amount of computation required compared to stepwise regression and also yields stable models. This approach relies on the use of a penalty function and tuning parameter. The penalty function is then used in an estimator which should have a threshold (i.e. small variable coefficients should be set to zero to reduce the complexity of the model), and be unbiased and continuous (to prevent model instability). Starting with an initial value for the coefficient, and using a local quadratic approximation of the penalty function, iterations are performed by a statistical software package to simultaneously estimate the value of coefficients and eliminate insignificant variables.

The UD methodology has been applied to the optimization of plasma sprayed coatings. One investigation used UD to optimize the wear resistance properties of titanium nitride coatings [114]. The responses of interest in this study were: deposition efficiency, porosity, oxide content, microhardness, and fracture toughness. Five input parameters were considered: torch current, primary plasma gas flow rate (Ar), secondary plasma gas flow rate (H_2), standoff distance, and powder feed rate. For torch current and powder feed rate, 10 levels were considered while 5 levels were used for the remaining 3 parameters. The experiment involved 10 trials ($U_{10}(10^2 5^3)$). Regression analysis was used to model the responses as third order polynomials; elimination of insignificant variables was performed using a step-wise regression analysis. The deposition efficiency was found to depend significantly on the torch current, argon flow rate, and the hydrogen flow rate. There was also an interaction between the torch current and the hydrogen flow rate. Through optimization of these three parameters, a deposition efficiency of 50.5% was obtained. Porosity was found to depend only on the standoff distance, though the confidence level of this model was somewhat lower than that for the deposition efficiency. There was also rather large relative error between the experimental and predicted values (up to 72%). It was suggested that pores created during polishing of the specimens obscured the influence of the other process parameters. The lowest predicted porosity was 4.6% at a standoff distance of 130mm. The oxide content was found to depend on an interaction between torch current and argon flow rate and an interaction between current, hydrogen flow rate, and standoff distance. The minimum value for oxide content predicted by the model was 16.4%. Like deposition efficiency, the regression equation for microhardness had a very high confidence level (>0.99). The microhardness was influenced by interactions between the current and argon flow and between current, hydrogen flow, and powder feed rate. Fracture toughness was a function of

argon flow rate and an interaction between hydrogen flow rate and standoff distance. Validation experiments showed that the models provided reasonably good estimates for the mechanical properties of optimized coatings with low relative error between predicted and observed values. The predictions for microstructural properties (porosity and oxide content) were somewhat less accurate.

A similar experimental procedure has been used for the optimization of plasma sprayed YSZ TBC's [115]. As in the previously reviewed study, a $U_{10}(10^2 5^3)$ experimental design was used for the same five parameters: current, primary and secondary plasma gas flows, standoff distance, and powder feed rate. The coatings were characterized for deposition efficiency, porosity, and microhardness. The responses were each modelled with three separate regression analyses to generate first, second, and third order equations that were then compared for accuracy. Elimination of insignificant variables was done through stepwise regression. For each of the three responses, the first and second order equations were found to have too much error and, in each case, the third order equation was adopted. Deposition efficiency was found to depend on all five process parameters including interactions between the torch current, hydrogen flow rate, and standoff distance. A combination of low argon flow, small standoff distance, moderate powder feed rate, and high current and hydrogen flow gave the best deposition efficiency. The porosity was sensitive to all parameters except the torch current. There was again some concern expressed that the porosity data were inaccurate or that the porosity may have been dependent on a complex interaction between some parameters that were not modelled. Nevertheless, the third order regression equation obtained provided a very good fit with the experimental results. It was found that a low argon flow rate and high hydrogen flow, standoff distance, and powder feed rates gave the lowest porosity. Microhardness was found to be highest with low argon flow rates and high currents, hydrogen flow rates, and powder feed rates. Validation experiments confirmed that the predicted optimum parameter values yielded superior coatings. The relationship between the various responses was also considered. The deposition efficiency and porosity, and hardness and porosity were found to have inverse relationships, while deposition efficiency and hardness were found to be directly related. In each case the relationship between the responses was roughly linear.

Due to the apparent advantages of the Uniform Design method over other approaches, it will be the method for experimental design used throughout this project. In the work presented here, UD will be used to generate experimental grids to explore the effects of the various parameters. In future work, more refined experimental grids will be used along with regression analysis for cathode optimization.

1.6 Literature Review Summary

Research involving solid oxide fuel cells has been the focus of much attention recently as SOFC's have the potential to be widely used as efficient and fuel flexible electricity generators. While the technology holds promise, there are a number of factors that prevent immediate and wide scale adoption of SOFC technology. These include high unit expense due to high raw material costs and time consuming, energy intensive manufacturing processes. Currently SOFC's are also not sufficiently reliable or durable. At present, new manufacturing techniques are being developed in an attempt to remedy these deficiencies. Plasma spraying is one such technique that has the potential to greatly reduce manufacturing time and expense and simultaneously improve the structure and durability of the cell through real time control of process parameters.

Of the three active layers in an SOFC (anode, electrolyte, cathode), it is the cathode that is responsible for the majority of activation losses during operation with hydrogen as the fuel due to the sluggishness of the kinetics of the oxygen reduction reaction compared to hydrogen oxidation at the anode. The material most widely used in SOFC cathodes at present is lanthanum strontium manganite; a ceramic with a perovskite crystal structure that is an electronic conductor with slight oxygen ion conductivity at high temperatures and is catalytically active for the reduction of oxygen. Due to the low ionic conductivity of LSM, it has been found that adding an ionic conducting material (such as YSZ) to the cathode to produce a composite structure greatly improves cathodic performance by increasing the length of triple phase boundaries at which oxygen reduction can take place. Adding YSZ to the cathode also improves the mechanical compatibility between the cathode and YSZ electrolyte by reducing the difference of thermal expansion coefficients for the two layers. It is also important to have sufficient gas porosity, ideally around 40%, in the cathode to allow for the transport of oxygen gas to the reaction sites. Finally, it has also been observed that by grading the microstructure of the cathode layer across its thickness the performance can be further increased. The ideal cathode would have a very fine microstructure near the electrolyte interface consisting of narrow pores, small particles, and a high proportion of YSZ in order to maximize the area available for oxygen reduction. Away from the electrolyte, the cathode microstructure should gradually become coarser with larger pores and a higher fraction of LSM to allow for good gas transport and improved electronic current collection.

Plasma spraying has been used for the deposition of composite SOFC cathodes with graded microstructures. Most of these studies have involved the use of low pressure or vacuum plasma spraying. Results have generally been good, producing cathodes performing about as well as those produced by traditional methods but in a small fraction of the processing time. The most

significant challenges in producing good cathodes by VPS are in depositing LSM with the desired phase and with a sufficiently porous structure. In many studies some post spray heat treatment was necessary to recrystallize the LSM, though in others the as sprayed LSM possessed the desired phase. High levels of porosity have been realized through the use of an organic pore former that is sprayed together with the LSM then burned out after spraying. More recently, there has been interest in using atmospheric pressure plasma spraying to produce SOFC's, as it is a simpler and less expensive process than VPS. Most of the APS work conducted to date has focussed on deposition of SOFC materials designed for reduced temperature operation. The studies that have explored the deposition of LSM have focussed on producing single phase cathodes. The co-deposition of LSM and YSZ by APS for the production of two phase composite cathodes for SOFC's has not been previously explored in published work.

There are a number of steps involved before an optimized composite cathode can be produced by APS. The first is the identification of all of the independently controllable process parameters that significantly affect the quality of the coating and therefore the performance of the cathode. The range of values to be explored for each parameter must then be defined. This can be accomplished by carrying out preliminary screening tests exploring a wide range of each parameter in order to rule out the values which are not suitable for coating production. The range of parameter values remaining after these tests can then all be expected to produce useful coatings. The optimum combination of values that produce the cathode with the best performance will then be determined through the application of an experimental design technique, such as uniform design. Once an optimized cathode with a constant composition has been produced, the optimization of a cathode with a graded microstructure and composition can then be explored in hopes of further improving performance.

2.0 Air Plasma Spray System Description and Experimental Setup

The plasma spray system used in this project is an Axial III Series 600 system (Northwest Mettech Corp., Richmond, BC). As the name suggests, this particular torch system features axial powder injection. As discussed above, axial powder injection leads to very uniform and complete melting of the powder and, as a consequence, this type of system generally has higher deposition efficiency than the much more common radial injection systems. The torch contains three separate electrodes, each independently powered. As a result this system is capable of achieving much more energetic plasmas than many other systems; system power outputs of up to 150kW are achievable. The Axial III system can make use of three plasma gasses simultaneously: argon, nitrogen, and hydrogen or helium. The plasma spray setup used for this project contains four main components: powder feed hoppers, torch, manipulator, and sample mount. For these four components there are three independent operating systems that control the experimental parameters related to each part of the system.

The powder feed hopper system, Figure 3, consists of two separate feed hoppers that are connected to powder feed lines that transport powder to the torch using an argon carrier gas. The system allows for both single and dual hopper operation. Single hopper operation can be controlled either from the torch control system software interface or from the hopper system control panel; dual hopper operation must be controlled from the hopper control panel. The hopper system parameters that can be independently controlled are the powder feed rate and the carrier gas flow rate. Feed rate is controlled by changing the rotational speed of the feed disk located in the bottom of the hopper. The powder feed rate generally increases in direct proportion to feed disk rotation speed. The powder mass flow rate is also dependent on each powder's flowability, requiring separate calibration for each different powder composition. Powder mass flow rate calibration is carried out by feeding a quantity of powder over a known period of time into a closed container, which is then weighed.

The plasma torch and associated components: power supplies, gas supply, water pump, and mass flow controllers, are the heart of the APS system. The torch and the power and gas supplies are shown in Figures 4 and 5. The torch system parameters are controlled by a programmable logic controller integrated into a PC, which is accessed through a graphic user interface, shown in Figure 6. Values for torch electrode current, plasma gas composition, and plasma gas flow rate are set through this interface. In addition, the torch nozzle diameter can be changed by physically replacing the nozzle. Five discrete sizes are available, 5/16", 3/8", 7/16", 1/2", and 9/16". Due to the extremely high amount of energy involved in the plasma spray process

it is imperative that steps are taken to ensure safe operation of the equipment. The controlling software has numerous safety limitations built into it, preventing dangerously high torch currents or gas mixtures. During operation, the torch generates intense noise and light; eye and ear protection are required for operators to avoid damage resulting from operation of this equipment.

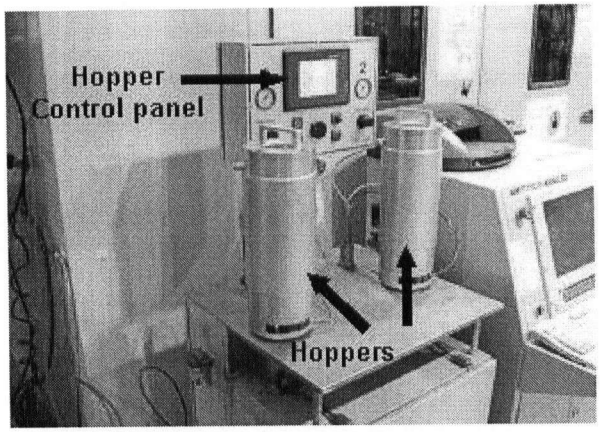

Figure 3: Powder feed hopper system.

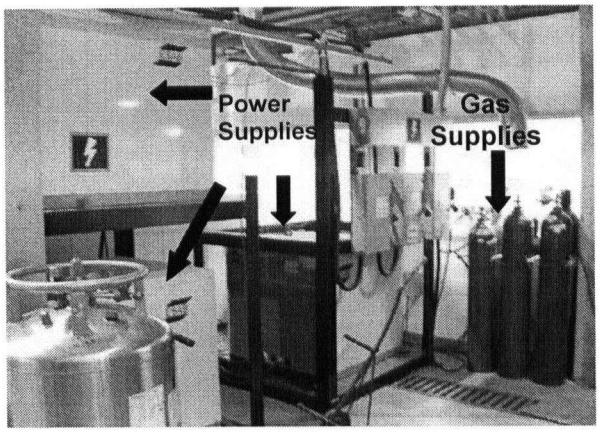

Figure 4: APS system power and gas supplies.

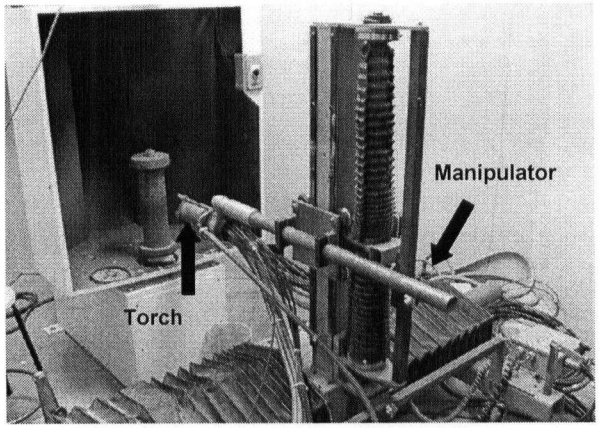

Figure 5: Plasma torch and manipulator robot.

Finally, the manipulator robot and sample mounting system are controlled from the consoles pictured in Figure 7. The mounting system consists of a metal drum bolted to the top of a turntable. Samples are then secured to the drum using a clamping system. The mounting system control console is used to set the rotation speed, anywhere from 0 to >600 rpm. The robot is a 2-axis programmable manipulator; though in practice only y-axis movement is used (x-axis movement is governed by the mounting system rotation). The programmable controller allows the number of torch passes over the sample to be set; which, together with the powder feed rate, determines coating thickness. The robot movement speed and movement distance can also be controlled from this console.

Figure 6: APS system control console.

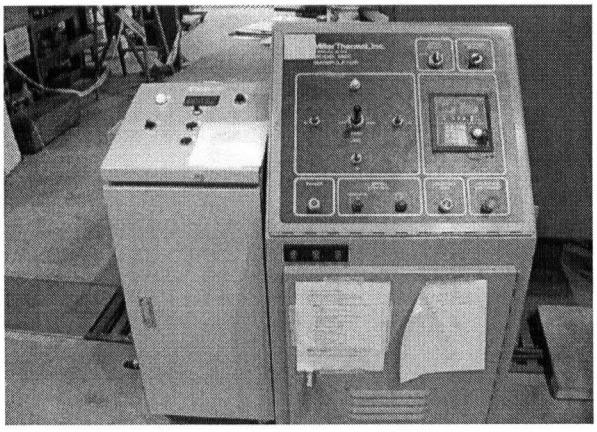

Figure 7: Manipulator (right) and sample mounting system (left) control consoles.

3.0 Plasma Spray Feedstock Preparation

3.1 Introduction

For composite cathode production by APS, both LSM and YSZ plasma spray grade powders were acquired. Infrox^{TM} S5725SR (Inframat Advanced Materials, CT, USA) was used as the LSM powder feedstock for experiments. The as received powder had the composition $(La_{0.8}Sr_{0.2})_{0.98}MnO_3$. As previously discussed, the use of an A site deficient, non-stoichiometric composition is believed to suppress the formation of undesirable lanthanum zirconate phases. The LSM powder was spray dried with a spherical morphology, as seen in Figure 8, to allow good flowability for feeding in a plasma spray application.

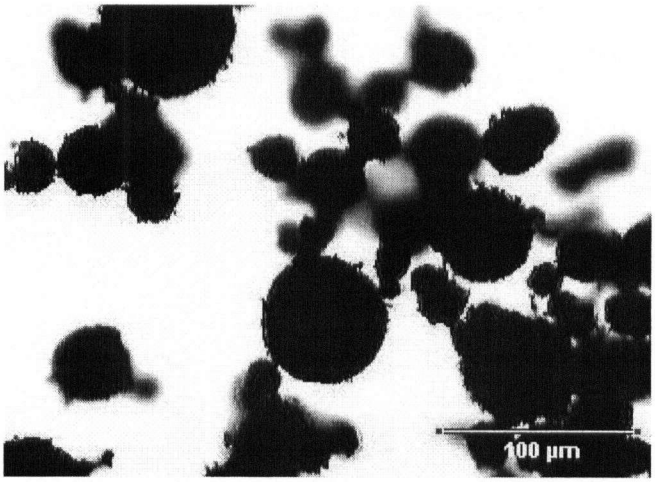

Figure 8: Typical optical micrograph of plasma spray grade $(La_{0.8}Sr_{0.2})_{0.98}MnO_3$ (x40 magnification)

The YSZ powder used for the initial screening tests, 920410-75MIC (St. Gobain, Worcester, MA, USA) had a hollow spherical morphology (Figure 9) and contained 4.7 mol% Y_2O_3, which is typical for TBC quality YSZ, but significantly lower than the 8-10 mol% normally used in SOFC applications. This powder also contained a fairly high level of impurities and, as a result, the electrical performance was expected to be rather poor. The decision to use this powder was based solely on its cost being significantly lower than electrical quality YSZ and the expectation that, in the initial stages of the screening trials, significant amounts of powder would be wasted in determining the appropriate deposition conditions for YSZ. The physical properties of this YSZ powder were expected to be largely similar to those of the electrical quality YSZ. Following the initial screening, high purity, electrical quality, spray dried 8 mol% YSZ (8YSZ) was used (Nanox S408A, Inframat Advanced materials, CT, USA).

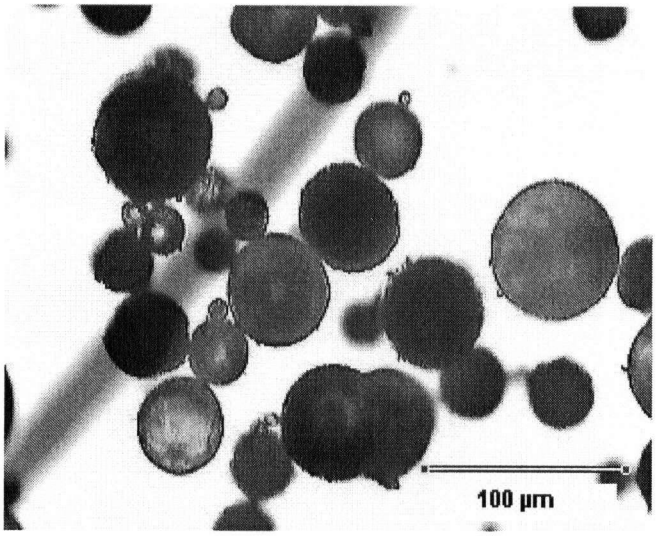

Figure 9: Typical optical micrograph of plasma spray grade 4.7 mol% YSZ (x40 magnification)

As it was desired to use particle size as one of the independent variables examined in these experiments, the as received powders needed to be separated into narrower size distributions. Additionally, it was necessary to ensure that the powders would be suitable for use in our powder feed hoppers.

3.2 Experimental Procedure

Particle size analysis was carried out using a Mastersizer 2000 (Malvern Instruments, Malvern, UK) particle size analyser. This equipment measures particle size by means of Low Angle Laser Light Scattering using a wet dispersion of the ceramic powder particles.

The as received powders were separated into narrower size distributions using sieves. The powders were sieved in batches of approximately 200g for approximately 30 min by an automated sieve shaker (Ro-Tap RX-29, WS Tyler, St. Catherines, Ontario, Canada).

3.3 Results and Discussion

The as received LSM powder had an average particle size (on a volume basis) of approximately 47µm, with sizes ranging from 10µm to 100µm. Figure 10 shows the particle size distribution of the as received powder.

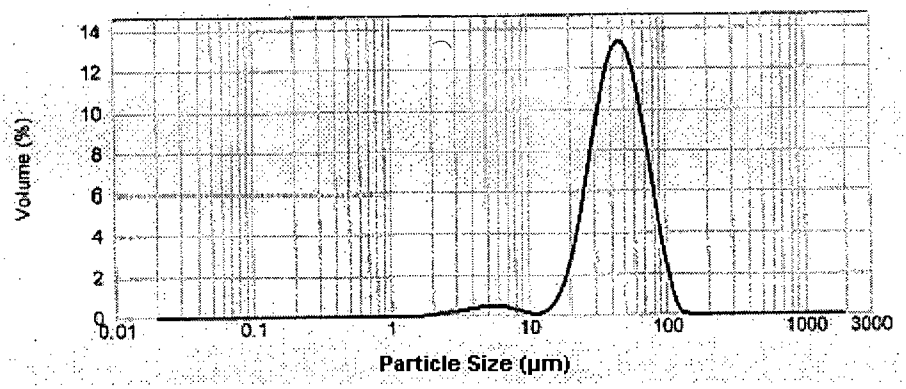

Figure 10: Particle size distribution of the as received LSM powder

After sieving, the resulting size distributions of the LSM powder were: -106+75µm, 75+45µm, -45+32µm, –32µm. The particle size distributions within each size range can be seen in Figure 11. Upon feeding the sieved, as received LSM, it was found that the powder quickly clogged the powder feed lines, effectively preventing the production of a coating.

Analysis of powder collected from the clogged lines revealed a drastically altered particle size profile, Figure 12. Particle size analysis revealed that, after passing through the feed hopper, the LSM particles had a bimodal size distribution. The larger size peak (~50µm) corresponds to average particle size of the original powder before feeding (-75+45µm) as seen in Figure 11b. The second peak centred at approximately 6µm, however, contains a significantly higher percentage of the total powder volume. The presence of these fines caused the previously free flowing powder to clump together, as seen in Figure 13, and adhere to the inside of the powder feed tube, leading to severe clogging. The distribution of the fine particles (<10µm) is very similar to the distribution of un-agglomerated LSM, which led to the conclusion that the ultimate cause of the problem was most likely the breaking up of the spray dried agglomerates due to the vibrations or a grinding action inside the powder feed hopper. To strengthen the agglomerates and prevent them from breaking up during feeding, it was necessary to first calcine the as received powder.

This heat treatment consisted of six steps: ramp from room temperature to 1000°C at 10°C/min, ramp to 1175°C at 5°C/min, dwell for 5 hours at 1175°C, cool to 1000°C at 5°C/min, dwell for 1 hour at 1000°C, cool to room temperature at 10°C/min. Particle size analysis of the calcined powder after feeding showed no change in the particle size profile, indicating the agglomerates were no longer breaking up. Also, no clogging of the lines was noted with the calcined LSM. The final preparation procedure for the LSM powder was to calcine the as received, spray dried LSM, and then sieve the powder into the size ranges described above.

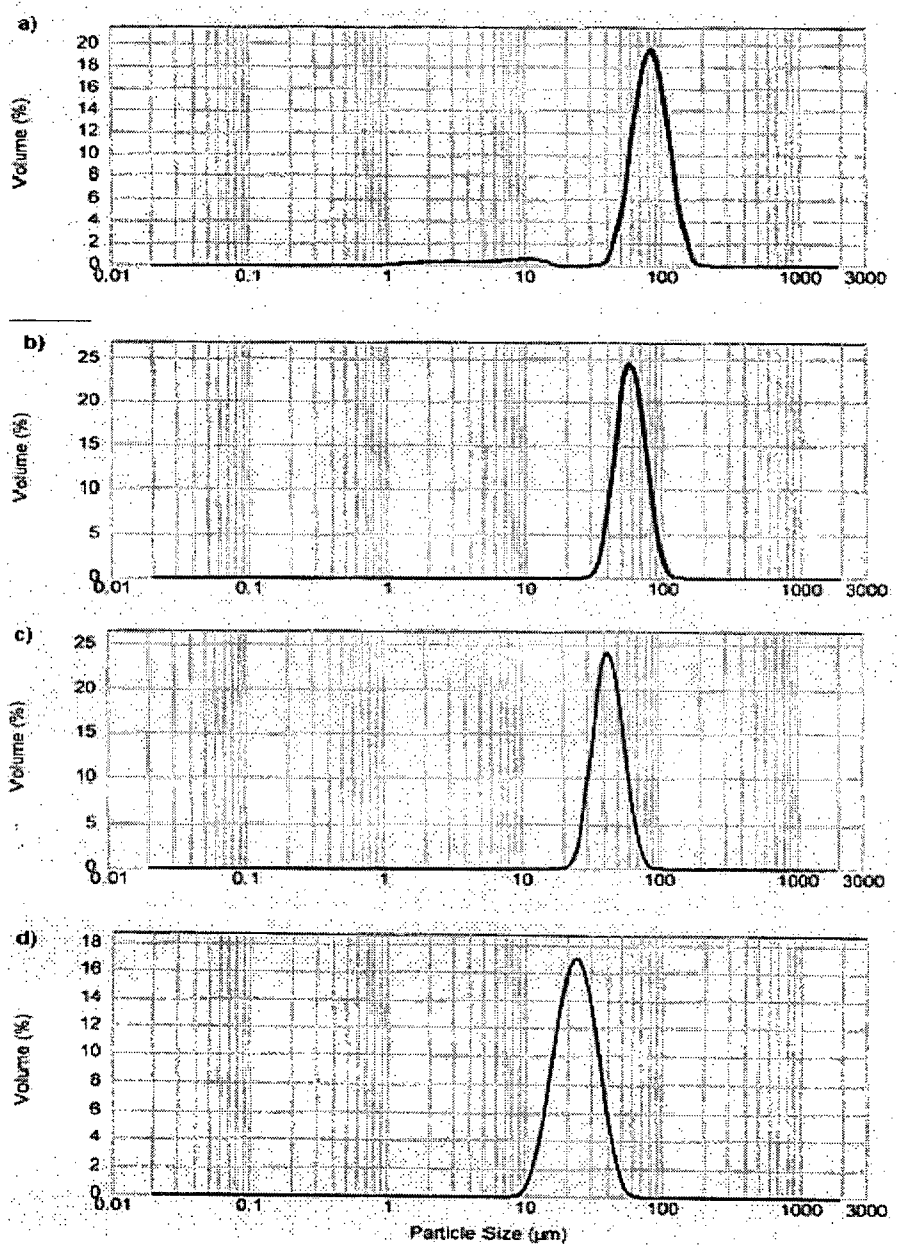

Figure 11: Particle size distribution of the a) -106+75µm, b) -75+45µm, c) -45+32µm, and d) -32µm sieved LSM powder

The as received 4.7 mol% YSZ powder had a size distribution from 124µm to 10µm with an average size of approximately 50µm. The as received powder was found to have excellent flowability and did not require any treatment prior to spraying other than sieving. The powder was sieved into the same size ranges used for the LSM powder.

In the 8 mol% YSZ powder, much like the as received LSM powder, the agglomerates were found to break up during feeding, causing severe clogging of the powder feed lines. The remedy for this problem was again to first calcine the as received powder prior to sieving. As the melting

temperature of YSZ is significantly higher than LSM, a higher calcining temperature was required.

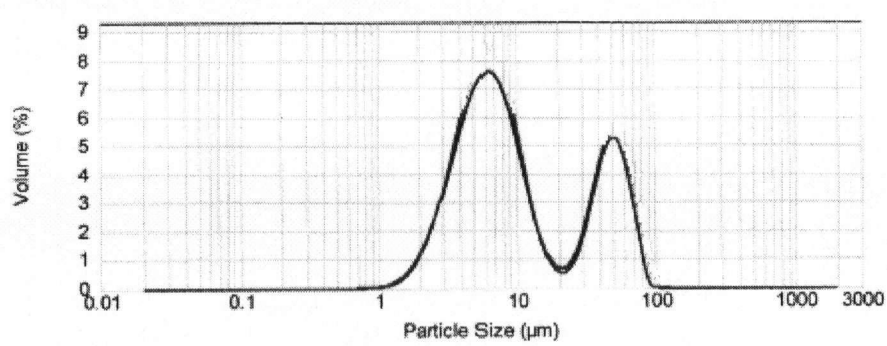

Figure 12: Particle size distribution of -75+45µm unsintered LSM powder after feeding.

The following heat treatment schedule was used: ramp to 1000°C at 10°C/min, ramp to 1350°C at 5°C/min, dwell for 5.5 hours, cool to 1000°C at 5°C/min, dwell for 1 hour, cool to room temp at 10°C/min. Following heat treatment the YSZ powder was sieved into several size ranges, -106+75µm, -75+45µm, -45+32µm, -32+25µm, and -25µm.

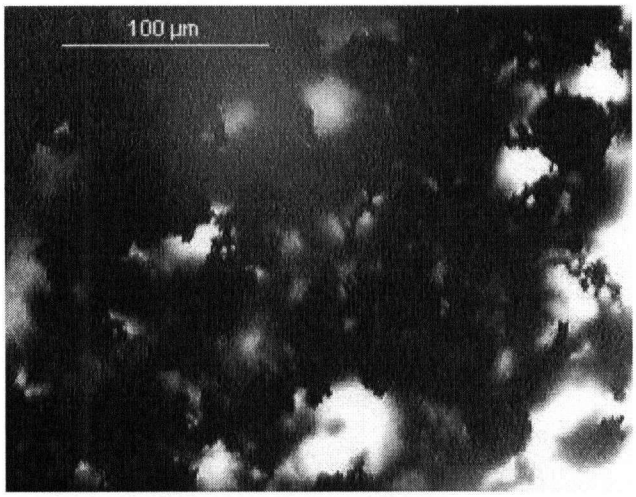

Figure 13: As received LSM powder after feeding (x40 magnification) showing clumping of broken agglomerates.

4.0 Single Material Coating Production and Parameter Range Screening

4.1 Introduction

Preliminary screening tests were carried out with both LSM and YSZ in order to determine the range of parameter values over which each material could be successfully deposited. This was done in order to determine the overlapping range of conditions over which it would be possible to co-deposit the two materials for composite cathode production.

LSM coatings were considered viable if there was minimal decomposition of the LSM phase and the coatings were well adhered to the substrate. As YSZ is a much more stable compound than LSM, decomposition was not an issue. YSZ coatings were considered viable if a coating was present and if the coating stayed was reasonably well adhered to the substrate.

4.2 Experimental Procedure

These tests were conducted by varying one or two process parameters while fixing the rest of the parameters at intermediate values. A range of values for each parameter was thereby determined over which it could be reasonably expected that a viable coating of each individual material could be produced. All of the coatings produced for the screening tests were deposited onto sandblasted stainless steel coupons for convenience.

X-Ray diffraction (XRD) analysis was used to determine if decomposition of the LSM had occurred. Comparison of the relative intensity of the diffraction pattern peaks of the LSM and the decomposition products (e.g. La_2O_3) offered some indication of the extent of the decomposition. The LSM and YSZ coatings were also evaluated for mechanical adhesion to the substrate through the use of a simple scratch test. The coatings tended to either be "dusty" and very easily removed, or well adhered to the substrate.

4.3 Results and Discussion

Initial tests quickly determined that the use of hydrogen as a plasma gas causes extensive decomposition of the LSM. This can be clearly seen in Figure 14d, where the LSM powder has been completely decomposed as a result of spraying with a very energetic plasma that contained 20% H_2. The extent of decomposition was found to increase with an increasing proportion of hydrogen in the plasma. Even the presence of a small amount of hydrogen, ~5%, was found to cause an unacceptable level of decomposition as seen in Figure 14c. This is thought to be due to the occurrence of a reducing reaction between the hydrogen and LSM in the plasma flame. When

deposition was carried out in the absence of hydrogen, the extent of decomposition was greatly reduced or eliminated altogether, as seen in the XRD pattern of such a coating in Figure 14b. Thus, it was concluded that the deposition of LSM should be carried out with only argon and nitrogen as plasma gasses. In plasmas using pure nitrogen slight decomposition of the LSM was noted, particularly when small powder particles (-45+32μm) were used. This is thought to have occurred due to thermal effects, i.e. decomposition stemming from exposure to excessively high temperatures. A similar effect was noted when depositing the as received LSM powder using plasmas containing more than about 40% N_2, likely the result of the decomposition of the fine particles contained in the as received powder. When larger powders were used, the extent of the decomposition was slight; though even very small levels of decomposition below the detection threshold may have a significant adverse effect on the performance of the cathode.

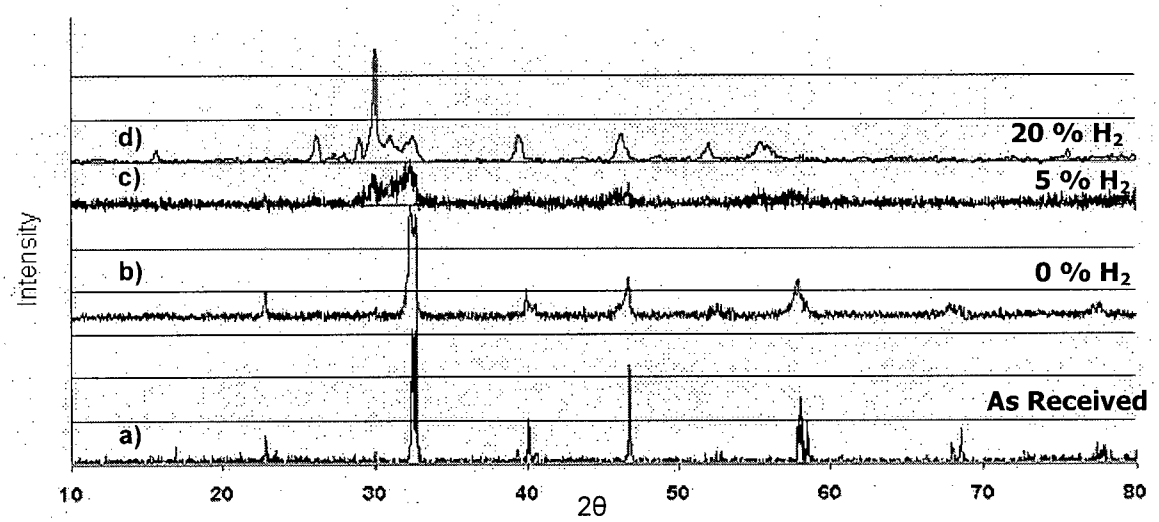

Figure 14: XRD patterns of, a) as received LSM feedstock and plasma sprayed LSM coatings produced with, b) 20% Ar, 80% N_2; c) 55% Ar, 40 % N_2, 5% H_2; d) 0% Ar, 80% N_2, 20% H_2.

While successful in preventing decomposition due to reduction, the exclusion of hydrogen as a plasma gas reduces the energy of the plasma that can be generated. The presence of hydrogen also increases the thermal conductivity of the plasma gas, enhancing heat transfer between the plasma and the entrained particles. Helium can be used as an inert replacement for hydrogen in order to achieve high energy plasmas and high thermal conductivity; but, because of the high cost of helium, the decision was made to try and produce high quality coatings using only argon and nitrogen. Pure argon generates a plasma with low energy (due to low arc voltage) and low thermal conductivity. The addition of nitrogen leads to a hotter, more energetic plasma; though the effect is much less than is achieved with the addition of the same proportion of hydrogen. For LSM, it was found that plasmas consisting of only argon and nitrogen were sufficient to produce good coatings over a wide range of input parameters. This is due in no small part to the relatively low melting point of the LSM (~1800°C).

The challenges involved in the production of viable YSZ coatings are considerably different than those encountered in the production of LSM coatings. Viable YSZ coatings were generally produced if the spraying conditions were such that at least some of the feedstock reaching the substrate was still in a molten (or partially molten) state. YSZ requires very high temperature plasmas in order to melt the powder feedstocks due to its high melting point (2680°C). YSZ is also more stable than LSM and does not decompose under any of the spraying conditions explored. However, due to the desire to co-deposit LSM and YSZ simultaneously in later stages of the project it was necessary to also produce YSZ coatings without the use of hydrogen in the plasma, making it much more difficult to achieve conditions that would produce a good coating. As was expected, YSZ coatings could be produced with less energetic plasmas when the smallest powder particles were used. Coatings were only successfully produced with the two smallest particle sizes available, -32+10μm and -45+32μm. The argon/nitrogen plasma used was not sufficiently energetic to melt particles above 45μm in diameter.

The maximum and minimum values established for each independent parameter and one dependent parameter (enthalpy) for the production of viable LSM/YSZ composite coatings can be seen in Table 4. The enthalpy of the torch is dependent on the plasma flow rate, plasma composition, and torch current and gives an indication of the energy density of the plasma jet. While enthalpy often correlates with the extent of melting of the powder particles, this is not always the case, especially when changes in enthalpy are due to a change in the hydrogen content of the plasma or changes in the plasma gas flow rate. In these cases adding hydrogen or increasing the gas flow rate will produce a drop in measured enthalpy while particle melting conditions are improved due to an increase in the thermal conductivity of the plasma and/or an increase in torch voltage.

The agglomerate sizes available are restricted by the particle size distribution of the source powder and the available sieves. 100 mm was set as the minimum standoff distance to be used as it was felt that smaller values would lead to excessive heating of the substrate and failure of the coating. The maximum standoff distance was determined by the limit at which it was still possible to produce a viable YSZ coating using an energetic plasma. The minimum values for the vol. % of N_2 and the arc current were selected as the points where plasma energy became sufficient to produce a viable YSZ coating. Up to 100% N_2 plasmas could be successfully used to deposit both materials. The maximum current of 250 Amps/source was the maximum allowable current that could be used in the torch. The minimum and maximum plasma gas and carrier gas flow rates were again determined by safety limitations set by the equipment manufacturer. The range of nozzle sizes available for use with the torch determined the minimum and maximum

values of that parameter. It was found that for both YSZ and LSM a viable coating could be produced with every nozzle size over a wide range of conditions.

	Minimum Value	Maximum Value
Standoff Distance (mm)	100	340
Vol. % N_2 in Plasma Gas	30	100
Vol. % H_2 in Plasma Gas	0	0
Arc Current (A/source)	150	250
Plasma Gas Flow Rate (slpm)	120	250
Carrier Gas Flow Rate (slpm)	5	25
Nozzle Size (1/16")	5	9
Total Enthalpy (kJ/L)	~48	~75

Table 4: Maximum and minimum values for each input parameter that allows for the production of a viable LSM/YSZ composite coating

5.0 Initial Composite Coating Production and Proof of Concept Cathode Testing

5.1 Introduction

Using the information gathered in the screening tests performed as described in the previous section on the two materials individually, the range of conditions over which it was expected that viable composite coatings could be produced was established. The next series of tests undertaken were designed to explore challenges of depositing the LSM and YSZ simultaneously and examine the characteristics of the coatings produced. The composite coatings were deposited onto the same stainless steel substrates used previously.

The most promising of the cathodes produced here was also subjected to electrochemical testing in order to confirm that the coatings produced would indeed function as SOFC cathodes.

5.2 Experimental Procedure

The composite coatings were initially produced using a mixture of LSM and YSZ (4.7 mol%) powders fed from a single feed hopper. As it was thought that the porosity of these coatings would be insufficient, graphite pore former was also introduced into the powder mixture in an attempt to increase the porosity of the final coating. The graphite was in the form of flakes which had a size < 45μm. The goal was to introduce carbon into the coating then to remove it with post-deposition heat treatment by combustion, leaving behind open porosity in the coating. Flowability of the powders was judged qualitatively by the extent of cohesive agglomerates in the powder mixtures.

Energy dispersive X-ray spectroscopy (EDX) was performed on the coatings in order to determine the relative quantity of elements present in the coating, used to establish the approximate coating composition.

For electrochemical testing, the complete cell was composed of a 1.4mm thick, 1" diameter, tape cast YSZ electrolyte, onto which was deposited the plasma sprayed LSM/YSZ composite cathode. A custom designed substrate holder was used to mask the electrolyte, and create the electrode outline, as shown in Figure 15. After spraying, platinum paste was applied to the opposite side of the

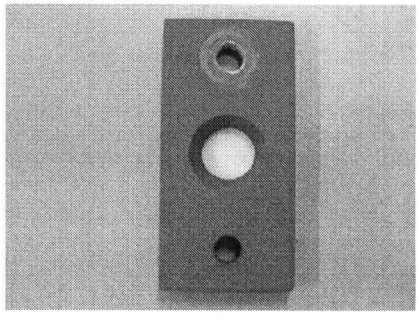

Figure 15: YSZ substrate holder and mask.

electrolyte to function as the anode. Testing was performed in humidified hydrogen and air (both at 0.1 slpm) at 1000°C.

Image analysis, performed on the SEM micrographs, was also used to determine the relative porosity of the coatings. The software used to perform the image analysis was Motic Images Plus 2.0 (Motic China Group Co., Ltd., Xiamen, China). Due to the limitations of this technique, the porosity values obtained cannot be used to determine the absolute porosity of the coatings. Image analysis was performed using micrographs of the top surface of the cathode coatings which have a three dimensional topography. Thus, distinguishing shallow pores from the coating surface was rather difficult. The micrographs used also represent only a very small portion of the total coating surface, so while effort was made to choose areas that were representative of the coating microstructure, some additional error would be introduced by the smallness of the area of the surface sampled. The software distinguishes pores by sensing differences in the brightness and contrast between the pores and the solid coating. As the brightness/contrast of the original micrographs is not standardized, the brightness and contrast had to be individually adjusted for each image. These adjustments are made at the discretion of the software user. It was found, however, that the reproducibility of the calculated porosity value was quite good. Repetition of the analysis typically yielded porosity values that were the same to within a percentage point. By using the same relative standards for each image, it is believed that the values obtained are suitable for comparisons of porosity values between the coatings, but not for absolute porosity level determinations.

5.3 Results and Discussion

The flowability of the final mixtures of graphite, LSM, and YSZ was found to be inferior to that of the separate ceramic powders, mostly due to the presence of the graphite flakes which tended to clump due to their highly non-spherical shape. The higher the proportion of graphite, the less "flowable" the final mixture was. Nevertheless, all of the mixtures used were able to be fed into the torch without the occurrence of significant clogging.

The most significant difficulty with the simultaneous deposition of multiple materials vs. the deposition of individual materials is the difference in relative deposition efficiency (DE) of the materials; with YSZ having a DE significantly lower than that of LSM. Thus, the composition of the initial powder mixture is quite different than that of the final coating. The extent to which the final coating composition differs from the initial powder mixture changes with variation of the input parameters. The differences in deposition efficiency ultimately stem from the large difference in the melting temperatures of the two materials. In an attempt to minimize the difference in DE between the two materials, the smallest powder size was used for the YSZ while larger particle

sizes were used for LSM. EDX analysis found that the YSZ content of the final coating was significantly lower than in the initial mixture. Table 5 shows the variation in relative deposition efficiency of the two materials over a range of spray conditions. SEM images of the composite coatings produced (after burning out graphite flakes) can be seen in Figures 16-18.

	Powder Mixture (LSM/YSZ)	LSM Powder Size	Arc Current (A/source)	Plasma Gas Composition (Ar/N_2, slpm)	Plasma Enthalpy (kJ/L)	Coating Composition (LSM/YSZ)	YSZ DE (Relative to LSM)
1	54.5/45.5	-45+32μm	200	50/50, 200	50.1	87.5/12.5	17.1%
2	37.0/63.0	-75+45μm	230	50/50, 200	56.1	76.1/23.9	18.5%
3	54.5/45.5	-45+32μm	200	60/40, 200	43.5	88.5/11.5	15.5%
4	54.5/45.5	-45+32μm	220	60/40, 200	48.3	85.5/14.5	20.4%
5	54.5/45.5	-45+32μm	220	25/75, 220	63.9	79.9/20.1	30.2%

Table 5: Relative deposition efficiency of LSM and 4.7 mol% YSZ over a range of plasma conditions (YSZ particle size -32+10μm). All ratios are on a mass basis.

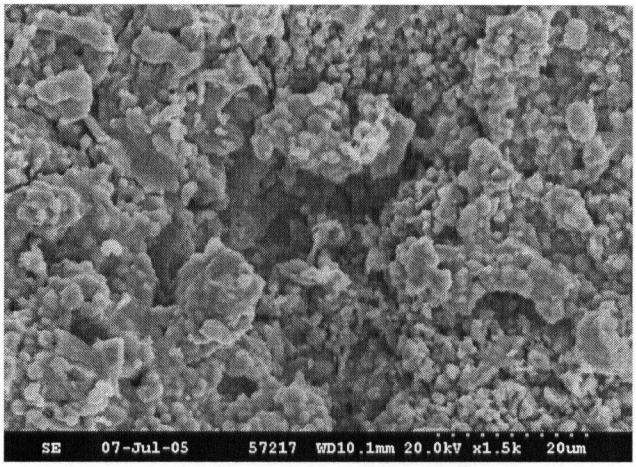

Figure 16: SEM image of LSM /YSZ composite coating #2 containing 23.9 wt% YSZ, 19% porosity.

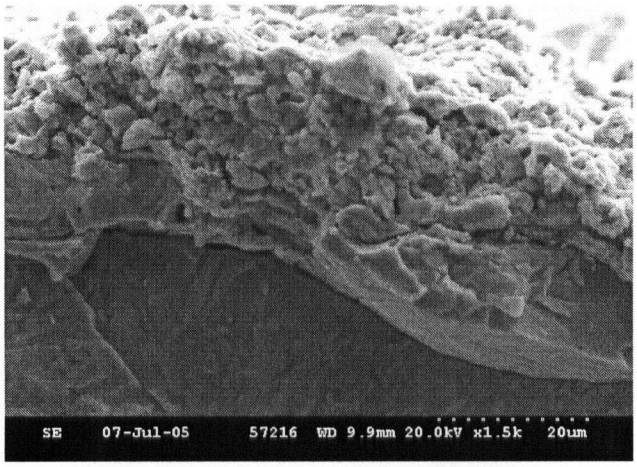

Figure 17: SEM cross section image of LSM /YSZ composite coating #2 deposited on a YSZ electrolyte substrate. Coating contains 31.9 wt% YSZ.

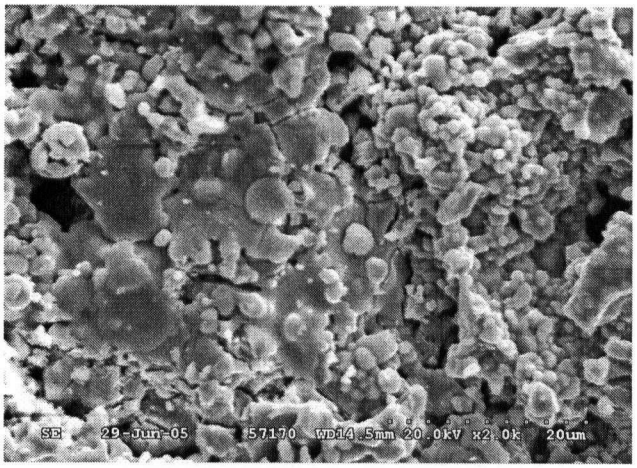

Figure 18: SEM image of LSM /YSZ composite coating # 4 containing 14.5 wt% YSZ, 8.4% porosity.

Over the range of conditions examined the deposition efficiency of the YSZ was 30% or less than that of the LSM. The YSZ relative DE is calculated as follows:

$$YSZ\ \mathrm{Re}l\ DE = \frac{LSM\ Powder\ Fraction}{LSM\ Coating\ Fraction} \times \frac{YSZ\ Coating\ Fraction}{YSZ\ Powder\ Fraction} \qquad \text{(Eq. 1)}$$

The DE can be calculated using either volume or weight fractions, provided that the use is kept consistent in all four terms.

The relative deposition efficiency is clearly dependent on the energy of the plasma; with higher energies giving a higher relative DE for the YSZ, as shown in Figure 19. It should be noted that all other factors are not being held constant in this plot and their variation likely has some influence on the relative DE. However, it can be seen that there is a correlation between plasma enthalpy and YSZ relative DE. It should also be noted that plasma enthalpy itself is not an independent variable, but rather is dependent on other factors; mainly plasma composition, arc current, and the plasma gas flow rate. Increasing either the N_2 content of the plasma or the arc current results in the coating containing more YSZ compared to coatings prepared with lower N_2 content plasmas or lower arc currents. Altering the initial powder mixture may also have an effect, as the mixture containing a higher percentage of YSZ had a lower relative DE than other mixtures, even when deposited using more energetic plasma. In an attempt to raise deposition efficiency coatings were also produced using a powder mixture containing very fine (<10μm) 8 mol% YSZ. This mixture did not, however, prove suitable for plasma spraying, as the fine YSZ clogged the powder feed lines very quickly.

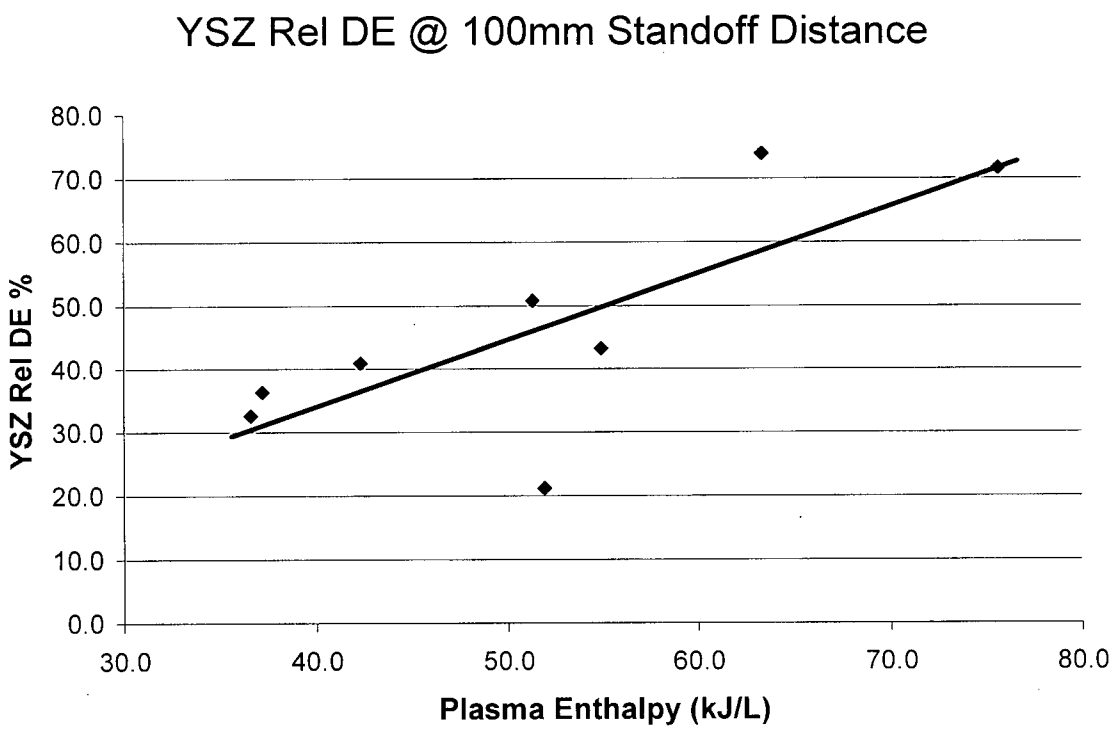

Figure 19: Variation in YSZ relative deposition efficiency with total plasma enthalpy

The desired ratio of YSZ to LSM in the final coating is approximately 50/50 vol%, or 52.8/47.2 LSM/YSZ on a mass basis, taking into account the respective densities of the two materials (6.6 g/cm^3 for LSM, 5.9 g/cm^3 for YSZ). It is clear from Table 5 that in order for a final coating to contain the desired proportion of YSZ, significantly more YSZ than LSM will have to be present in the initial powder mixture. By knowing the approximate value of the YSZ relative DE in particular plasma conditions and the target coating composition, the initial ceramic powder mixtures can be adjusted to yield a final coating with the desired composition.

A series of experiments were also conducted to determine the relative DE of the various powder sizes over a range of plasma conditions when co-deposited with LSM. The DE of the 8YSZ powder was expected to be somewhat different than that of the 4.7 mol% YSZ due to differences in the structure of agglomerates (hollow spheres for the 4.7 mol% YSZ, solid agglomerates for the 8YSZ) and differences in the particle sizes. The initial powder mixture used was 50/50 vol% LSM (-75+45μm) and 8YSZ (-45+32μm); no carbon pore former was included. Coatings were produced using conditions similar to those previously used for the deposition of the 4.7mol% YSZ to allow comparison. Visually, the coatings produced with the 8YSZ appeared to contain much more YSZ than the previously prepared coatings. EDX compositional analysis confirmed this assessment. The coating produced in 75% N_2 was found to have a relative DE for the YSZ of nearly 60%. This is approximately twice the best deposition efficiency previously found

in coatings deposited using the 4.7 mol% YSZ for the same conditions. These coatings containing 8YSZ also appeared to be much more porous. This seems to confirm previous speculation that the presence of YSZ contributes significantly to the porosity of the coating, and that by having a higher YSZ content, the level of porosity can be enhanced.

Through the course of these explorations, there were several instances when coatings were deposited using conditions identical to previous runs. Comparison of micrographs of these coatings revealed that, in each case, the microstructures of the coatings appeared very similar. Furthermore, EDX analysis of these coatings revealed that the coating compositions and the corresponding relative YSZ DE's, were fairly consistent from coating to coating and within the observed variability typically found within each particular coating (± 2-3%). Thus, any variability in the torch from run to run using identical parameters does not seem to be sufficient to significantly affect the properties of the coating produced and careful monitoring of the torch operating points (voltage, power, and enthalpy) should be sufficient to ensure reproducibility of the coatings.

The coating produced with the highest YSZ (using the 4.7 mol% composition) content produced at this stage (#2 in Table 5) was then subjected to electrochemical testing in order to validate that the manufacturing procedure developed was suitable for the production of functioning SOFC composite cathodes. The finished cathode can be seen in Figure 20.

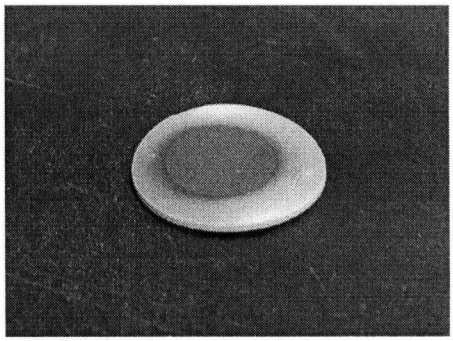

Figure 20: APS LSM/YSZ composite cathode on YSZ electrolyte.

The cell's active electrode area was 1.47 cm^2. The cell polarization and power curves can be seen in Figure 21. The cell OCV of 1.01 V is very close to the theoretical value, indicating no significant gas leakage in the cell. The cell achieved a peak power density of 80.6 mW/cm^2 at a current density of 0.24 A/cm^2 and a voltage of 0.34V. The performance of the cell was severely limited both by high electrode activation losses and very high ohmic losses across the thick electrolyte. Based on the theoretical ionic area specific resistance of the electrolyte at 1000°C, 1.4 Ωcm^2, the ohmic drop in this layer at 0.24 A/cm^2 is 0.34 V. Most of the remaining voltage drop, 0.33 V, is likely the result of activation and ohmic losses in the electrodes. The short triple-phase boundary (TPB) length and low porosity in the Pt paste would have contributed to activation losses in the anode. On the cathode side, the low YSZ content in addition to the low conductivity of the YSZ present likely contributed to the cathode polarization.

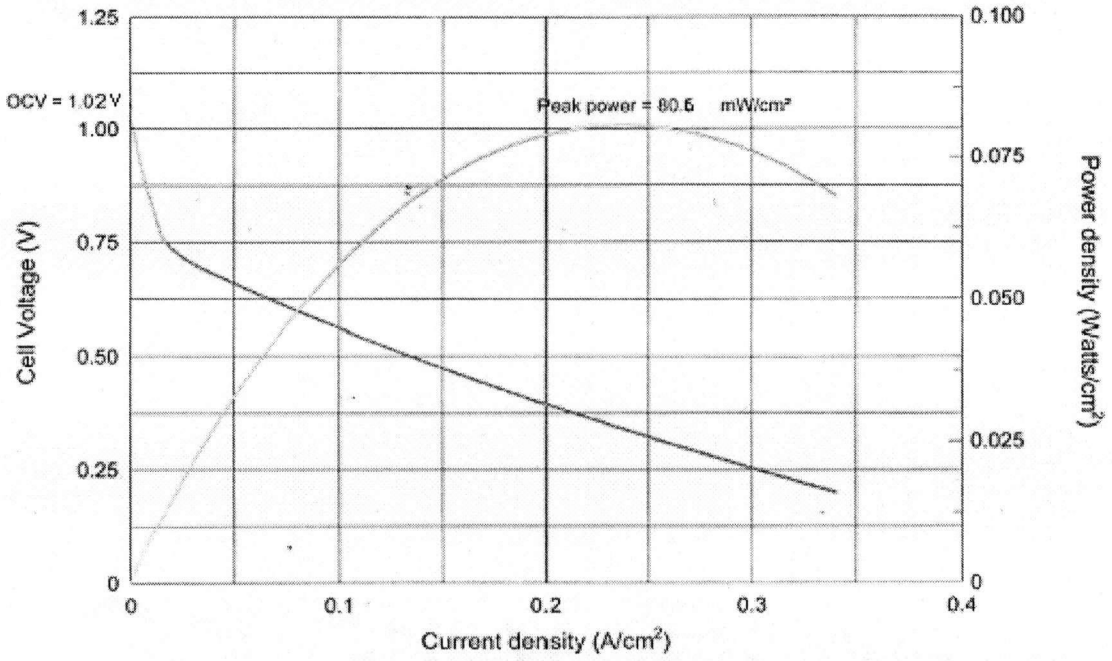

Figure 21: I-V characteristics of an SOFC with a plasma sprayed LSM/YSZ cathode, YSZ electrolyte, and Pt anode tested in H_2/Air at 1000°C.

Despite the higher content of YSZ in the initial powder mixture, the final volume of YSZ in the coating is still lower than the target amount. This would limit the performance of the cathode as there is likely not full percolation of the YSZ phase in the cathode, significantly reducing the length of triple phase boundaries, and therefore the number of reaction sites available for oxygen reduction. However, the very low current density at 0.2 V (the termination voltage), just 0.35 A/cm^2, is largely the result of the high ohmic resistance of the electrolyte (Ohmic drop = 0.49 V @ 0.35 A/cm^2). Nevertheless, these tests do confirm that the developed procedure is suitable for the production of functioning SOFC cathodes. They also indicate that significant optimization and improvement is required to produce a cathode with sufficiently high electrochemical performance.

6.0 Preliminary Coating Optimization Study

6.1 Introduction

Following the establishment of a procedure for their production, a large number of composite coatings were then produced using a variety of parameter value combinations within the identified ranges (Table 6) and their suitability for use as cathodes was evaluated. A sufficiently large number of experiments (40) were to be performed in order to examine the effect of each of the parameters on the quality of the coating produced.

6.2 Experimental

Again, coatings were deposited onto sandblasted stainless steel coupons. These experiments, and all further ones, were performed exclusively with the 8 mol% YSZ powder. The experimental grid used in this experiment considers the nine parameters thought to most affect the coating quality: plasma gas flow rate, carrier gas flow rate, % N_2 in the plasma, arc current, standoff distance, LSM particle size, YSZ particle size, powder feed rate, and nozzle diameter. Since only two viable size ranges were available for each powder, the number of levels to be explored for all parameters must be a multiple of two to satisfy the requirements of the Uniform Design Method used to generate the grid. As only 5 nozzle sizes were available, it was decided to drop the smallest nozzle size and proceed with a table using four levels. To have adequately covered an experimental grid consisting of 10 levels (the lowest common multiple of 2 and 5) would require a very large number of experiments. The experimental grid consisted of 40 parameter combinations so as to still yield a sufficiently large number of coatings (>20) to analyse after coatings which were not viable were discarded.

All of the coatings produced were examined with SEM and characterized for composition using EDX. As before, image analysis was used to estimate the relative porosity levels of the coatings.

6.3 Results and Discussion

The experimental grid used is shown in Table 6 along with the resulting YSZ relative deposition efficiency for each coating, as determined by EDX analysis.

Run #	ST D (mm)	PG (slpm)	N2 %	CG (slpm)	Current (A)	LSM Size	YSZ Size	Feed rate (g/min)	Nozzle (1/16")	YSZ Rel DE (%)
1	100	183.3	53.3	25	183.3	-75+45	-32+25	40	9	50.74
2	260	150	30	11.7	216.7	-75+45	-32+25	30	9	
3	260	216.7	30	25	250	-45+32	-45+32	40	8	
4	340	150	76.7	18.3	150	-45+32	-45+32	30	6	
5	260	250	76.7	5	216.7	-45+32	-32+25	20	7	38.30
6	180	183.3	30	11.7	150	-45+32	-32+25	40	7	
7	340	183.3	53.3	25	216.7	-45+32	-45+32	30	9	25.66
8	260	216.7	76.7	5	183.3	-45+32	-32+25	40	9	18.91
9	180	150	76.7	5	216.7	-75+45	-45+32	20	9	37.34
10	100	183.3	76.7	18.3	216.7	-75+45	-45+32	40	8	71.56
11	100	150	30	18.3	250	-75+45	-45+32	10	7	21.16
12	340	183.3	30	11.7	150	-45+32	-45+32	10	9	
13	260	150	53.3	5	150	-75+45	-45+32	40	8	17.16
14	100	216.7	100	25	216.7	-45+32	-45+32	20	6	
15	180	250	76.7	25	150	-75+45	-45+32	10	8	25.90
16	180	183.3	76.7	11.7	250	-75+45	-32+25	30	6	62.19
17	100	250	100	11.7	250	-45+32	-32+25	30	9	
18	180	250	53.3	18.3	250	-75+45	-32+25	20	8	56.52
19	340	216.7	76.7	25	250	-75+45	-32+25	10	9	20.25
20	180	216.7	100	18.3	150	-75+45	-32+25	30	9	
21	260	183.3	100	25	183.3	-45+32	-45+32	10	7	38.97
22	100	216.7	53.3	11.7	150	-75+45	-45+32	20	7	32.56
23	260	150	100	11.7	250	-45+32	-45+32	10	8	40.05
24	340	250	100	5	183.3	-75+45	-45+32	30	8	
25	100	250	76.7	11.7	183.3	-45+32	-45+32	40	6	43.15
26	260	250	53.3	11.7	216.7	-75+45	-45+32	10	6	61.81
27	340	216.7	53.3	18.3	183.3	-45+32	-32+25	10	6	
28	100	150	76.7	18.3	150	-45+32	-32+25	20	8	73.84
29	100	216.7	30	5	183.3	-75+45	-45+32	30	7	36.31
30	340	250	30	18.3	216.7	-75+45	-32+25	40	6	
31	180	183.3	53.3	5	250	-45+32	-45+32	30	6	31.23
32	100	216.7	30	5	216.7	-45+32	-32+25	10	8	40.84
33	180	183.3	100	5	150	-75+45	-32+25	10	6	39.07
34	260	150	30	25	183.3	-75+45	-32+25	20	6	
35	180	250	30	18.3	183.3	-45+32	-45+32	20	9	47.02

Run #	ST D (mm)	PG (slpm)	N2 %	CG (slpm)	Current (A)	LSM Size	YSZ Size	Feed rate (g/min)	Nozzle (1/16")	YSZ Rel DE (%)
36	180	150	100	25	216.7	-45+32	-32+25	40	7	51.75
37	340	150	53.3	5	250	-45+32	-32+25	20	7	6.82
38	260	250	53.3	25	150	-45+32	-32+25	30	7	
39	340	216.7	100	18.3	250	-75+45	-45+32	40	7	
40	340	183.3	100	11.7	183.3	-75+45	-32+25	20	8	7.13

Table 6: 9-4-40 Uniform Design Grid.

The runs highlighted in red represent runs that were not performed either because the conditions will not be suitable for the deposition of the LSM or YSZ (due either to decomposition of the LSM or insufficient melting of the YSZ) or are physically impossible (e.g. require a flow rate of N_2 higher than the system is capable of achieving). These combinations of conditions are included in the grid because of the algorithms used to ensure uniformity in the experimental design and the desire to avoid excluding any combinations which may produce promising coatings. However, these runs will represent gaps in the response data (coating porosity, composition, etc.) and will prevent us from performing regression analyses on the data collected from this set of experiments.

The factors which appeared to have the most significant, direct, influence on the coating composition are the standoff distance, plasma gas composition, and relative particle size. The gun current, plasma gas flow rate, carrier gas flow rate, feed rate, and nozzle diameter appear to be less important, though they may play a significant role in higher order interactions which will be considered in future experiments.

Shortening the standoff distance substantially improves the relative DE of YSZ while appearing to have much less effect on the LSM. The average YSZ relative DE was 46.3% at 100mm, 40.2 % at 180mm, 23.9% at 260mm, and 7.5% at 340mm (coatings not considered viable due to low plasma energy were counted as 0% DE). These numbers are not directly comparable due to the fact that each standoff distance was not a uniformly distributed subset, but rather only a part of a larger Uniform Design, and the necessity to exclude some trials due to equipment limitations. Nevertheless, it does give some idea as to the effect of increasing standoff distance. The average coating thickness showed a similar trend, decreasing from an average of over 71μm at 100mm to just over 21μm at 340mm. Standoff distance also appears to have a significant effect on the coating porosity, which appears in most cases to be related to the coating composition. The greater the proportion of YSZ in the coating, the higher the porosity generally appears to be. The LSM phase morphology in the coating seems to be relatively independent of standoff distance for relatively energetic plasma conditions (>~20kJ/l); in all cases it appears very

melted with little porosity. Standoff distance will, however, determine the lower bound of plasma energy at which it is possible to produce an LSM coating at all. At 100mm and 180mm it was possible to produce reasonably good LSM coatings at plasma energy densities as low as 11 or 12 kJ/l. At 260mm nearly 17 kJ/l was required and at 340mm nearly 20 kJ/l was needed to successfully deposit LSM.

The plasma gas composition also appears to have a significant effect on the relative deposition efficiency of the YSZ. Higher nitrogen contents generally produce coatings containing a greater percentage of YSZ, though this effect can be overwhelmed by variation in other parameters. Higher nitrogen content also causes the LSM phase in the coating to appear more melted, thus lowering the apparent coating porosity. This is offset, however, in the coatings produced at shorter standoff distances by porosity generated by the higher YSZ content, as shown in Figures 22 and 23. The coatings produced with high plasma nitrogen content at higher standoff distances that contained little YSZ appear to have very low porosity (<5%) and consist almost entirely of highly melted LSM, as seen in Figures 24 and 25.

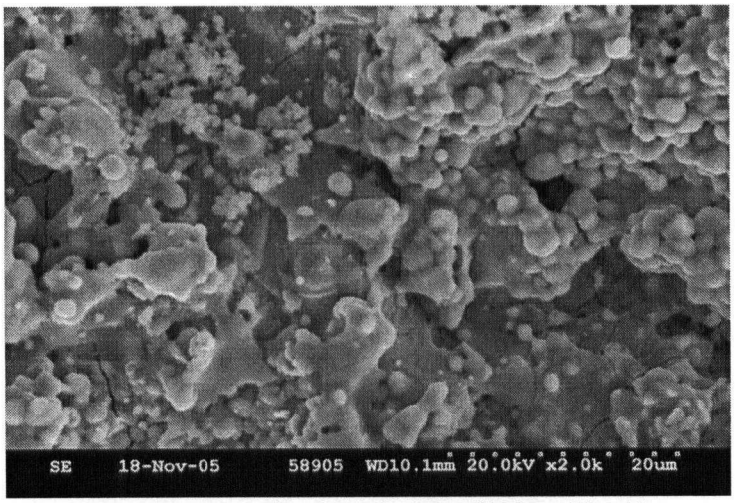

Figure 22: Micrograph of surface of coating #16 from UD table, containing 33.8 wt% YSZ, 15.6% porosity.

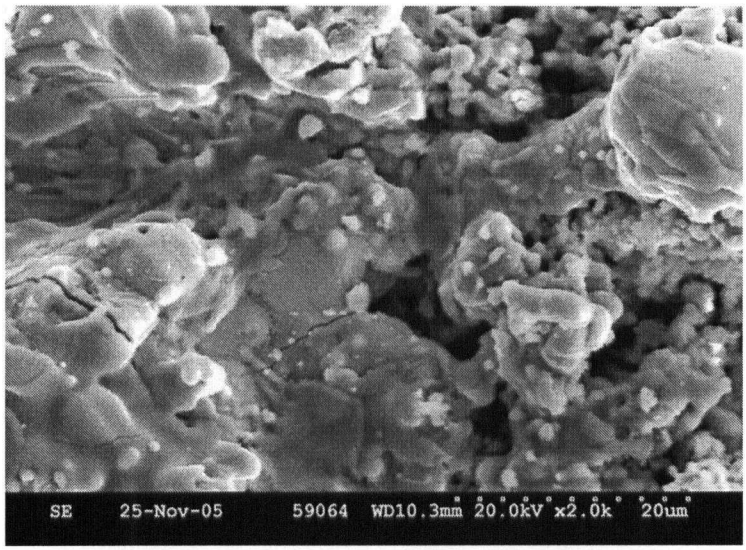

Figure 23: Micrograph of surface of coating #10 from UD table, containing 36.9 wt% YSZ, 12.5% porosity.

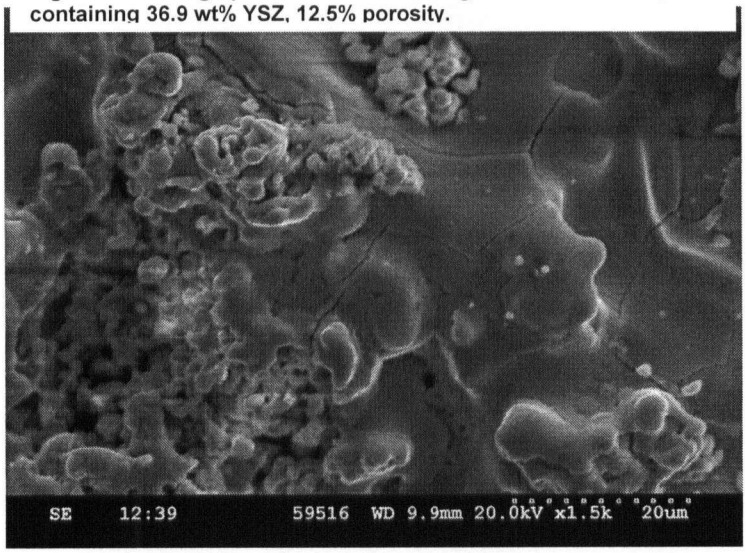

Figure 24: Micrograph of surface of coating #8 from UD table, containing 31.7 wt% YSZ, 4.0% porosity.

The particle size of the two materials also seems to play an important role in the relative deposition efficiency by partially compensating for the large difference in melting temperature between the LSM and YSZ. By using large LSM particles (-75+45μm) and small YSZ particles (-32+25μm) the relative deposition efficiency of the YSZ is increased. Unfortunately, the resulting powder mixture from using two very different particle sizes causes the segregation into layers of each of the two materials in the powder hopper during feeding as a resulting from the hopper vibration. The coatings resulting from these mixtures also appear less uniform, with large LSM splats and finer YSZ structures, as seen in Figure 26. The remaining four parameters included in this experimental grid do not appear to have a significant direct influence on the coating composition or microstructure, though they may become important when higher order and multiple parameter interactions are considered.

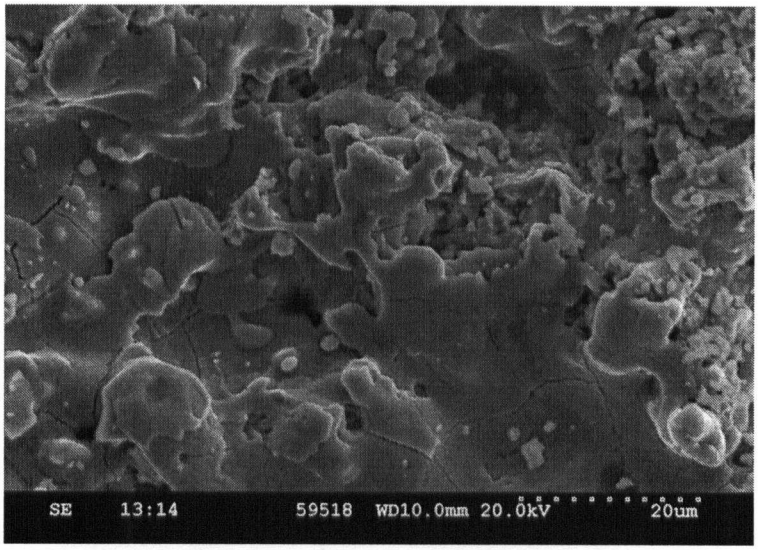

Figure 25: Micrograph of surface of coating #19 from UD table, containing 14.3 wt% YSZ, 4.5% porosity.

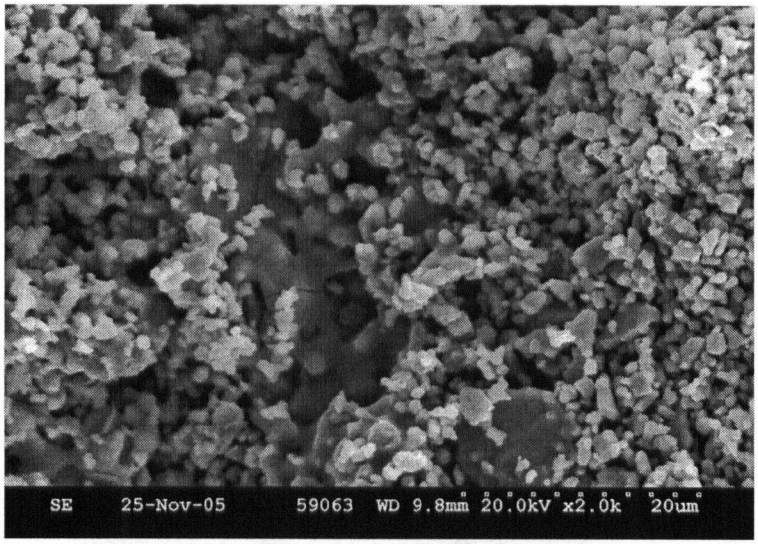

Figure 26: Micrograph of surface of coating #1 from UD table, containing 29.4 wt% YSZ, 16.3% porosity.

The coatings which appear the best in terms of both microstructure and composition are those produced in low energy plasmas at small standoff distances, as shown in Figures 27 and 28. The low energy allows the LSM in the coating to remain somewhat porous as a result of not having fully melted in the plasma, while the short standoff distance allows more YSZ to reach the substrate in a partially molten state. This combination of parameters results in coatings that are reasonably good in terms of composition and have the highest levels of porosity measured (17%-19%). Identifying the most significant parameters and their effect on the properties of these LSM/YSZ composite coatings, along with the most suitable deposition conditions, are the most significant achievements of this preliminary optimization study.

Future tests will also consider the use of an organic pore former, which would be particularly useful for those coatings produced in energetic plasmas and which contain a lot of YSZ, but appear to have very low porosity due to the LSM phase being completely molten upon impact. There were also several "anomalous" coatings that contained significantly more YSZ and appeared to have better microstructure than other coatings produced under very similar conditions. Examples are shown in Figures 29 and 30.

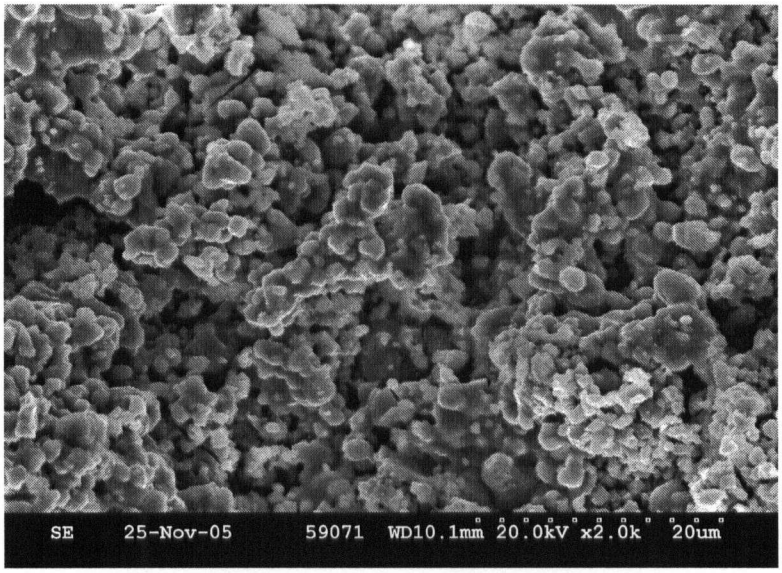

Figure 27: Micrograph of surface of coating #32 from UD table, containing 25.1 wt% YSZ, 18.6% porosity.

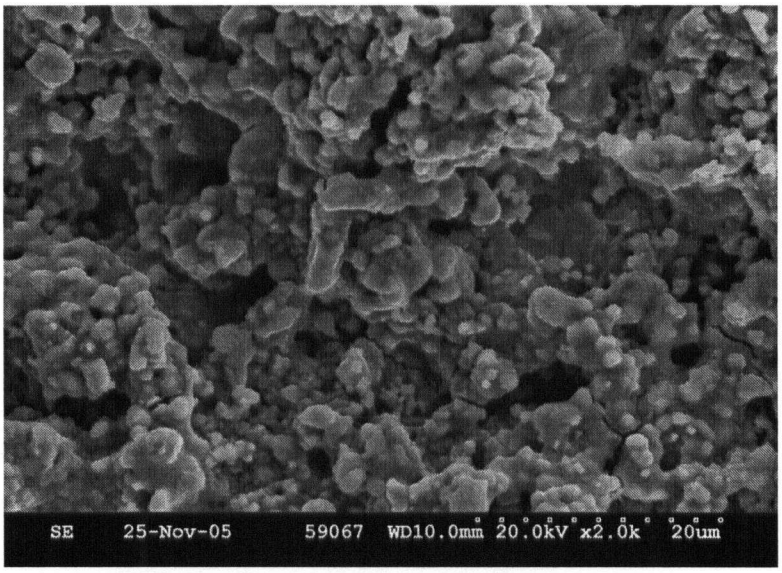

Figure 28: Micrograph of surface of coating #25 from UD table, containing 26.1 wt% YSZ, 16.7% porosity.

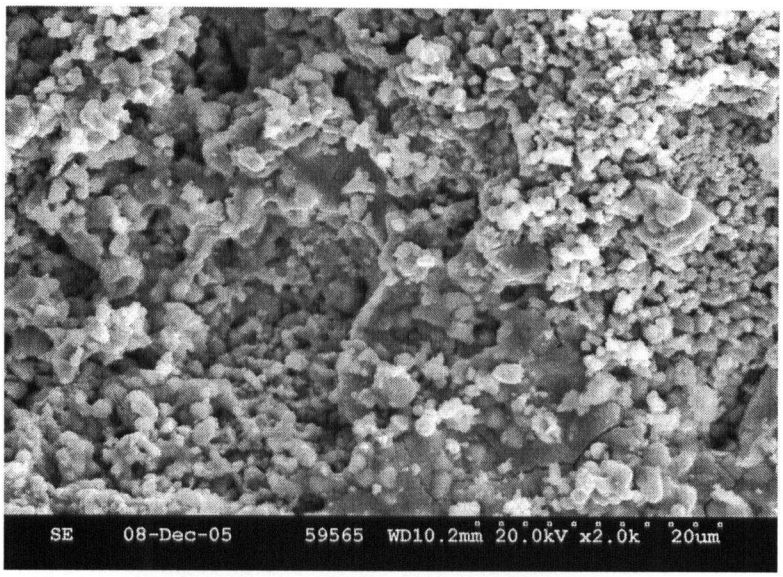

Figure 29: Micrograph of surface of coating #26 from UD table, containing 33.6 wt% YSZ, 11.0% porosity.

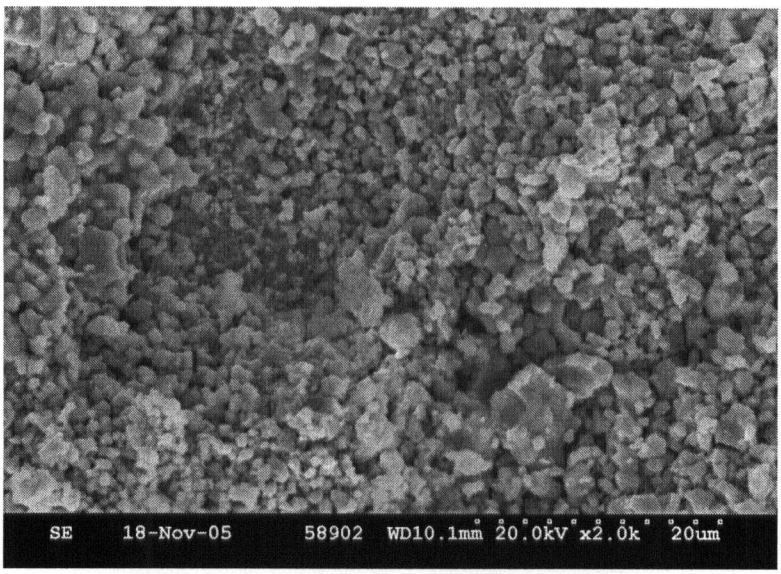

Figure 30: Micrograph of surface of coating #35 from UD table, containing 30.1 wt% YSZ, 8.9% porosity.

7.0 Cathode Electrochemical Evaluation

7.1 Introduction

The next step was to produce cathode-cathode symmetric cells on YSZ electrolyte substrates for electrochemical evaluation of representative coatings produced in the experimental study discussed above using EIS. These tests were designed to assess the coating quality based on electrochemical performance in order to confirm the previous evaluation of coating quality based on the appearance of the microstructure.

7.3 Experimental Procedure

The circular YSZ pellets used as substrates were produced from uniaxially pressed powder (Inframat Advanced Materials, Farmington, CT, USA). The powder was pressed in a 32mm diameter die using between 6-8 tonnes of pressure. The pellets were then sintered to produce substrates with a diameter of ~23mm and a thickness of ~1.5mm. After sintering, various methods were used to roughen the pellet surface to improve coating adhesion. These are discussed in more in the results section. Fabrication of the symmetric cells involved the deposition of cathode coatings using identical conditions on either side of the pellet in two sequential runs. Electrode alignment, which is essential for accurate EIS measurements, was ensured by using the circular substrate holder/mask shown in Figure 15. As before, the coatings were examined using SEM and EDX to evaluate their microstructure and composition and image analysis to asses their porosity.

Prior to mounting the cells on the test stand, LSM slurry was applied to the surface of each cathode to act as a current collecting layer and to reduce the contact resistance between the electrodes and platinum mesh on the test stand. Several different LSM slurry recipes, based on a recipe previously used for YSZ tape casting, were developed and tested to evaluate their suitability for use in this application. The slurry recipe eventually selected for use formed the strongest and most flexible bond when dried, ensuring good contact between the current collector and platinum mesh until the organic components have been burned out of the slurry. The recipe used was as follows: 50.9 wt% LSM powder (<32μm), 3.8 wt% graphite, 12.7 wt% ethanol solvent, 15.3 wt% toluene solvent, 0.8 wt% fish oil dispersant, 6.4 wt% polyvinyl butyral binder, and 10.1 wt% butyl benzyl phthalate plasticizer. Graphite powder was added to the LSM slurry to ensure good porosity in the current collecting layer.

Electrochemical testing was carried out using a 1" test stand (AMEL, Italy) with EIS measurements (SI 1260 frequency response analyzer, Solartron Analytical, Farnborough, UK) to determine the electrodes' polarization resistance and activation energy taken at four

temperatures between 715°C and 950°C in an ambient air atmosphere. Impedance measurements were carried out at OCV with an AC voltage amplitude of 100 mV over a range of frequencies between 1 MHz and 0.1-0.01 Hz, depending on the measurement temperature.

7.4 Results and Discussion

It was immediately discovered that coatings produced on the YSZ substrates had significantly different microstructures than those produced on steel substrates using identical plasma conditions, as seen in Figure 31. The coating produced on steel appears to have a much more porous microstructure with more discrete particles of LSM visible. The coating produced on YSZ, on the other hand, appears much more melted and less porous (11.1% porosity on zirconia vs. 18.6% on steel).

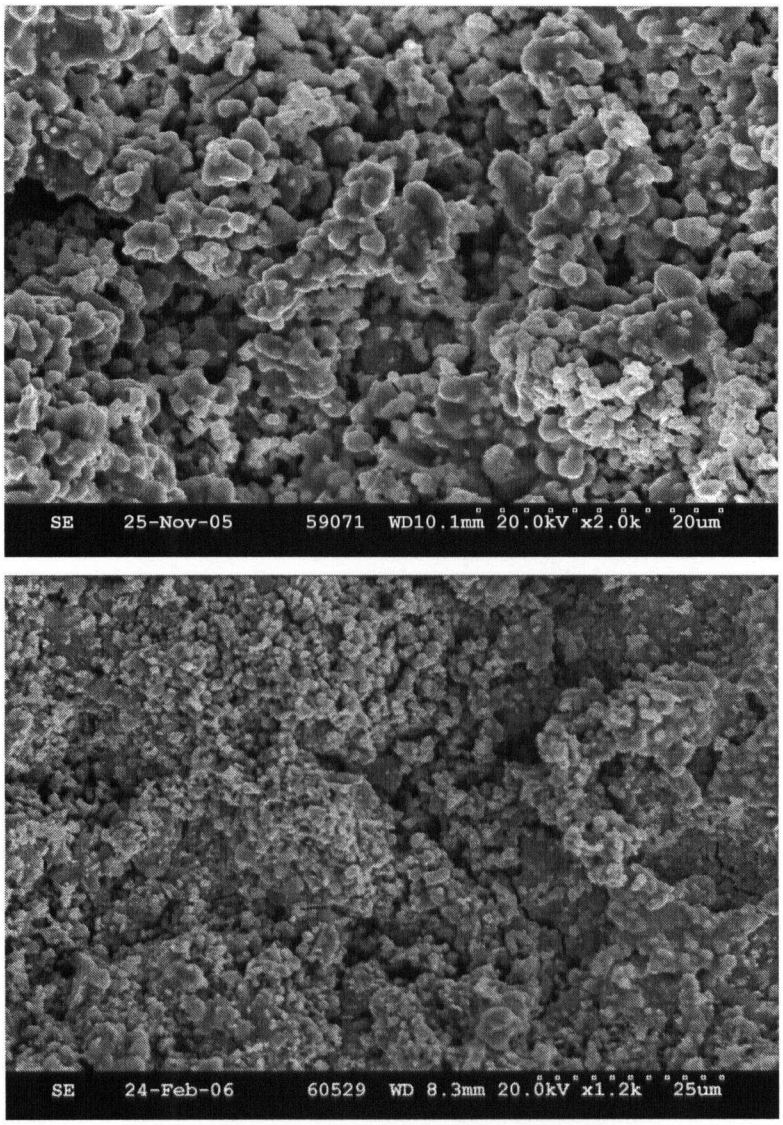

Figure 31: Top surface of LSM/YSZ coatings produced under identical conditions (30%N_2, 100mm, 217A, 217slpm) on (bottom) zirconia and (top) stainless steel.

This seems likely to be the result of the different heat conduction rates of the two substrate materials, with the steel having much higher heat conductivity, resulting in faster cooling rates for the deposited particles, leading ultimately to faster solidification of the plasma sprayed particles upon impact. The cross section of the coating produced on zirconia also shows that the coating porosity appears rather low (Figure 32).

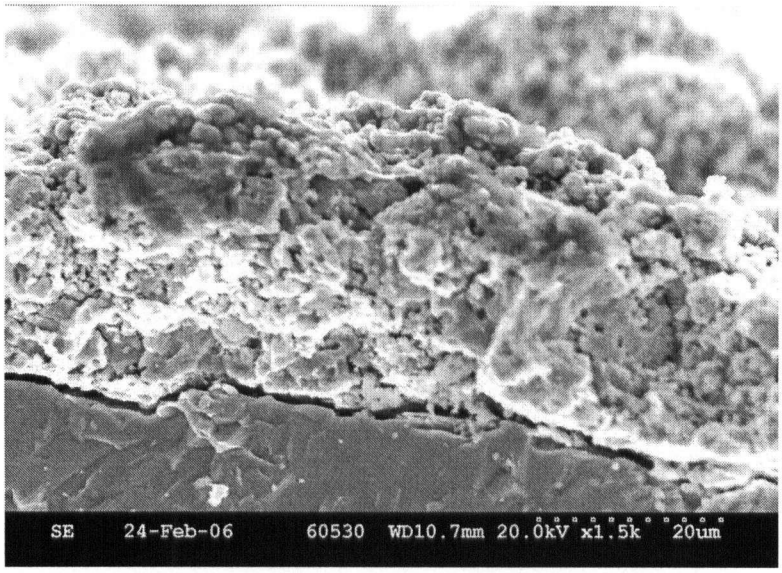

Figure 32: Cross section of coating produced on zirconia substrate at 30%N_2, 100mm, 217A, 217slpm.

Other issues also arose related to the use of zirconia substrates. Frequent breakage of the zirconia electrolytes occurred during deposition. This tended to occur more frequently with thinner substrates due to their lower strength. The breakage of the cells appears ultimately to be caused by excessive heating of the substrates during spraying, rather than by mechanical stress. Measurements taken of the substrate surface temperature with an infrared pyrometer immediately following spraying showed a strong correlation between this temperature and the likelihood of substrate fracture. Substrates with surface temperatures above ~150°C immediately following spraying were nearly always found to be fractured. Fractures always occurred in the same location, directly through the middle of the part of the substrate exposed to the plasma flame. Below this temperature the probability of fracture seemed to be reduced, though not zero; indicating that a critical temperature may exist for these substrates which should not be exceeded in order to reduce the probability of substrate breakage. In some cases substrates that were not fractured during spraying were found to be substantially weakened and were easily broken during handling. Plasma energy, torch standoff distance, and spray time were found to strongly influence the substrate surface temperature and therefore the likelihood of the electrolyte fracturing. At short standoff distances, ~100mm, only low energy plasmas (generally containing no more than

40% N_2) could be successfully used. At longer standoff distances, higher plasma energies could be used, but the N_2 content still needed to be below approximately 70 vol%.

Problems were also encountered related to coating adhesion on the YSZ substrates. Coatings deposited on YSZ using conditions identical to those used for steel produced much thinner and more poorly adhered coatings. This problem seemed to stem from the smoothness of the zirconia pellet surface compared to the sandblasted surface of the steel substrates. Using coarse sandpaper (80 grit) to roughen the substrate surface seemed to offer some improvement over the original surface, but the coating thickness and adhesion was still inferior to that of the coatings on the steel. It was found, however, that sandblasting of the YSZ substrates prior to deposition allowed for coatings of comparable thickness and adhesion to those sprayed on the steel to be produced.

Further experiments involving a variety of different deposition conditions were successful in producing a number of coatings on zirconia with significantly different microstructures. However, none of the conditions explored were successful in reproducing what appeared to be the best microstructures found using steel substrates. A selection of the coatings produced can be seen in Figures 33-36.

Those microstructures largely represent the types of microstructures that were found to be possible to produce on zirconia. The coatings in Figures 33 and 34 are relatively porous, having been produced in low-intermediate plasma energy. The coating pictured in Figure 35 was produced in a low energy plasma, resulting in a very thin coating with some bare substrate visible. The coating shown in Figure 36 was produced in a high energy plasma and appears to have lower porosity due to the presence of a large quantity of completely melted LSM. For each of these coatings, the relative deposition efficiency of the YSZ was quite high, 40 - 50%, resulting in coatings containing 40 - 50 vol% YSZ.

To compare the electrochemical performance of these various cathode microstructures a series of symmetric cell (cathode-cathode) impedance tests were performed on these cathodes. For these tests, cathodes were deposited on both sides of the zirconia electrolyte using identical plasma spray conditions. The powder mixtures used to create each coating were adjusted to yield a final coating composition of ~50 vol.% each of YSZ and LSM. It was found that the coating produced using the conditions shown for Figure 33 could not be deposited without fracturing the substrate due to excessive heating from the plasma, and was therefore not tested. The other three coatings were successfully deposited on both sides of the zirconia substrates.

For the symmetric cell deposited using low energy plasma conditions (Figure 35), some substrate was still visible as it was not fully covered by the plasma sprayed cathode. It is therefore quite likely that some of the applied LSM slurry would be in direct contact with the electrolyte and would be electrochemically active. As the LSM slurry would produce a cathode with very different properties from the plasma sprayed electrodes, the performance of this cell would not be directly comparable to that of the cells in which only the plasma sprayed layer is electrochemically active.

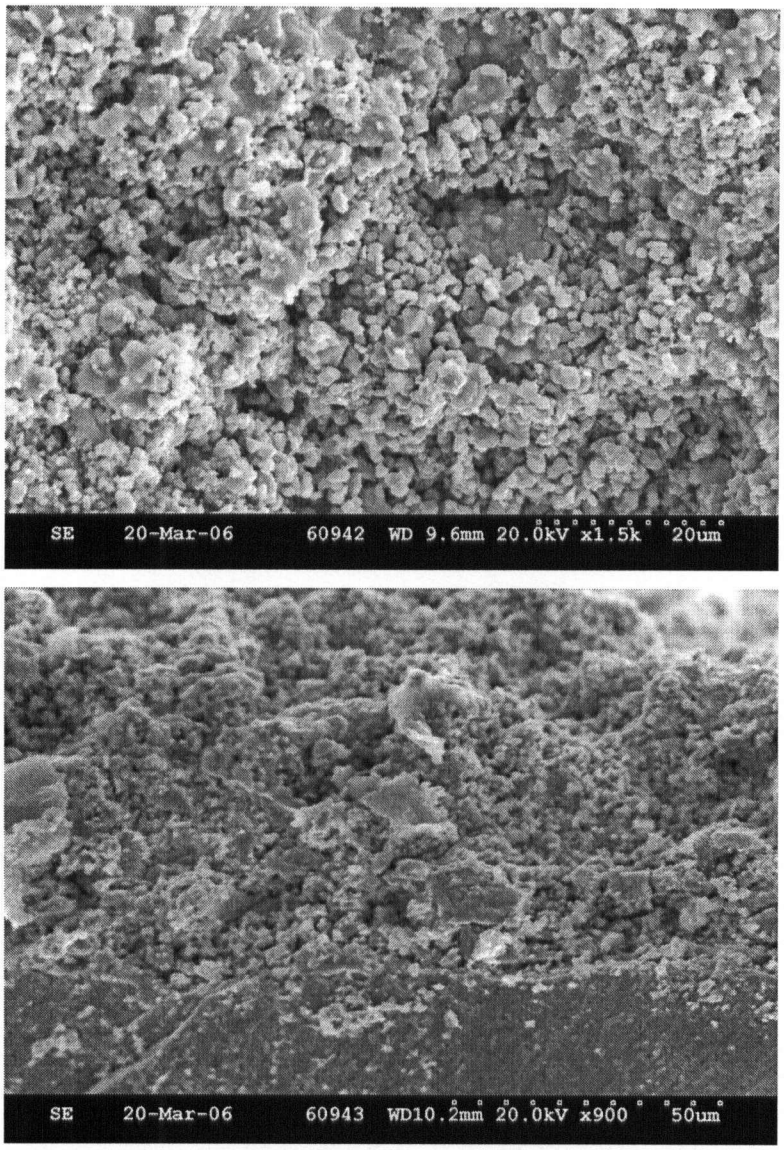

Figure 33: Top surface (top) and cross section (bottom) of a LSM/YSZ composite cathode deposited on a thick YSZ electrolyte (100mm, 220 slpm, 30%N_2, 250A, -45+32µm LSM, -32+25µm YSZ), 10.5% porosity.

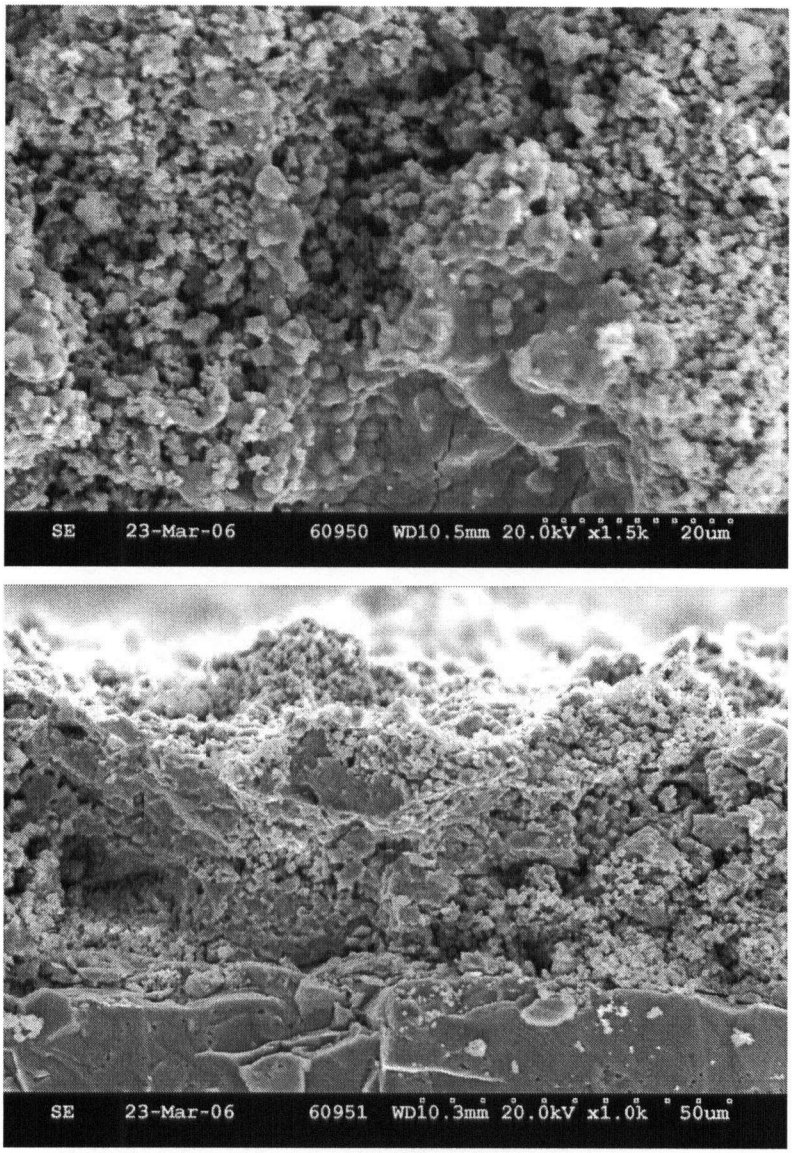

Figure 34: Top surface (top) and cross section (bottom) of a LSM/YSZ composite cathode deposited on a thick YSZ electrolyte (150mm, 200 slpm, 50%N_2, 220A, -75+45μm LSM, -45+32μm YSZ), 11.0% porosity.

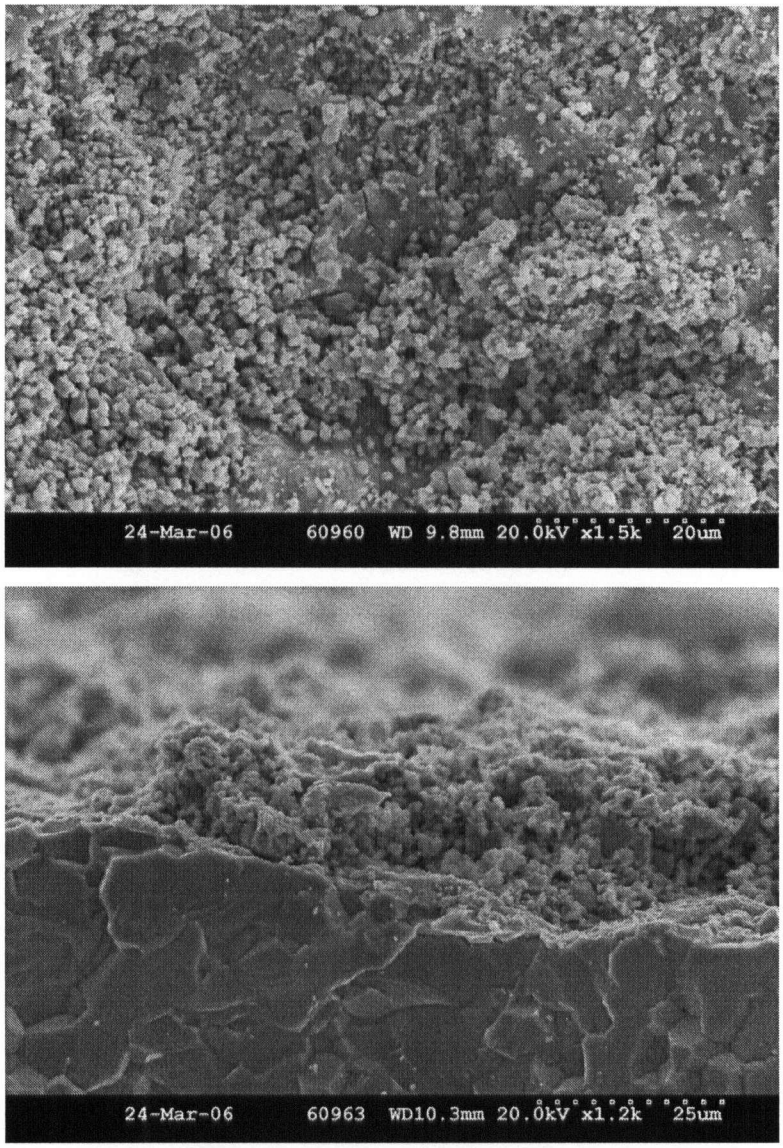

Figure 35: Top surface (top) and cross section (bottom) of a LSM/YSZ composite cathode deposited on a thick YSZ electrolyte (150mm, 220 slpm, 50%N_2, 150A, -75+45µm LSM, -45+32µm YSZ), 7.2% porosity.

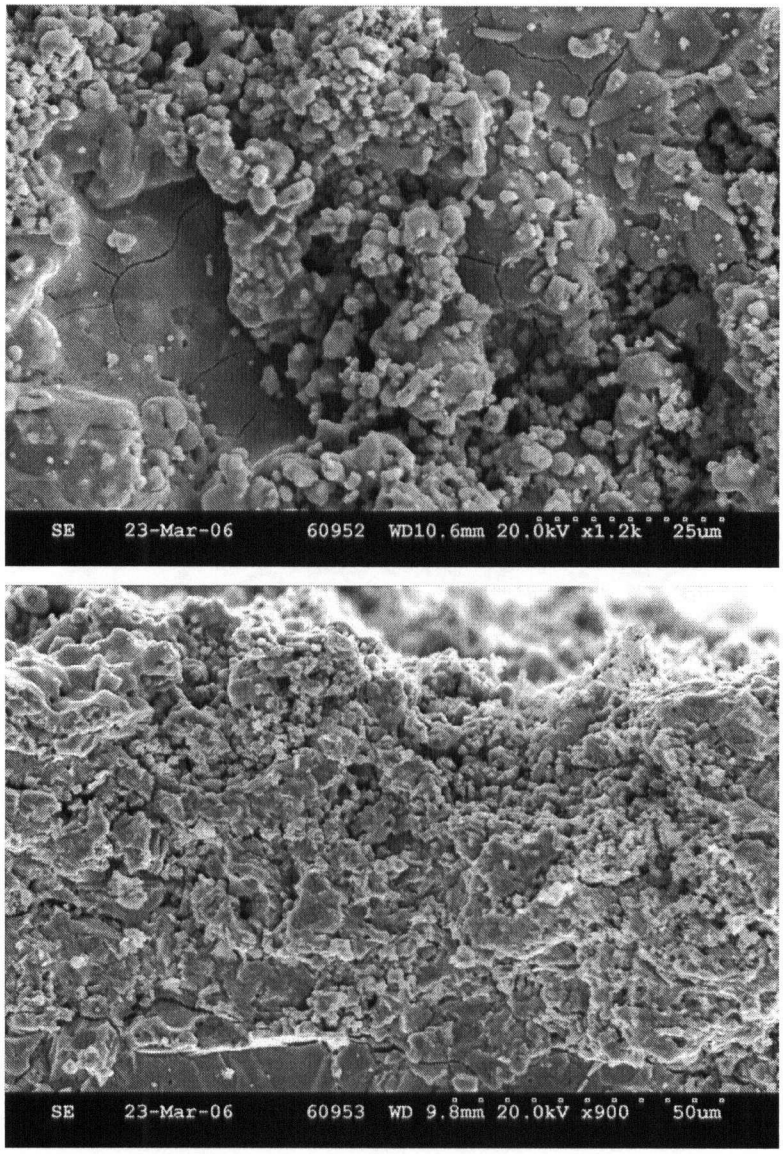

Figure 36: Top surface (top) and cross section (bottom) of a LSM/YSZ composite cathode deposited on a thick YSZ electrolyte (180mm, 180 slpm, 70%N_2, 220A, -75+45μm LSM, -32+25μm YSZ), 9.1% porosity.

The impedance spectra for the two cells tested at four of the temperatures examined can be seen in Figures 37-40. As expected, due to the higher internal surface area available for electrochemical activity at each temperature examined, the more porous (11.0%) cathode deposited in the lower N_2 plasma (Figure 34), had significantly lower polarization resistance (R_p) than the cathode processed using the more energetic plasma (Figure 36). As expected due to the logarithmic nature of variations in R_p with temperature, the relative difference between the R_p values for the two cells is much larger at higher temperatures. At 950°C the measured R_p for the low porosity coating (9.01 Ωcm^2) is nearly double that of the more porous coating (5.09 Ωcm^2). At 715°C the R_p of the less porous coating (260.24 Ωcm^2) is just 20% higher than that of the more

porous coating (216.74 Ωcm^2). At each temperature examined, the series resistance, R_s, was found to correspond generally with the expected resistance of the YSZ electrolyte.

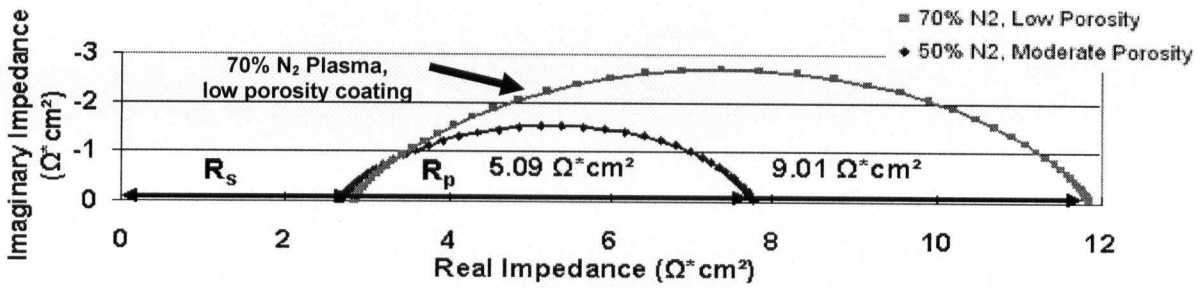

Figure 37: Electrochemical Impedance Spectra of LSM/YSZ cathode half cells tested at 950°C. 100mV AC amplitude, 1 MHz to 0.1 Hz frequency range.

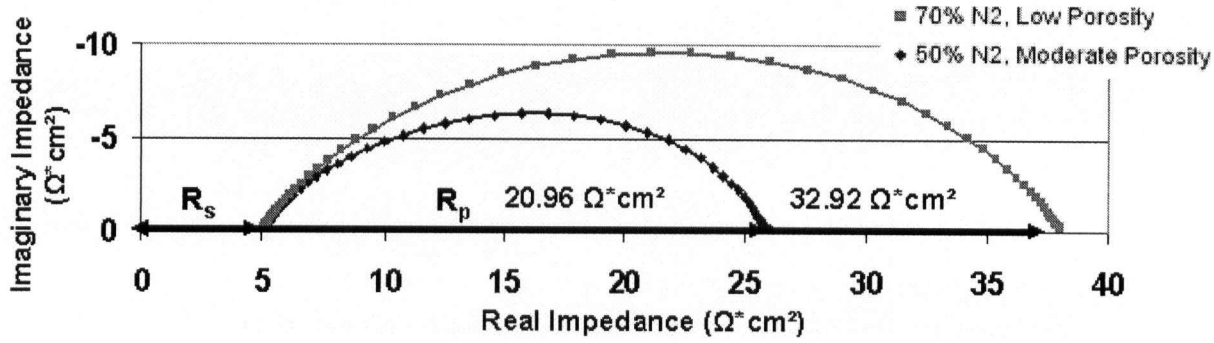

Figure 38: Electrochemical Impedance Spectra of LSM/YSZ cathode half cells tested at 860°C. 100mV AC amplitude, 1 MHz to 0.1 Hz frequency range.

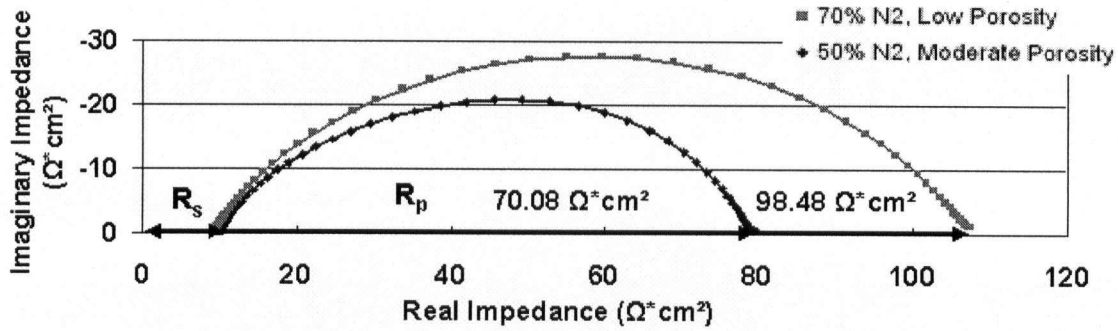

Figure 39: Electrochemical Impedance Spectra of LSM/YSZ cathode half cells tested at 780°C. 100mV AC amplitude, 1 MHz to 0.05 Hz frequency range.

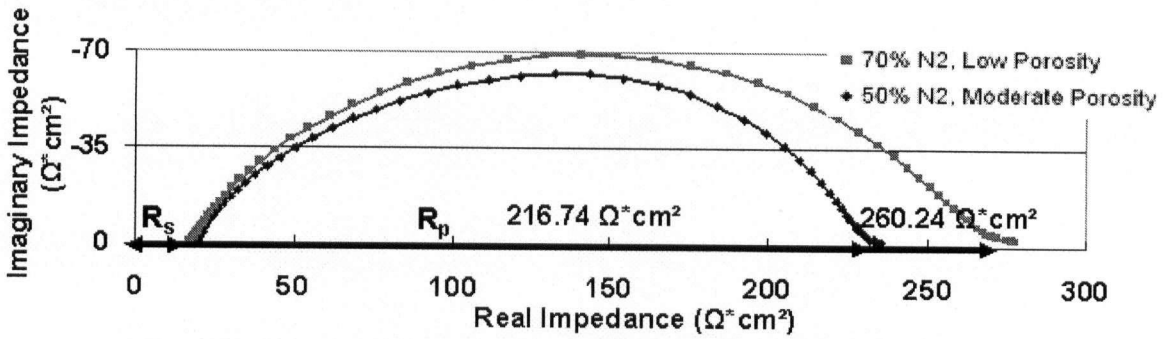

Figure 40: Electrochemical Impedance Spectra of LSM/YSZ cathode half cells tested at 715°C. 100mV AC amplitude, 1 MHz to 0.01 Hz frequency range.

From the linear nature of the plot of the logarithm of the area specific polarization resistance vs. 1/T (Figure 41) we can see that both symmetric cells display the expected Arrhenius behaviour. From the slope of this plot, the cathode activation energy can be calculated. In both cases it is approximately 1.5eV, suggesting that the polarization mechanism is the same in both cells.

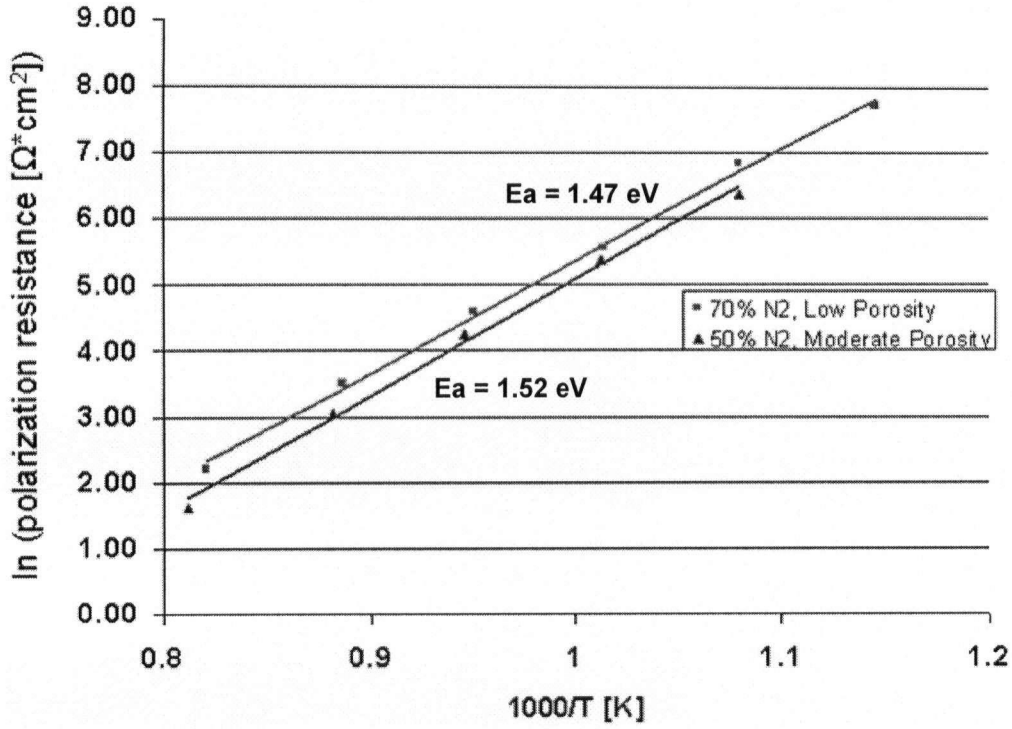

Figure 41: Arrhenius plot showing ASR vs. 1/T for both cells tested.

While the above results indicate that the coatings that appear to have the most promising microstructures do indeed perform the best, much further optimization is needed to approach the performance levels reported in the literature (<1 Ωcm^2 @ <900°C).

8.0 Symmetric Cell Production by APS

8.1 Introduction

In order to resolve the problems described above associated with the use of zirconia substrates for electrochemical testing, a procedure was developed for producing cathode-cathode symmetric cells entirely by APS supported by porous steel interconnects. This route offers four significant advantages over the use of dense, prefabricated, zirconia substrates. First, the properties of the porous metal substrates are closer to those of the metal substrates used in the initial composite cathode screening trials in which promising cathode structures were obtained, structures that have been irreproducible on the ceramic substrates. Secondly, the issue of substrate cracking during spraying is eliminated. This production method is also much closer to the technique that will ultimately be used to produce full cells by APS on metal interconnects, making these results more applicable to future work. Finally, the plasma sprayed electrolytes are significantly thinner (50-100μm) than the zirconia pellets previously used (1.5mm), giving significant performance improvements due to the reduction in ohmic resistance in the electrolyte. This approach will, however, limit electrochemical testing to short duration tests and relatively low temperatures (<800°C) in order to avoid excessive oxidation of the steel. Performance at higher temperatures can still be extrapolated, however, due to the linear nature of the Arrhenius ASR plots.

8.2 Experimental Procedure

In order to develop a procedure for the fabrication of the cathode-cathode symmetric cells, deposition was first carried out using solid stainless steel coupons. Cathodes were deposited onto the steel followed by a YSZ electrolyte deposited onto the cathode. In some cases a second cathode was deposited onto the electrolyte layer. Cathode layers were fabricated as before. Electrolyte layers were fabricated using 8YSZ powder with a particle size <25μm, the smallest size available. Small YSZ powder was used in order to achieve better particle melting in the hopes of producing a reasonably dense electrolyte layer. Electrolytes were deposited without hydrogen, using argon/nitrogen plasmas, in order to avoid the possibility of reduction of the previously deposited cathode layer. Numerous different deposition conditions were explored in order to find conditions most suitable for the deposition of the electrolytes. The deposited layers, both surfaces and polished cross sections, were examined by SEM. Symmetric cells were also deposited onto YSZ pellets in order to examine fractured cross sections.

Following the development of an appropriate production procedure, symmetric cells were then to be deposited onto porous metal substrates, 1" diameter 316ss discs, fabricated by powder metallurgy, with 49% porosity (Mott Corporation, Farmington, CT, USA).

8.3 Results and Discussion

The first attempts at depositing electrolyte layers examined the quality of the coatings produced using three different plasma compositions, 60%, 70%, and 80% N_2 by volume (balance Ar). All other parameters were held constant (200 slpm plasma gas, 150mm stand-off, 220 A, 20g/min powder feed rate). All three electrolytes utilized a common cathode (#32 from Table 6) with a thickness of approximately 50μm deposited on a solid steel coupon substrate. The electrolyte deposition conditions were chosen in order to reduce the heat load on the substrate while still providing enough power to melt the YSZ particles. Unfortunately, the electrolytes produced appeared to be rather thin in all cases (10-20μm) and not particularly dense.

A second set of electrolytes were produced using an 80% N_2 plasma, 250 A arc current and a plasma gas flow rate of 220 slpm. Standoff distance was maintained at 150mm to avoid excessive heating of the substrate. This electrolyte was then deposited onto three different cathodes (#'s 32, 18, and 10 from Table 6) which had been previously deposited onto the steel. Each of the cathodes deposited onto the steel had a thickness of approximately 50μm. Finally, another cathode layer identical to the first was deposited onto the electrolyte. These three cathodes were also deposited separately, to facilitate comparison between the cathodes deposited directly on steel and those deposited on top of the electrolyte. Upon examination of the cross sections of the symmetric cell coatings, it was observed that the majority of the thickness consisted only of YSZ electrolyte, with none of either cathode visible, as seen in Figure 42. The electrolyte also appears to still be rather porous. EDX mapping of the image indicated small patches of LSM present along the top and bottom of the electrolyte layer in each case. The thickness of the coating cross sections observed in the micrographs (~60 μm) was not in agreement with caliper measurements of the as sprayed coating, which indicated a coating thickness of approximately 100-120μm. As well, a continuous cathode layer is clearly visible on top of the electrolyte layer in the as sprayed coatings. These observations seem to indicate that the cutting and/or polishing of the coating cross sections caused significant potions of the cathode coatings to be removed.

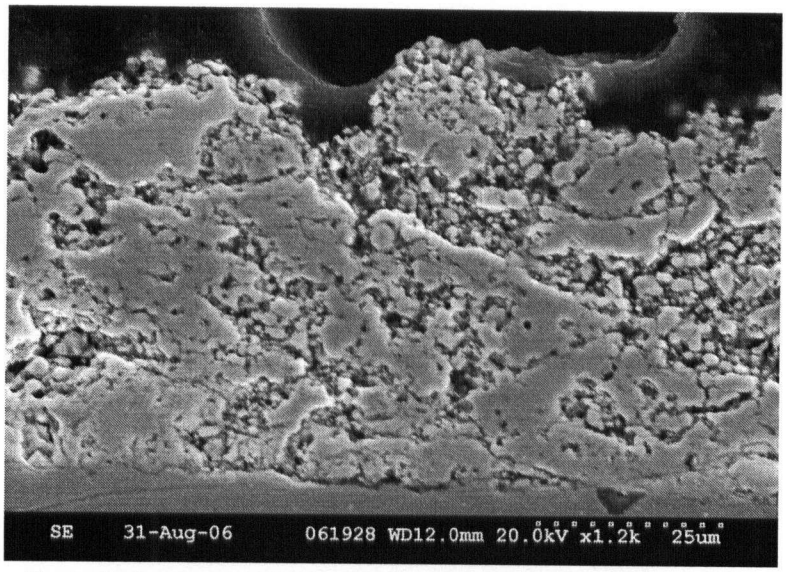

Figure 42: Cross section of plasma sprayed electrolyte (80% N_2, 220 slpm, 250 A, 150mm).

In order to avoid the introduction of microstructural changes caused by polishing of the coating cross sections, a symmetric cell was next deposited onto a sandblasted YSZ pellet which could be easily broken to allow the fracture cross section of the coatings to be examined. Due to the relatively poorer adhesion on YSZ substrates, the cathodes deposited only had a thickness of ~20μm using the same conditions that yielded a 50μm layer on the steel substrates. The cathodes were again deposited with previously used conditions (#32 from Table 3). The electrolyte deposition conditions were very similar to those used in the preceding experiment for the cross section examination on steel, only with a slightly lower plasma gas flow rate (200 slpm).

After spraying, the YSZ substrates that did not break during spraying were fractured. Caliper measurements indicated a total coating thickness of 100-120μm (caliper measurements of coating thicknesses on the YSZ substrates are less accurate than those on steel as the thickness of the YSZ substrates can vary substantially, ±100μm, across the disc). When the fractured cross sections were examined by optical microscopy and SEM, the coating appeared again to be mostly composed of YSZ electrolyte. However, EDX mapping indicated a thin (10-20μm), but continuous, cathode layer on top of the electrolyte. Surface imaging of the same sample confirms the presence of a continuous cathode layer. No cathode appeared to be present next to the substrate, though there was a 10-20μm gap where the electrolyte layer appeared to have delaminated from the substrate. It was suspected from these observations that while the cathode on top of the electrolyte appeared to be present, the bottom cathode was being removed during the deposition of the electrolyte layer. This was thought to be occurring due to the presence of un-melted YSZ particles impacting the cathode layer at high velocity and acting as an abrasive, much like sandblasting.

To remedy this problem, electrolyte deposition conditions were altered to result in YSZ particles being more melted and impacting at a slower speed. To reduce the YSZ particle velocity, the plasma gas and carrier gas flow rates were reduced to 150 slpm and 5 slpm respectively, and the nozzle diameter was increased from 1/2" to 9/16", the largest size diameter. To prevent YSZ particles from re-solidifying in flight, the standoff distance was decreased from 150mm to 120mm. Only one cathode, directly on the substrate, was deposited in this case. The electrolyte deposited using these conditions was approximately the same thickness (100μm) as those in the preceding experiments. However, when the sample was examined after spraying it was found that the entire coating had largely delaminated from the substrate and could be easily pealed off in one piece. No cathode coating was visible remaining on the substrate, however, a cathode was visible attached to the underside of the plasma sprayed electrolyte. Examination of this cathode revealed it to be approximately the same thickness as the originally sprayed cathode (20μm), as determined by caliper measurements. Inspection of the cathode surface revealed it to be continuous with no gaps in coverage through which the substrate was visible. It therefore seemed that the cathode layer was not removed by the electrolyte deposition, in this case, and that the adhesion between the cathode and electrolyte was quite good.

In light of this result, an attempt was made to spall the coating from the sample that was previously found to have a 10-20μm gap between the electrolyte and substrate at the fracture surface. Some small flakes of this coating were successfully obtained. These symmetric cell coating flakes, when examined, were found to have a cathode coating on both sides of the electrolyte. The cathodes both appeared to be approximately 20μm thick. Thus, it seemed the absence of a cathode coating adjacent to the substrate occurred only at the point of fracture, and that the three plasma sprayed layers are well adhered to one another. Since the adhesion of cathode coatings on metal substrates has been observed to be superior to that of the YSZ substrates, it is likely that the cathode layer is present as well in the samples prepared using the stainless steel coupons, and is not visible due to the effects of cutting or polishing. Still, the final set of conditions appear to be the best for the production of an electrolyte, as the coating appears to be the strongest (as evidenced by the obtaining of very large pieces of the coating intact) and is likely more dense due to the presence of more fully melted particles. A 50μm electrolyte coating produced using these conditions (-25μm YSZ, 150 slpm plasma gas, 100% N_2, 250 A, and 9/16" nozzle at 120mm) should be suitable for electrochemical testing of these symmetric cells.

Examination of the surface of cathodes deposited onto the substrate and cathodes deposited onto the electrolyte reveals that they are largely similar in appearance and composition, as seen

in Figure 43. It therefore appears that the assumption of cathode symmetry for the purposes of EIS testing may be reasonable.

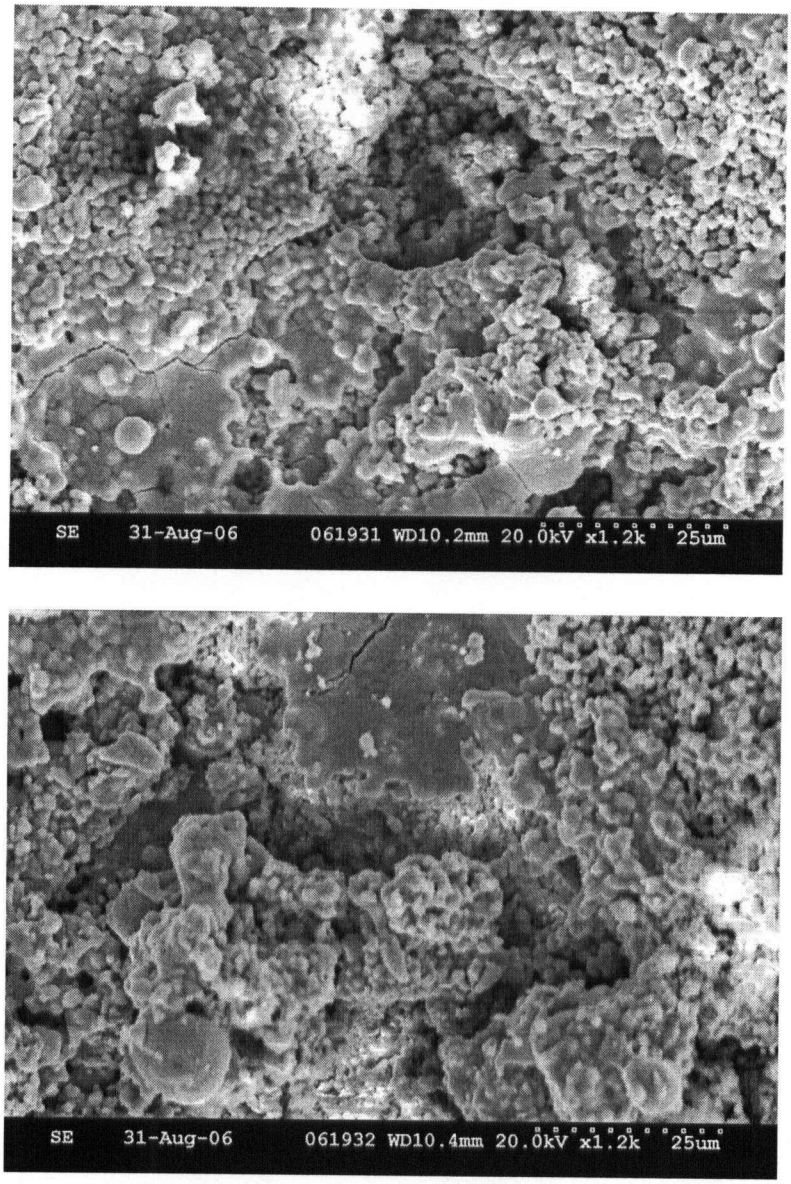

Figure 43: Surface view micrographs of cathodes deposited on substrate (top) and on plasma sprayed electrolyte (bottom). Coating compositions 31-35wt% YSZ and porosities 16-19%. Both cathodes deposited using -75+45μm LSM, -45+32μm YSZ, 183 slpm, 77% N_2, and 217A at 100mm.

Through the use of porous metal interconnect substrates, and the procedure developed above, it is possible to produce cathode-cathode symmetric cells in a suitable configuration for EIS testing. This allows for electrochemical evaluation, in addition to evaluations of microstructure and composition, for cells produced as part of future optimization studies.

9.0 Conclusion

9.1 Summary

The research described above represents the preliminary stages of inquiry into the development of an optimized LSM/YSZ composite cathode for SOFC's produced by APS. The initial work focussed on becoming familiar with the operation of the air plasma spray system, a complex piece of equipment, and determining the preparation required to ready the feedstock material for spraying. A series of screening tests were then performed with both materials (LSM and YSZ) individually, in order to determine the full range of deposition parameters over which it was possible to produce a coating with each material. The most significant discovery was that LSM deposition was not possible in the presence of a hydrogen containing plasma due to decomposition of the material. This had significant implications for the production of composite coatings due to the high melting point of the YSZ. These tests also provided valuable information and experience regarding the behaviour of the materials under a wide range of spraying conditions. From these data, it was possible to identify a region of overlap in the parameter ranges in which it was thought to be possible to successfully deposit both materials simultaneously.

The information from the screening tests was then used to produce a few trial composite cathodes using different conditions. Composite cathodes were successfully produced, though it was clear that the low deposition efficiency of the YSZ relative to the LSM was going to be a significant difficulty in the production of these coatings. From this first group of composite coatings, the one with the most promising microstructure was selected for electrochemical testing to confirm that the coatings produced would function as SOFC cathodes. While the performance of this cell was limited by a number of factors, including the quality of the cathode, the coating did function as a reasonable cathode.

The next step was to begin to explore the characteristics of composite cathode coatings produced over the full range of deposition conditions identified in the screening trials. The purpose of these tests was to identify the combinations of parameters which yielded the cathodes with the best microstructures and to determine which parameters most significantly affected coating quality. These tests were successful in obtaining a large number of composite cathodes with very different properties. The most promising of these coatings, with high porosity and sufficient YSZ content, were found to be produced at fairly low plasma energies and short standoff distances. Low plasma power allowed some partially melted LSM to be incorporated into the coating, generating significant porosity. Short standoff distances reduced the time of flight for

the powder particles and allowed YSZ to reach the substrate in a partially melted state and be incorporated into the coating. Additionally, coatings produced using similarly sized particles of LSM and YSZ were found to have the most uniform microstructural features.

Following these results, there was a desire to confirm, with electrochemical testing, that the coatings with best microstructures would indeed have the best performance in a fuel cell. For this purpose, these microstructures were to be reproduced as symmetric cells using YSZ pellets as substrates and electrolytes. However, it was found that these microstructures previously produced on steel substrates could not be reproduced on YSZ due to cracking of the substrates resulting from excessive heat loads and differences in heat conduction in the two substrates. Eventually, cathodes were successfully obtained on the YSZ substrates with substantially different microstructures, suitable for testing. EIS testing confirmed that the more porous cathode produced in a lower energy plasma had significantly better performance than the cathode with less porous microstructure resulting from more extensive particle melting during spraying.

The final work presented here was the development of a procedure for producing symmetric cells entirely by APS, eliminating the problems previously encountered while producing these cells using YSZ substrates. The principal challenge here was to determine appropriate conditions for the deposition of the YSZ electrolyte. Despite problems encountered in evaluating these cells, a suitable electrolyte was produced, along with two cathodes in a configuration suitable for EIS testing. When deposited onto porous metal substrates, this cathode-electrolyte-cathode symmetrical cell will allow for electrochemical evaluation, in addition to evaluation of the microstructure, of cathodes produced in future optimization studies.

The primary motivation behind producing SOFC cathodes by APS is to improve the speed and scalability of the manufacturing process while achieving performance comparable to, or exceeding, that achieved by more traditional fabrication routes. The work presented here has shown that there is the potential to realize these goals. The expectations of fabrication speed have been realized, with production times on the order of several minutes being typical for the cathodes produced. While no attempt has been made to scale up the process for simultaneous fabrication of multiple cells, the equipment on hand could be very easily modified to do so. While preliminary efforts at optimization of the cathodes have been made here, there remains much to be done in order to achieve the performance levels sought. The above research lays the groundwork for these future optimization studies to be carried out.

9.2 Recommendations for Future Work

The next work to be carried out will involve the reproduction of a set of representative microstructures, using the APS half cell production process developed, from the optimization study already performed. EIS testing of these cells will be used to quantify the performance of the different microstructures and further confirm our assessment of coating quality. This data will allow for a more refined cathode optimization study to be performed in the next stage of the project. Information from the first optimization study will permit a narrower range of parameter values to be examined and allow for better resolution with equal or fewer trials. Most notably, very high N_2 containing plasmas (>80%) and large standoff distances (>180mm) can likely be excluded in future studies.

Sufficient information should now be available to allow the studies to be designed in such a way that gaps in the experimental data can be eliminated, allowing for regression analysis to be performed on the data obtained. This will allow the relationship between variations in production parameters and variations in coating properties to be examined in much more detail and with more certainty. This should allow for better control over coating properties in the future. Finally, by applying half cell production process developed it will be possible to include electrochemical performance data, in addition to physical and microstructural properties, in the evaluation of the cathode coatings produced. This will allow for a more relevant determination of the quality of the cathodes produced in the study.

Using the optimized constant composition and microstructure cathode as a starting point, work could then commence on the development of functionally graded cathode layers. By modifying the composition and microstructural properties of the cathode across it's thickness it has been shown that substantial performance improvements can be obtained. The APS process should be well suited to the production of graded cathode layers. An optimization process conducted in a similar manner to those performed on the constant composition and microstructure cathodes could be carried out.

The optimized cathodes, both constant and graded, could also benefit from the application of new features and techniques. In particular a pure LSM current collecting layer should be developed. Such a layer, present between the composite cathode and the interconnect, should offer improved performance through reduced ohmic losses resulting from electrical resistance in the cathode layer. The application of liquid based suspension plasma spraying should also be investigated. Suspension spraying allows for the use of much finer starting particles and can be

used to produce microstructures with much finer features than are possible with powder based feedstocks.

As the ultimate goal of this project is the production of an entire SOFC by APS in a continuous deposition process, a major element in the future of this project is the integration of cathode production with the production of the electrolyte and anode. This will introduce a new set of considerations in the cathode design and will likely require compromises to be made between cathode performance and compatibility with the other layers. Full optimization of each layer in isolation from the others is not plausible if the goal of producing the best overall fuel cell by APS is to be reached. For example, the production of a thin plasma sprayed electrolyte could require a cathode with low surface roughness, a factor not previously considered. This would likely result in a stage of simultaneous iterative design of the multiple SOFC layers, fine tuning each until the best complete fuel cell has been produced.

References

[1] Schiller, G., Henne, R., Lang, M., Muller, M., "Development of Solid Oxide Fuel Cells (SOFC) for stationary and mobile applications by applying plasma deposition processes", Mat. Sci. Forum, Pt. 3, pp. 2539-44, 2003.

[2] Yokokawa, Harumi, "Recent Development of Solid Oxide Fuel Cells in Japan", Electrochemical Society Proceedings, Vol. 99-19, pp. 10-18, 1998.

[3] Matsushima, T., Ohrui. H.; Hirai, T.; "Development of Solid Oxide Fuel Cell with a New Structure", NTT-Review, V 9 N 5, pp. 76-82, 1997.

[4] England, Gordon, "Plasma Spray – Thermal Spray Coating Process", *http://www.gordonengland.co.uk/ps.htm*, retrieved October 2004.

[5] Ross, D.A., Patent US 5,008,511, April 6th, 1991.

[6] Karthikeyan, J., Berndt, C.C., Tikkanen, J., Reddy, S. and Herman, H., "Plasma spray synthesis of nanomaterial powders and deposits", Materials Science and Engineering A, Vol. 238, pp. 275-286, 1997.

[7] Xie, L., Ma, X., Jordan, E.H., Padture, P., Xiao, D.T. and Gell, M., "Identification of coating deposition mechanisms in the solution-precursor plasma-spray process using model spray experiments", Materials Science and Engineering A, Vol. 362, pp. 204-212, 2003.

[8] Sobolev, V.V. and Guilemany, J.M., "Flattening of Droplets and Formation of Splats in Thermal Spraying: A Review of Recent Work – Part 1", Journal of Thermal Spray Technology, (8)1, pp. 87-101, 1999.

[9] Smith, R.W., "Thermal Spray of Ceramic Materials", Fourth Euro Ceramics, Vol. 9, pp. 365-382, 1995.

[10] van den Frank, M.J. Berge, "Stork Materials Technology – Thermal Spray Processes", Stork Cellramic, Inc., http://www.storksmt.com/page7.html?p=4545, Milwaukee, Wisconsin, retrieved January 2005.

[11] Devasenapathi, A., Ng, H.W., Yu, S.C.M., and Indra, A.B., "Forming near net shape free-standing components by plasma spraying", *Materials Letters,* 57, pp. 882-886, 2002.

[12] Troczynski, Tom, "MTRL 482 Course Notes", University of British Columbia Dept. of Materials Engineering, 2004.

[13] Fauchais, P., Vardelle, M., Vardelle, A. and Bianchi, L., "Plasma Spray: Study of the Coating Generation", Ceramics International, 22, pp. 295-303, 1996.

[14] Sobolev, V.V. and Guilemany, J.M., "Flattening of Droplets and Formation of Splats in Thermal Spraying: A Review of Recent Work – Part 2", Journal of Thermal Spray Technology, (8)2, pp. 301-313, 1999.

[15] Kucuk, A., Lima, R.S., and Berndt, C.B., "Influence of Plasma Spray Parameters on In-Flight Characteristics of ZrO_2 – 8 wt% Y_2O_3 Ceramic Particles", J. Am. Ceram. Soc., 84, [4], pp. 685-692, 2001.

[16] Borisov, Yu., Murashov, A. and Saakov, A., "Effect of Different Factors on Plasma Spraying Efficiency and Metallization Pattern", Proc. 3rd National Thermal Spray Conference, Long Beach Ca., 1990.

[17] Osaki, Katashi, Fukumasa, Osamu, Fujimoto, Satoru and Kobayashi, Akira, "Plasma electrode-type plasma spray gun – effect of powder loading on the behaviour of plasma jet", Vacuum, 65, pp. 305-309, 2002.

[18] Fauchais, P., Vardelle, M., Vardelle, A., Prouix, P. and Boulos, M.I., "Loading effect by oxide powders in DC Plasma Jets", Proc. International Thermal Spray Conference & Exposition, Orlando Fl., pp. 321-332, 1992.

[19] Fauchais, Pierre, Vardelle, Michel, "Control of Plasma Spray Process", 10th International Ceramics Congress – Part C, pp. 543-547, 2003.

[20] Choi, B.L. and Hong, S.H., "Theoretical Investigations on Sprayed Particle-Plasma Interactions to Optimize Processing Parameters in D.C. Thermal Plasma Spraying", Materials and Manufacturing Processes, Vol. 12, No.2, pp. 309-328, 1997.

[21] Fincke, J.R., Swank, W.D., "Air Plasma Spraying of Zirconia: Spray Characteristics and Standoff Distance Effect on Deposition Efficiency and Porosity", Proc. International Thermal Spray Conference & Exposition, Orlando Fl., 1992.

[22] Cetegen, B.M. and Yu, W., "In-Situ Particle Temperature, Velocity, and Size Measurements in DC Arc Plasma Thermal Sprays", ASM International, JTTEE5 8, pp. 57-67, 1998.

[23] Parker, Ron, and Allor, Richard, "Imaging pyrometer for monitoring the surface temperature of a spray-formed steel billet", *Proceedings of SPIE - The International Society for Optical Engineering*; vol. 4360, pp. 80-89, 2001.

[24] Leblanc, L. and Moreau, C., "The Long-Term Stability of Plasma Spraying", ASM International, JTTEE5 11, pp. 380-386, 2001.

[25] Leblanc, L., Moreau, C., Gougeon, P., "Investigation of the Long-Term Stability of Plasma Spraying by Monitoring Characteristics of the Sprayed Particles", *Thermal Spray: A United Forum for Scientific and Technological Advances,* ASM International, Materials Park, Ohio, USA, pp. 567 – 574, 1997.

[26] Northwest Mettech Corp., http://www.mettech.com/, 2004, Retrieved October 2004.

[27] Minh, Nguyen Quang and Takahashi, Takehiko, *Science and Technology of Ceramic Fuel Cells,* Elsevier, 1995.

[28] Minh, Nguyen Q., "Ceramic Fuel Cells", *J. Am. Ceram. Soc.,* 76, [3], pp. 563-588, 1993.

[29] Mogensen, Mogens, Jensen, Karin Vels, Jørgensen, Mette Juhl, and Primdahl, Søren, "Progress in understanding SOFC electrodes", *Solid State Ionics,* 150, pp. 123– 129, 2002.

[30] Fleig, Jurgen, "Solid Oxide Fuel Cell Cathodes: Polarization Mechanisms and Modeling of the Electrochemical Performance", *Annu. Rev. Mater. Res.* 33, pp. 361– 82, 2003.

[31] Virkar, Anil V., Chen, Jong, Tanner, Cameron W., and Kim, Jai-Woh, "The role of electrode microstructure on activation and concentration polarizations in solid oxide fuel cells", *Solid State Ionics,* 131, pp. 189–198, 2000.

[32] Murray, Erica P., Tsai, Tsepin, Barnett, Scott A., "Oxygen Transfer Processes in (La,Sr)MnO_3/Y_2O_3 – stabilized ZrO_2 cathodes: an impedance spectroscopy study", *Solid State Ionics*, 110, pp. 235-243, 1998.

[33] Jiang, S.P., "Issues on development of (La,Sr)MnO3 cathode for solid oxide fuel cells", *Journal of Power Sources*, 124, pp. 390–402, 2003.

[34] Kuznecov, M., Otschik, P., Obenaus, P., Eichler, K., Schaffrath, W., " Diffusion controlled oxygen transport and stability at the perovskite/electrolyte interface", *Solid State Ionics,* 157, pp. 371-378, 2003.

[35] Horita, Teruhisa, Yamaji, Katsuhiko, Sakai, Natsuko, Yokokawa, Harumi, Kawada, Tatsuya, Kato, Tohru, "Oxygen reduction sites and diffusion paths at $La_{0.9}Sr_{0.1}MnO_{3-x}$/ yttria-stabilized zirconia interface for different cathodic overvoltages by secondary-ion mass spectrometry", *Solid State Ionics*, 127, pp. 55–65, 2000.

[36] Juhl, Mette, Primdahl, Seren, Manon, Carrie, and Mogensen, Mogens, "Performance / structure correlation for composite SOFC cathodes", *Journal of Power Sources*, 61, pp. 173-181, 1996.

[37] Barbucci, A., Bozzo R., Cerisola G., Costamagna, P., "Characterisation of composite SOFC cathodes using electrochemical impedance spectroscopy. Analysis of Pt/YSZ and LSM/YSZ electrodes", *Electrochimica Acta*, 47, pp. 2183 – 2188, 2002.

[38] Jùrgensen, M.J., Primdahl, S., Mogensen, M., "Characterisation of composite SOFC cathodes using electrochemical impedance spectroscopy", *Electrochimica Acta*, 44, pp. 4195 – 4201, 1999.

[39] Lee, You-Kee, Kim, Jung-Yeul, Lee, Young-Ki, Kim, Insoo, Moon, Hee-Soo, Park, Jong-Wan, Jacobson, Craig P., and Visco, Steven J., "Conditioning effects on $La_{1-x}Sr_xMnO_3$-yttria stabilized zirconia electrodes for thin-film solid oxide fuel cells", *Journal of Power Sources,* 115, pp. 219–228, 2003.

[40] Fukunaga, Hiroshi, Ihara, Manabu, Sakaki, Keiji, and Yamada, Koichi, "The relationship between overpotential and the three phase boundary length", *Solid State Ionics*, 86-88, pp. 1179-1185, 1996.

[41] Tsai, Tsepin, and Barnett, Scott A., "Effect of LSM-YSZ cathode on thin-electrolyte solid oxide fuel cell performance", *Solid State Ionics*, 93, pp. 207-217, 1997.

[42] Herbstritt, D., Weber, A., and Ivers-Tiffee, E., "Modelling and DC-polarisation of a three dimensional electrode/electrolyte interface", *Journal of the European Ceramic Society*, 21, pp. 1813–1816, 2001.

[43] Choi, Jin H., Jang, Jong H., Ryu, Ji H., and Oh, Seung M., "Microstructure and cathodic performance of $La_{0.9}Sr_{0.1}MnO_3$ electrodes according to particle size of starting powder", *Journal of Power Sources,* 87, pp. 92–100, 2000.

[44] Ostergard, M. J. L., Clausen, C., Bagger, C., and Mogensen, M., "Manganite-Zirconia Composite Cathodes for SOFC: Influence of Structure and Composition, *Electrochimica Acta.*, Vol. 40., No. 12, pp. 1971-1981, 1995.

[45] Holtappels, P., Bagger, C., "Fabrication and performance of advanced multi-layer SOFC cathodes", *Journal of the European Ceramic Society,* 22, pp. 41–48, 2002.

[46] Liu, Ying, Compson, Charles and Liu, Meilin, "Nanostructured and functionally graded cathodes for intermediate temperature SOFCs", *Fuel Cells Bulletin*, v 2004, n 10, pp. 12-15, October, 2004.

[47] Stöver, D., Buchkremer, H.P., Uhlenbruck, S., "Processing and properties of the ceramic conductive multilayer device solid oxide fuel cell (SOFC)", *Ceramics International,* 30, pp. 1107–1113, 2004.

[48] Ohrui, Himeko, Matsushima, Toshio, and Hirai, Toshiro, "Performance of a solid oxide fuel cell fabricated by co-firing", *Journal of Power Sources,* 71, pp. 185-189, 1998.

[49] Kamata, Hiroyuki, Hosaka, Akio, Mizusaki, Junichiro, and Tagawa, Hiroaki, "High temperature electrocatalytic properties of the SOFC air electrode $La_{0.8}Sr_{0.2}MnO_3$/YSZ", *Solid State Ionics,* 106, pp. 237–245, 1998.

[50] Charojrochkul, S., Choy, K.L., and Steele, B.C.H., "Flame assisted vapour deposition of cathode for solid oxide fuel cells. 1. Microstructure control from processing parameters", *Journal of the European Ceramic Society*, 24, pp. 2515–2526, 2004.

[51] Matsuzaki, Yoshio, and Yasuda, Isamu, "Relationship between the steady-state polarization of the SOFC air electrode, $La_{0.6}Sr_{0.4}MnO_{3+\delta}$/YSZ, and its complex impedance measured at the equilibrium potential", *Solid State Ionics*, 126, pp. 307–313, 1999.

[52] Kleitz, M. and Petitbon, F., "Optimized SOFC electrode microstructure", *Solid State Ionics,* 92, pp. 65-74, 1996.

[53] Steele, B.C.H., Hori, K.M., and Uchino, S., "Kinetic parameters influencing the performance of IT-SOFC composite electrodes", *Solid State Ionics*, 135, pp. 445–450, 2000.

[54] Leng, Y.J., Chan, S.H., Khor, K.A., and Jiang, S.P., "Performance evaluation of anode-supported solid oxide fuel cells with thin film YSZ electrolyte", *International Journal of Hydrogen Energy*, 29, pp. 1025 – 1033, 2004.

[55] Charpentier, P., Fragnaud, P., Schleich, D.M., and Gehain E., "Preparation of thin film SOFCs working at reduced temperature", *Solid State Ionics,* 135, pp. 373–380, 2000.

[56] de Souza, Selmar, Visco, Steven J., and C. De Jonghe, Lutgard, "Thin-film solid oxide fuel cell with high performance at low temperature", *Solid State Ionics,* 98, pp. 57–61, 1997.

[57] Basu, Rajendra N., Tietz, Frank, Wessel, Egbert, and Stöver, Detlev, "Interface reactions during co-firing of solid oxide fuel cell components", *Journal of Materials Processing Technology,* 147, pp. 85–89, 2004.

[58] Harta, N.T., Brandon, N.P., Daya, M.J., and Lapena-Rey, N., "Functionally graded composite cathodes for solid oxide fuel cells", *Journal of Power Sources*, 106, pp. 42–50, 2002.

[59] Matsuzaki, Yoshio, and Yasuda, Isamu, "Electrochemical properties of reduced-temperature SOFCs with mixed ionic–electronic conductors in electrodes and/or interlayers", *Solid State Ionics,* 152–153, pp. 463– 468, 2002.

[60] Wang, S., Kato, T., Nagata, S., Kaneko, T., Iwashita, N., Honda, T., and Dokiya, M. "Electrodes and performance analysis of a ceria electrolyte SOFC", *Solid State Ionics*, 152– 153, pp. 477– 484, 2002.

[61] Murray, E. Perry, Sever, M.J., and Barnett, S.A., "Electrochemical performance of $(La,Sr)(Co,Fe)O_3$–$(Ce,Gd)O_3$ composite cathodes", *Solid State Ionics*, 148, pp. 27– 34, 2002.

[62] Huang, Keqin, Hou, Peggy Y., and Goodenough, John B., "Characterization of iron-based alloy interconnects for reduced temperature solid oxide fuel cells", *Solid State Ionics,* 129, pp. 237–250, 2000.

[63] Matsuzaki, Yoshio and Yasuda, Isamu, "Electrochemical properties of a SOFC cathode in contact with a chromium-containing alloy separator", *Solid State Ionics*, 132, pp. 271–278, 2000.

[64] Jianga, S.P., Zhangb, J.P., and Zhengb, X.G., "A comparative investigation of chromium deposition at air electrodes of solid oxide fuel cells", *Journal of the European Ceramic Society,* 22, pp. 361–373, 2002.

[65] Žadvydas, Marius, Tamulevičius, Sigitas, and Grinys, Tomas, "Relation Between the YSZ Powder Properties and Vacuum Plasma Spray Deposited Layers", *Materials Science (Medžiagotyra),* Vol. 10, No. 4., pp. 349-352, 2004.

[66] Li, Chang-Jiu, Li, Cheng-Xin, and Ning, Xian-Jin, "Performance of YSZ electrolyte layer deposited by atmospheric plasma spraying for cermet-supported tubular SOFC", *Vacuum,* 73 pp. 699–703, 2004.

[67] Li, Chang-Jiu, Ning, Xian-Jin, and Li, Cheng-Xin, "Effect of densification processes on the properties of plasma-sprayed YSZ electrolyte coatings for solid oxide fuel cells", *Surface & Coatings Technology,* 190, pp. 60– 64, 2005.

[68] Okumura, K., Aihara, Y., and Kawasaki, S., "Development of Thermal Spraying-Sintering Technology for Solid Oxide Fuel Cells", *Journal of Thermal Spray Technology*, 9(3), pp. 354-359, 2000.

[69] Khor, K.A., Yu., L.G., Chan, S.H., and Chen, X.J., "Densification of plasma sprayed YSZ electrolytes by spark plasma sintering (SPS)", *Journal of the European Ceramic Society,* 23, pp. 1855-1863, 2003.

[70] Zhang, H., Ma, X., Dai, J., Hui, S., Roth, J., Xiao, T.D., and Reisner, D.E., "Structure and Electrochemical Behaviour of Plasma-Sprayed LSGM Electrolyte Films", *Materials Research Society Symposium Proceedings,* Vol. 756, pp. 491-496, 2003.

[71] Hui, S., Ma, X., Zhang, H., Dai, J., Roth, J., Xiao, T.D., and Reisner, D.E., "Plasma Sprayed LSGM Electrolyte For Intermediate Temperature Solid Oxide Fuel Cells", *Electrochemical Society Proceedings,* Vol. 2003-07, pp. 330-339, 2003.

[72] Nie, Huaiwen, Huang, Wenhua, Wen, Ting-Lian, Tu, Hengyong, and Zhan, Zhongliang, "LSM Cathodes for SOFC Prepared by Plasma Spraying", Journal *of Materials Science Letters,* 21, pp. 1951-1953, 2002.

[73] Barthel, Knut, and Rambert, Serge, "Processing and Electrochemical Behaviour of LSM-YSZ Composite Cathodes by Vacuum Plasma Spraying", *3rd European Solid Oxide Fuel Cells Forum,* pp. 11-18, 1998.

[74] Barthel, K., and Rambert, S., "Thermal Spraying and Performance of Graded Composite Cathodes as SOFC-Component", *5th International Symposium on Functionally Graded Materials,* pp. 800-805, 1998.

[75] Barthel, K., Rambert, S., and Siegmann, St., "Microstructure and Polarization Resistance of Thermally Sprayed Composite Cathodes for Solid Oxide Fuel Cell Use", *Journal of Thermal Spray Technology,* Vol. 9(3), pp. 343-347, 2000.

[76] Tai, Lone-Wen and Lessing, Paul A., "Plasma Spraying of Porous Electrodes for a Planar Solid Oxide Fuel Cell", *J. Am. Ceram. Soc.*, 74, pp. 501-504, 1991.

[77] Marinković, Z.V., Mančić, L., Cribier, J.F., Ohara, S., Fukui, T., and Milošević, O., "Nature of structural changes in LSM-YSZ nanocomposite material during thermal treatments", *Materials Science and Engineering A,* 375–377, pp. 615–619, 2004.

[78] Bertrand. G., Meunier, C., Bertrand, P., and Coddet, C., "Dried particle plasma spray in-flight synthesis of spinel coatings", *Journal of the European Ceramic Society*, 22, pp. 891-902, 2002.

[79] Batawi, E., Honegger, K., Diethelm, R., Wettstein, M., "The Selection and Optimisation of Thermally Sprayed Perovskite-Based Coatings for Improved Long-Term Electrochemical Performance", 2nd Eur. *SOFC Forum Proc.,* pt. 1, Vol. 1, pp. 307-314, 1996.

[80] Fendler, E., Henne, R., Ruckdaschel, R., Schmidt, H., "Protecting Layers for the Bipolar Plates of Planar Solid Oxide Fuel Cells Produced by Vacuum Plasma Spraying", *2nd Eur. SOFC Forum Proc.*, pt. 1, Vol. 1, pp. 269 – 277, 1996.

[81] Schiller, G., Henne, R., Ruckdaeschel, R., "Vacuum Plasma Sprayed Protective Layers for Solid Oxide Fuel Cell Application", *J. Adv. Mat.*, vol. 32, no. 1, pp. 3-8, 2000.

[82] Schiller, G., Henne, R., and Lang, M., "Development of Plasma Sprayed Components for a new SOFC design", *Proc. 5th Int: Symp. SOFC - SOFC V.*, pp. 635-44, 1997.

[83] Schiller, G., Henne, R., Lang, M., and Müller, M., "Development of Solid Oxide Fuel Cells by Applying DC and RF Plasma Deposition Technologies", *Fuel Cells,* 4, No. 1-2, pp. 56-61, 2004.

[84] Franco, Thomas, Henne, Rudolf, Lang, Michael, Metzger, Patrick, Schiller, Günter, Szabo, Patric, and Ziehm, Sebastian, "Metallic Components for a Plasma Sprayed Thin-film SOFC Concept", *Electrochemical Society Proceedings,* Volume 2003-07, pp. 923-931, 2003.

[85] Lang, Michael, Franco, Thomas, Henne, Rudolf, Metzger, Patrick, Schiller, Günter, and Ziehm, Sebastian, "Electrochemical Characterisation of Vacuum Plasma Sprayed SOFCs on Different Porous Metallic Substrates", *Electrochemical Society Proceedings,* Volume 2003-07, pp. 1059-1067, 2003.

[86] Lang, M., Franco, T., Schiller, G., and Wagner, N., "Electrochemical characterization of vacuum plasma sprayed thin-film solid oxide fuel cells (SOFC) for reduced operating temperatures", *Journal of Applied Electrochemistry*, 32, pp. 87-874, 2002.

[87] Schiller, G., Henne, R., Lang, M., Ruckdaeschel, R., and Schaper, S., "Fabrication of Thin-Film SOFC by Plasma Spray Techniques", *4th Eur. SOFC Forum Proc.*, Vol. 1, pp. 37-46, 2000.

[88] Schiller, Günter, Henne, Rudolf H., Lang, Michael, Ruckdäschel, Robert, and Zentrum, Deutsches, "Development of vacuum plasma sprayed thin-film SOFC for reduced operating temperature", *Fuel Cells Bulletin*, vol. 3, No. 21, pp. 7-12, 2000.

[89] Henne, R., Lang, M., Muller, M., and Schiller, G., "Thermal Plasma Deposition Technologies for Producing Advanced High Temperature Fuel Cells of SOFC-type", Czechoslovak Journal of Physics, 52, pp. D896-D904, 2002.

[90] Chen, H.C., Heberlein, J., and Henne, R., "Integrated Fabrication Process for Solid Oxide Fuel Cells in a Triple Torch Plasma Reactor", *Journal of Thermal Spray Technology,* vol. 9(3), pp. 348-353, 2000.

[91] Gitzhofer, Francois, Boulos, Maher, Heberlein, Joachim, Henne, Rudolf, Ishigaki, Takamasa, and Yoshida, Toyonobu, "Integrated Fabrication Processes for Solid-Oxide Fuel Cells using Thermal Plasma Spray Technology", *MRS Bulletin*, vol. 25, no. 7, pp. 38-42, 2000.

[92] Nikravech, Mehrdad, Rousseau, Frederic, Marvan, Daniel, and Amouroux, Jacques, "Development of Cathode Materials by Plasma Process at Room Temperature", *Electrochemical Society Proceedings,* Volume 2003-07, pp. 414-421, 2003.

[93] Notomi, Akira, and Hisatome, Nagao, "Application of plasma spraying to solid oxide fuel cell production", *Pure&Appl. Chem.,* vol. 68, No. 5, pp. 1101-1106, 1996.

[94] Nagata, M., Iwasawa, C., Yamaoka, S., Seino, Y., and Ono, M., "Development of Self-supporting Air Electrode SOFC", *Proc. 4th Int. Symp. SOFC - SOFC-IV*, pp. 173-179, 1995.

[95] Hui, Shiqiang, Ma, Xinqing, Zhang, Heng, Chen, Hhuimin, and Roth, Jeffery, "Solid oxide fuel cell components and method of manufacture thereof", Patent WO 03/075383 A2, September 12th, 2003.

[96] Ma, X.Q., Hui, S., Zhang, H., Dai, J., Roth, J., Xiao, T.D., and Reisner, D.E., "Intermediate Temperature SOFC Based on Fully Integrated Plasma Sprayed Components", *Thermal Spray 2003,* pp. 163-168, 2003.

[97] Zheng, R., Zhou, X.M., Wang, S.R., Wen, T.-L., and Ding, C.X., "A Study of Ni+8YSZ/8YSZ/$La_{0.6}Sr_{0.4}CoO_{3-\delta}$ ITSOFC fabricated by atmospheric plasma spraying", *Journal of Power Sources,* 140, pp.217-225, 2005.

[98] Fehringer, G., Janes, S., Wildersohn, M., and Clasen, R., "Proton—conducting ceramics as electrode/electrolyte—materials for SOFCs: Preparation, mechanical and thermal-mechanical properties of thermal sprayed coatings, material combination and stacks", *Journal of the European Ceramic Society,* 24, pp. 705–715, 2004.

[99] *NIST/SEMATECH e-Handbook of Statistical Methods*, http://www.itl.nist.gov/div898/handbook/, accessed April 25th, 2005.

[100] Willen, W.S., "Parametric Sensitivities of Copper-Nickel-Indium and Inconel 718 Plasma Spray Coatings", *Proc. 4th National Thermal Spray Conference,* pp. 21-28, 1991.

[101] Walter, J., and Riggs, W.L., "Plasma Spray Coating Parameter Development", *Proc. 3rd National Thermal Spray Conference,* pp. 729-746, 1990.

[102] Steeper, T.J., Rotolico, A.J., Nerz, J.E., Riggs, W.L., Varacalle Jr., D.J., and Wilson, G.C., "A Taguchi Experimental Design Study of Plasma Sprayed Alumina-Titania Coatings", *Proc. 4th National Thermal Spray Conference,* pp. 13-20, 1991.

[103] Novinski, Edward R., Rotolico, A.J., and Cove, Edward J., "Process Parameter Impact in the Physical Properties of an Advanced Abradable Coating", *Proc. 3rd National Thermal Spray Conference,* pp. 151-158, 1990.

[104] Huston, Roberta P., "Role of Designed Experiments to Evaluate Factors that Influence Measured Properties of Sprayed Coatings", *Proc. 3rd National Thermal Spray Conference,* pp. 675-680, 1990.

[105] Box, George, Bisgaard, Søren, and Fung, Conrad, "An Explanation and Critique of Taguchi's Contributions to Quality Engineering", *Quality and Reliability Engineering International,* 4, pp. 123-131, 1988.

[106] Bisgaard, Søren, "(Invited Paper) Optimizing Thermal Spray Processes Going Beyond Taguchi Methods", *Proc. 3rd National Thermal Spray Conference,* pp. 661-667, 1990.

[107] Hermanek, F., and Riggs, W.L., "Iterative Design of Experiments to Optimize Plasma Sprayed Chrome Carbide/Nickel Chromium", *Proc. 3rd National Thermal Spray Conference,* pp. 695-710, 1990.

[108] Chon, T., Nerz, J.E., Kushner Jr., B.A., Rotolico, A.J., and Riggs, W.L., "Design of Experimental Study of Plasma Sprayed Chromium Carbide/Nickel Chromium and Aluminum Oxide Coatings", *Proc. 4th National Thermal Spray Conference,* pp. 3-11, 1991.

[109] Box, George E.P., and Draper, Norman R., *Empirical Model Building and Response Surfaces*, John Wiley & Sons, New York, 1987.

[110] Fang, Kai-Tai, Lin, Dennis, K.J., Winker, Peter, and Zhang, Yong, "Uniform Design: Theory and Application", *Technometrics,* vol. 42, no. 3, pp. 237-248, 2000.

[111] Fang, Kai-Tai, "Theory, Method and Applications of the Uniform Design", *International Journal of Reliability, Quality and Safety Engineering,* vol. 9, no. 4, pp. 305-315, 2002.

[112] Li, Runze, "Model Selection for Analysis of Uniform Design and Computer Experiment", *International Journal of Reliability, Quality and Safety Engineering,* vol. 9, no. 4, pp. 367-381, 2002.

[113] Jiping, Shao, Bochu, Wang, Meisheng, Liu, Hongyang, Zhang, Xin, Chen and Chuanren, Duan, "Optimal designs for sound wave simulation on the growth conditions of Chrysanthemum callus", *Colloids and Surfaces B: Biointerfaces,* 30, pp. 93-98, 2003.

[114] Li., J.F., Liao, H., Normand, B., Cordier, C., Maurin, G., Foct, J., and Coddet, C., "Uniform design method for optimization of process parameters of plasma sprayed TiN coatings", *Surface Coatings and Technology,* 176, pp. 1-13, 2003.

[115] Li, J.F., Liao, H.L., Ding, C.X., and Coddet, C., "Optimizing the plasma spray process parameters of yttria stabilized zirconia coatings using a uniform design of experiments", *Journal of Materials Processing Technology,*160, pp. 34-42, 2005.